POSTBUCKLING ANALYSIS OF ISOTROPIC AND ORTHOTROPIC RECTANGULAR PLATES SBJECTED TO EDGE COMPRESSION/SHEAR USING FINITE ELEMENT METHOD

A Thesis Submitted
In Partial Fulfillment of the Requirements
for the Degree of

DOCTOR OF PHILOSOPHY

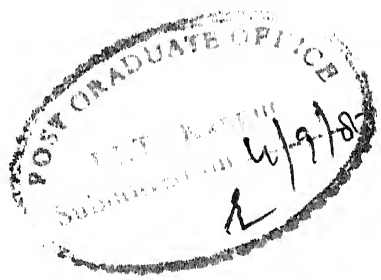

By
PARAS RAM SINDHI

to the

DEPARTMENT OF CIVIL ENGINEERING

INDIAN INSTITUTE OF TECHNOLOGY, KANPUR

SEPTEMBER, 1987

Dedicated

to

My Parents

CERTIFICATE

This is to certify that the thesis "Postbuckling Analysis of Isotropic and Orthotropic Rectangular Plates Subjected to Edge Compression/Shear Using Finite Element Method" submitted by Paras Ram Sindhi in partial fulfilment of the requirements for the degree of Doctor of Philosophy of the Indian Institute of Technology, Kanpur, is a record of bonafide research work carried out by him under our supervision and guidance. The work embodied in this thesis has not been submitted elsewhere for a degree.

Ashwini 4.9.87

ASHWINI KUMAR
Professor
Department of Civil Engineering
Indian Institute of Technology
Kanpur

Bhupinder Pal Singh Sept 4, 87

B.P. SINGH
Assistant Professor
Department of Mechanical Engineeri
Indian Institute of Technology
Kanpur

Date : September, 1987

TABLE OF CONTENTS

LIST OF TABLES

LIST OF FIGURES

NOTATIONS

(All notations are also defined whenever they appear first in the text)

a	:	length of the plate (in x-direction)
b	:	width of the plate (in y-direction)
$\{B\}$	:	vector of boundary forces
b_e	:	effective width of the plate
$\bar{b}_e$	:	non-dimensional effective width ($= b_e/b$)
D	:	flexural rigidity (of an isotropic plate)
D_1	:	$D_x \nu_y = D_y \nu_x$
D_x, D_y	:	flexural rigidities of an orthotropic plate
D_{xy}	:	shear rigidity of an orthotropic plate
E	:	modulus of elasticity of an isotropic plate
E_x, E_y	:	modulii of elasticity of an orthotropic plate
$\bar{E}$	:	degree of orthotropy or rigidity ratio ($= E_x/E_y$)
$\{g\}$	:	vector of unbalanced forces
G	:	shear modulus of elasticity of an isotropic plate
G_{xy}	:	shear modulus of elasticity of an orthotropic plate
H	:	$D_1 + 2\,D_{xy}$
k_c	:	compressive buckling coefficient
	:	$N_{xcr}\, b^2/\pi^2 D$ for isotropic plates
	:	$N_{xcr}\, b^2/\pi^2 \sqrt{D_x D_y}$ for orthotropic plates
k_s	:	shear buckling coefficient
	:	$N_{xycr}\, b^2/\pi^2 D$ for isotropic plates
	:	$N_{xycr}\, b^2/\pi^2 \sqrt{D_x D_y}$ for orthotropic plates

$[K_T]$: tangent stiffness matrix (for the plate)

: $[K_o] + [N_1] + [N_2]$

$[K_S]$: secant stiffness matrix (for the plate)

: $[K_o] + \frac{1}{2}[N_1] + \frac{1}{3}[N_2]$

$[K_o]$: conventional linear stiffness matrix of zero order (for the plate)

$[k_{11}] \cdots [k_{33}]$: submatrices of $[K_o]^{(e)}$ for an element

$[N_1]$: non-linear stiffness matrix of first order (for the plate)

$[n_{1,13}] \cdots [n_{1,33}]$: submatrices of $[N_1]^{(e)}$ for an element

$[N_2]$: non-linear stiffness matrix of second order (for the plate)

$[n_{2,33}]$: the only non-zero submatrix of $[N_2]^{(e)}$ for an element

$\lfloor M \rfloor$: row matrix of shape functions $M_1 \cdots M_{16}$

$M_1 \cdots M_{16}$: shape (or interpolating) functions in displacement model of w

$\{M,x\}, \{M,y\}$: $\frac{\partial\{M\}}{\partial x}$ and $\frac{\partial}{\partial y}\{M\}$ respectively

$\{M,xx\}, \{M,yy\}$: $\frac{\partial^2}{\partial x^2}\{M\}$ and $\frac{\partial^2}{\partial y^2}\{M\}$ respectively

$\{M,xy\}$: $\frac{\partial^2}{\partial x \partial y}\{M\}$

$\lfloor N \rfloor$: row matrix of shape functions $N_1 \cdots N_4$

$N_1 \cdots N_4$: shape functions in displacement model of u (and v)

m,n : number of half waves along the centre line of a longitudinally compressed plate in x- and y-direction respectively

n_x, n_y : direction cosines of the outer normal

N_x, N_y : inplane (membrane) forces/loads in x- and y-direction respectively (per unit length)

N_{xy} : membrane shear force/load (per unit length)

N_{xi} : value of the load N_x at which the two load-shortening lines intersect

N_{xp} : critical load for primary mode

N_{xs} : critical load for secondary mode

$\bar{N}_x$: non-dimensional compressive load

$= N_x b^2/\pi^2 D$ for isotropic plates

$= N_x b^2/\pi^2 \sqrt{D_x D_y}$ for orthotropic plates

$\bar{N}_{xy}$: non-dimensional shear load

$= N_{xy} b^2/\pi^2 D$ for isotropic plates

$= N_{xy} b^2/\pi^2 \sqrt{D_x D_y}$ for orthotropic plates

N_{xcr} : critical load (in compression) per unit length

N_{xycr} : critical load (in shear) per unit length

$\bar{N}$: load ratio

$= N_x/N_{xcr} = \bar{N}_x/k_c$ for compression loaded plates

$= N_{xy}/N_{xycr} = \bar{N}_{xy}/k_s$ for shear loaded plates

P_{cr} : total critical load (for compression as well as shear)

q : lateral load on the plate (in z-direction)

$\{q\}$: displacement vector

$\{\Delta q\}$: vector of incremental displacements

Q_x, Q_y : shear forces (in z-direction)

$\{Q\}$: load vector

$\{\Delta Q\}$: vector of incremental loads

t : thickness of the plate

u, v, w : middle surface displacements in x-, y- and z-direction respectively

$\{u\}$: vector of displacements $u_1 \ldots u_4$ at the 4 nodes of an element (4x1)

$\{v\}$	:	vector of displacements $v_1 \cdots v_4$ at the 4 nodes of an element (4x1)
$\{w\}$	:	vector of displacements w_1, $\partial w/\partial x|_1 \cdots \cdots \partial^2 w/\partial x \partial y|_4$ at the 4 nodes of an element (16x1)
U	:	total strain energy
	=	$U_o + U_1 + U_2$
U_o	:	linear part of strain energy U
	=	$U_{o,m} + U_{o,b}$
$U_{o,m}$	:	strain energy due to stretching (quadratic order)
$U_{o,b}$	:	strain energy due to bending (quadratic order)
U_1	:	strain energy due to coupling between stretching and bending (cubic order)
U_2	:	strain energy due to effect of rotations due to large deflections (quartic order)
V	:	total work done by forces
w_o	:	maximum value of the lateral (out of plane) deflection w, for a plate buckling in a particular mode
$\bar{w}_o$	:	non-dimensional lateral deflection ($= w_o/t$)
$\partial w/\partial x$, $\partial w/\partial y$	:	slopes or rotations about y- and x-axis respectively
$\partial^2 w/\partial x \partial y$	:	twist
x-, y-, z-	:	reference axes
π	:	total potential energy (= U-V)
ν	:	Poisson's ratio (for isotropic plates)
ν_x, ν_y	:	Poisson's ratios, associated with x- and y-axis respectively (for orthotropic plates)

λ : aspect ratio of the plate (= a/b)

λ' : mb/na ($= \frac{mb}{a}$, with n = 1)

Δ : average axial shortening of a plate subjected to longitudinal compression

Δ_{sh} : relative displacement of the longitudinal edges, parallel to x-direction, for plates subjected to shear loading

$\bar{\Delta}$: non-dimensional shortening

$= \Delta E b^2 t/a \pi^2 D$ for an isotropic plate

$= \Delta E_x b^2 t/a \pi^2 \sqrt{D_x D_y}$ for an orthotropic plate

$\bar{\Delta}_{sh}$: non-dimensional shear displacement

$= \Delta_{sh} G bt/\pi^2 D$ for an isotropic plate

$= \Delta_{sh} G_{xy} b t/\pi^2 \sqrt{D_x D_y}$ for an orthotropic plate

$\varepsilon_x, \varepsilon_y$: middle surface strains in x- and y-direction respectively

γ_{xy} : middle surface shear strain

σ_x , σ_y : longitudinal and transverse membrane stresses (in x- and y-direction respectively)

σ_{av} : average longitudinal stress (compressive)

σ_{cr} : critical compressive stress

$\bar{\sigma}_{cr}$: non-dimensional critical stress

: $\sigma_{cr} b^2 t/\pi^2 D$ for isotropic plates

: $\sigma_{cr} b^2 t/\pi^2 \sqrt{D_x D_y}$ for orthotropic plates

σ_{max} : maximum value of σ_x (for longitudinally compressed plates)

$\bar{\sigma}_{max}$: non-dimensional value of σ_{max}

: $\sigma_{max} b^2 t/\pi^2 D$ for isotropic plates

: $\sigma_{max} b^2 t/\pi^2 \sqrt{D_x D_y}$ for orthotropic plates

$\sigma_{x\ max}$: maximum tensile value of σ_x in shear loaded plate

$\sigma_{y\ max}$: maximum tensile value of σ_y in shear loaded plate

$\bar{\sigma}_{x\ max}$: non-dimensional value of $\sigma_{x\ max}$ $(= \sigma_{x\ max}/N_{xcr})$

$\bar{\sigma}_{y\ max}$: non-dimensional value of $\sigma_{y\ max}$ $(= \sigma_{y\ max}/N_{xcr})$

τ_{cr} : critical shear stress

τ_{max} : maximum value of τ_{xy} (for plates loaded in shear)

$\bar{\tau}_{max}$: non-dimensional value of τ_{max},

$= \tau_{max}\ b^2 t/\pi^2 D$ for isotropic plates

$= \tau_{max}\ b^2 t/\pi^2 \sqrt{D_x\ D_y}$ for orthotropic plates

$\oint$: line integral (integration to be carried along the boundary in anti-clockwise direction.

Superscripts

(e) : over an element

(ne) : at the nodes of the element

(n) : at all the nodes of the plate

Subscripts

i : iteration number

j : nodal displacement number

Explanation of abbreviations for journals, used in REFERENCES

AIAAJ	:	American Institute of Aeronautics and Astronautics Journal
AQ	:	Aeronautical Quarterly
CMAME	:	Computer Methods in Applied Mechanics and Engineering
CS	:	Computers and Structures
IJMS	:	International Journal of Mechanical Sciences
IJNLM	:	International Journal of Non-Linear Mechanics
IJNME	:	International Journal of Numerical Methods in Engineering
IJSS	:	International Journal of Solids and Structures
JAM	:	Journal of Applied Mechanics, Transactions American Society for Mechanical Engineers
JCM	:	Journal of Composite Materials
JEMD	:	Journal of Engineering Mechanics Division, Proceedings, American Society of Civil Engineers
JMES	:	Journal of Mechanical Engineering Sciences
JSD	:	Journal of Structural Division, Proceedings, American Society of Civil Engineers
PICEL	:	Proceedings Institute of Civil Engineers, London

SYNOPSIS

POSTBUCKLING ANALYSIS OF ISOTROPIC AND ORTHOTROPIC RECTANGULAR PLATES SUBJECTED TO EDGE COMPRESSION/SHEAR USING FINITE ELEMENT METHOD

(A thesis submitted in partial fulfilment of the requirements for the degree of Doctor of Philosophy by PARAS RAM SINDHI, to the Department of Civil Engineering, Indian Institute of Technology, Kanpur, India).

The postbuckling analysis of a plate requires the solution of a set of non-linear partial differential equations. The simplest form of such equations is that due to von Karman. The closed-form solution of these equations is rather tedius, if not impossible. In past, attempts have been made to solve them using different methods, for example, double Fourier series solution, perturbation technique, dynamic relaxation method, energy balancing technique, Galerkin method, finite difference and finite element methods. In some cases it has been found convenient to solve von Karman's equations in terms of three displacement functions while many investigators have preferred to solve these equations in their modified form involving only two variables, i.e. the stress function and the lateral deflection of the plate.

In this thesis, the postbuckling analysis of simply supported, rectangular, thin, flat plates is investigated in considerable detail. Two types of load are considered: longitudinal compression and edge shear. The basis of the formulation is limited to linear elastic plates only. Both, isotropic as well as orthotropic plates are analysed using finite element method. The finite element model used is a 4-noded rectangle with 6 degrees

of freedom, viz. u, v, w, $\partial w/\partial x$, $\partial w/\partial y$ and $\partial^2 w/\partial x \partial y$ at each node; this makes a total of 24 degrees of freedom for an element. Only a quadrant of the plate is analysed in the case of longitudinal compression (due to symmetry with respect to loading and geometry) while the full plate has to be analysed in the case of shear loading. A 16-element mesh is used to discretize the quadrant of the plate or the plate itself, as the case may be. The finite element matrix equations are derived by minimizing the total potential energy that takes into account the stretching of the middle surface of the plate as well; in the expression of strain energy, therefore, non-linear strain-displacement relations are used. Stiffness coefficients for linear and non-linear stiffness matrices are obtained as second partial derivative (with respect to nodal degrees of freedom), of the corresponding strain energy. The incremental method, supplemented with the Newton-Raphson iterative technique, is used to solve the resulting set of non-linear algebraic simultaneous equations.

For plates under longitudinal compression, two types of inplane boundary condition on unloaded edges are examined : (i) completely free (to move in its own plane), (ii) completely restrained (i.e. not allowed to move in the transverse direction). Plates with different aspect ratios and buckling in different modes are studied in detail. To study the effect of orthotropy, two materials, viz. the glass-epoxy and boron-epoxy are considered. Results such as critical load curves, load-deflection curves, load-shortening curves, changes in buckle pattern, effective width curves, and stress distributions are reported.

It is shown that the plate behaves quite differently under the two inplane boundary conditions.

A simple method is suggested to predict whether or not a changeover from one buckling mode to another takes place. Simple formulae are also devised to ascertain the magnitude of the possible secondary buckling load, under each inplane boundary condition. The effective-width curves presented are unique in that they account for the change in the buckle pattern of the plate, and are thus valid even after the plate has changed over to the higher mode of buckling.

To study the postbuckling analysis of a plate subjected to pure shear, the NASTRAN model is modified and used in the present work. Plates of different aspect ratios are analysed and results such as critical shear loads, load-deflection curves, deflection contours, load-shear displacement curves and stress distribution are reported. It is shown that a shear loaded plate buckles in a mode which is essentially a combination of either some uncoupled symmetric modes or some uncoupled anti-symmetric modes, and that the changeover from a symmetric to an anti-symmetric mode (or vice versa) is not possible. The reduction in the shear stiffness (from the prebuckling to the post-buckling stage) is very low as compared to the reduction in the axial stiffness for a longitudinally compressed plate. It is found that the tensile membrane stresses (longitudinal as well as transverse) get developed which tend to stiffen the plate.

A brief, yet complete, review of the existing literature on the subject of postbuckling has been presented. Wherever possible, the results of the present investigation are compared with those already available.

CHAPTER 1

INTRODUCTION

Plates are extensively used in aircraft construction, shipbuilding, plate girders and box girders used in buildings and bridges, and in many thin-walled structures. In recent years, the availability of high strength alloys and composites and the use of optimization techniques in designs for the minimum weight, have resulted in structures that are inherently very thin. This, in turn, has enhanced the possibility of buckling.

1.1 POSTBUCKLING - A GEOMETRICALLY NON-LINEAR PROBLEM

1.1.1 Buckling and Postbuckling Phenomena

A plate may be subjected to any type of inplane loads and load-combinations. Under these loads, a thin flat plate initially undergoes inplane displacements only. With increasing loads a stage is reached when the flat equilibrium configuration becomes unstable and the plate passes to a buckled configuration, (characterized by the out of plane deflection). The load at which this bifurcation of equilibrium takes place is called the critical load (or the buckling load).

Unlike a column for which the critical load is, more or less, the ultimate load, the plate does not fail immediately at the critical load. It is well established that plates have considerable reserved strength even beyond the classical buckling

i.e. in the postbuckling range. From Figure 1.1 it is noted that at the onset of buckling, the plate has zero flexural stiffness but it increases with the increase in lateral deflection. Thus, the plate is able to resist greater loads. The nature of the load-deflection curve for the plate in the postbuckling range is of 'stiffening' type - stiffness increasing with the load (as against the 'softening' type for shells in which the stiffness decreases with load).

In general, plates are not perfectly flat but have some initial geometric imperfections. The dashed curve in Figure 1.1 is for an imperfect plate. The out of plane deflection grows continuously with the load, right from the beginning; the curve coincides with that of a perfect plate only at higher loads.

The determination of the critical load for a particular structure is essentially an eigen-value problem based on linear (small deflection) theory. This yields only the critical load and provides no information about the magnitude of the lateral deflection at the onset of buckling and beyond. Therefore, the use of non-linear equations, based on the large deflection theory, becomes essential for studying the behaviours of the structure in the postbuckling regime.

1.1.2 Solving a Geometrically Non-Linear Problem

The formulation of a geometrically non-linear problem, in general, is based on the following two approaches :

(i) Total Lagrangian Approach

(ii) Updated Lagrangian Approach (or Eulerian Approach).

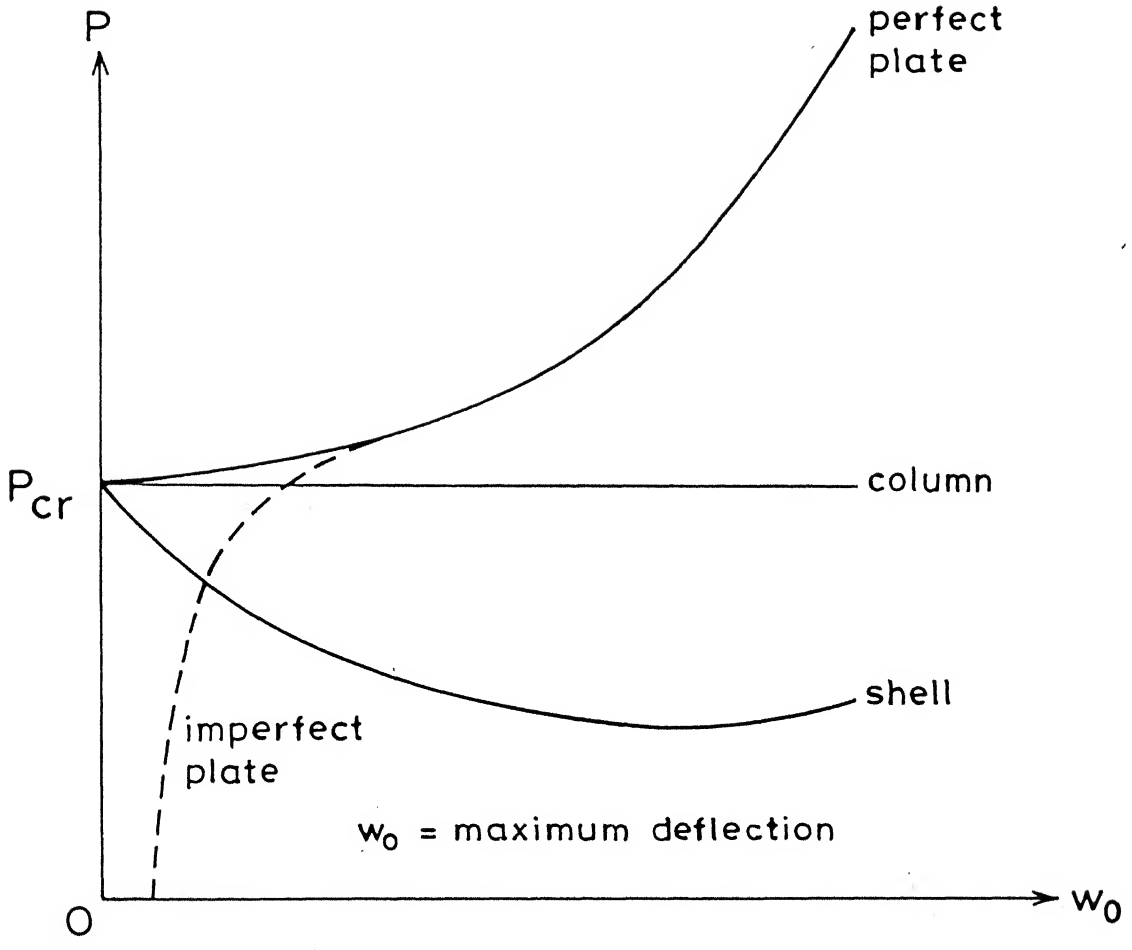

Fig. 1.1 Load-deflection curves in post-buckling range.

In total Lagrangian approach the formulation is always based on the initial undeformed configuration whereas in the updated Lagrangian approach, the problem is formulated with respect to the current deformed configuration of the structure. The total Lagrangian method is advantageous since the initial configuration of the structure remains fixed, thus resulting in the simplification of the formulation and the ensuing computations.

The finite element formulation of a non-linear problem is usually done in one of the following ways :

(i) The governing non-linear differential equations are converted into a matrix form, using Galerkin's weighted residual approach.

(ii) The equations of equilibrium are obtained by using the principle of stationary potential energy i.e. by setting the first variation of the potential energy with respect to the nodal displacements, to zero.

In both the cases the resulting non-linear simultaneous algebraic equations are solved by some iterative schemes, like Newton-Raphson method, as discussed in Chapter 2.

1.2 EFFECTIVE WIDTH CONCEPT

When a plate is loaded in uniaxial compression, membrane stresses are developed within it. So long as the load P is less than the critical load P_{cr} , the longitudinal stress, i.e. σ_x, is uniform at all points, (Figure 1.2a). Obviously at this stage,

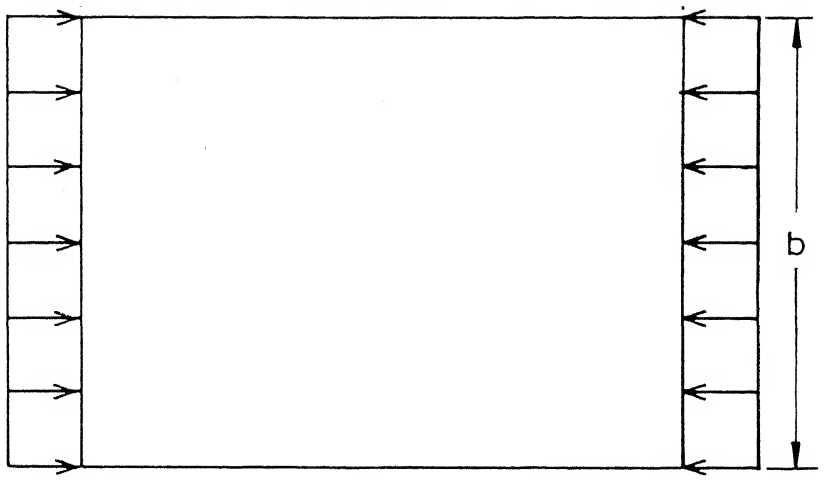

(a) $P \leqslant P_{cr}$

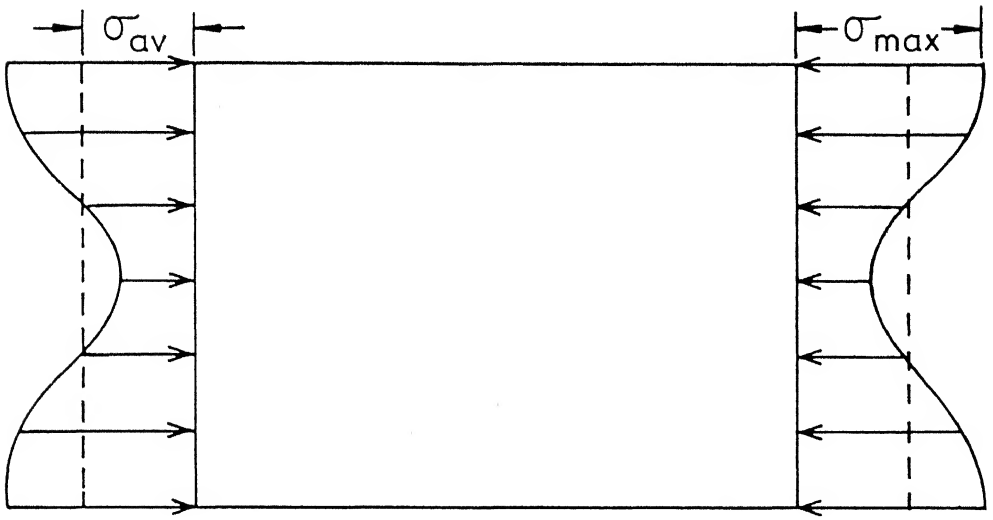

(b) $P > P_{cr}$

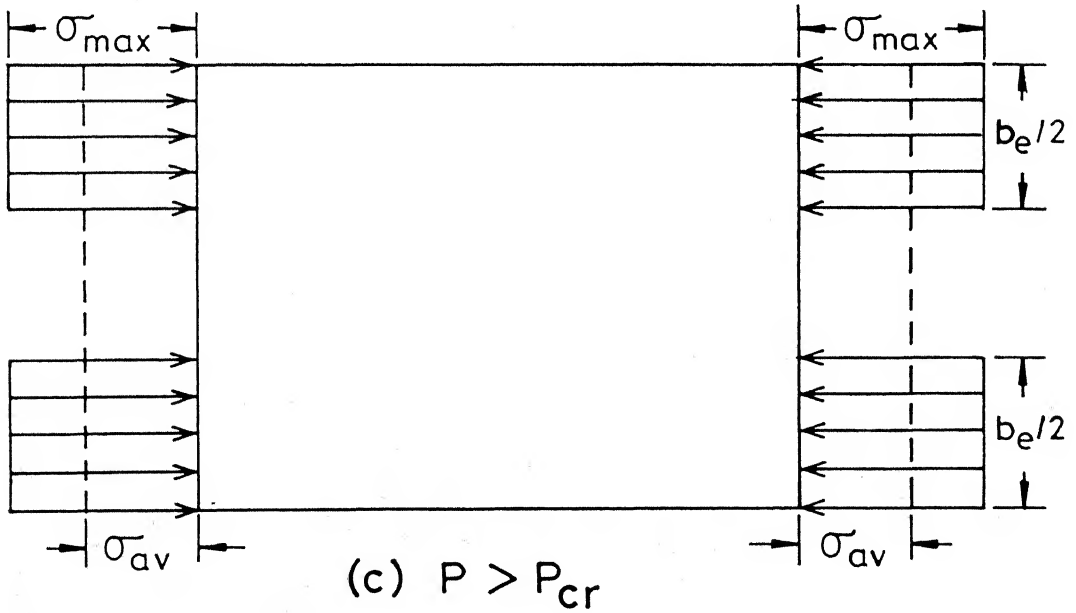

(c) $P > P_{cr}$

Fig. 1.2 Effective width concept.

$$P = \sigma_{av}\, b\, t = \sigma_x\, b\, t = \sigma_{max}\, b\, t \qquad (1.1)$$

where σ_{av} is the average longitudinal stress, σ_{max} the maximum stress, b the width and t the thickness of the plate. The stress distribution continues to be uniform until $P = P_{cr}$ when σ_x approaches σ_{cr} (the critical stress). For loads beyond P_{cr}, tensile membrane stresses σ_y (in the transverse direction) are developed within the plate, which retard the increase of the lateral deflection. The stresses on loaded edges, therefore, get redistributed in a manner that more and more stress is produced in the vicinity of the unloaded edges and the stress in the central portion remains low - generally less than σ_{cr} (Figure 1.2b). The nonuniformity in the stress pattern is actually due to the differential plate shortening along the longitudinal direction.

At any stage of loading ($P > P_{cr}$) the total compressive load may be assumed to be carried by the two strips of equal width, adjacent to the unloaded edges (Figure 1.2c), the central portion remaining ineffective in resisting the load. The effective width b_e is, thus, defined as

$$P = \sigma_{max}\, b_e\, t = \sigma_{av}\, b\, t \qquad (1.2)$$

i.e.

$$b_e = \frac{1}{\sigma_{max}} \int_0^b \sigma_x \, dy \qquad (1.3)$$

The concept of effective width is useful for design purposes; the ultimate strength of the plate is readily estimated by requiring σ_{max} not to cross the yield stress of the material.

From time to time, many empirical and semi-empirical effective width formulae have been proposed, the earliest being that of von Karman . A reference to these formulae can be made, for example, in Lind et. al. (1976) and Narayanan and Chow (1985).

1.3 BOUNDARY CONDITIONS

In this section the standard boundary conditions are summarized for rectangular plates in terms of flexural (out of plane) displacement/force and membrane (inplane) displacement/force.

1.3.1 Flexural Boundary Conditions

(a) Simply supported edges

The deflection and the bending moment along these edges is zero, i.e.

$$w = 0,\ M_x = 0 \quad \text{along} \quad x = \text{constant}$$
$$w = 0,\ M_y = 0 \quad \text{along} \quad y = \text{constant} \qquad (1.4)$$

(b) Clamped edges

Along such edges the deflection and the slope is required to be zero, i.e.

$$w = 0,\ \partial w/\partial x = 0 \quad \text{along} \quad x = \text{constant}$$
$$w = 0,\ \partial w/\partial y = 0 \quad \text{along} \quad y = \text{constant} \qquad (1.5)$$

(c) Free edges

On free edges the shear force and the bending moment are zero, i.e.

$$Q_x = 0,\ M_x = 0 \quad \text{along} \quad x = \text{constant}$$

$$Q_y = 0,\ M_y = 0 \quad \text{along} \quad y = \text{constant} \qquad (1.6)$$

1.3.2 Membrane Boundary Conditions

(i) Specified displacements

The inplane displacement on an edge may be specified as

$$u = u^* \quad \text{along} \quad x = \text{constant}$$

$$v = v^* \quad \text{along} \quad y = \text{constant} \qquad (1.7)$$

(ii) Specified normal membrane force

Along an edge, some normal membrane force of known value may be specified.

(iii) Shear-free edges

For an edge to remain shear free, the shear stress/force on the edge is assumed to be zero, such that

$$\partial v/\partial x + \partial u/\partial y = 0 \quad \text{along the edge} \qquad (1.8)$$

(iv) Stress-free edges

For an edge to remain stress free, both normal (direct) and shear stress/force on it are assumed to be zero.

The inplane boundary conditions for the straight edge (SE), movable edge (ME)-which is similar to the stress-free edge and fixed edge (FE) are separately dealt in Chapter 3, section 3.1.

1.4 LITERATURE REVIEW

1.4.1 Isotropic Plates Under Edge Compression

Levy (1942) and Coan (1951) are amongst the first few who initiated the study of the postbuckling behavior of rectangular plates by presenting approximate solutions of von Karman's large deflection equations. Yamaki (1960) extended the work of Levy and Coan by incorporating different inplane and flexural boundary conditions. A similar analysis for the case when unloaded edges of the plate are rigidly held apart, has been reported in Timoshenko and Gere (1961) and has also been independently attempted by Rushton (1969). Brown and Harvey (1969) studied the behavior of plates under the combined action of lateral and edge loads. The perturbation technique to investigate postbuckling problems was employed by many investigators, for example, Stein (1960), Walker (1969), Rhodes and Harvey (1971 , 1977), Dombourian et. al. (1976). Among other methods, Rushton (1969, 1970) used the dynamic relaxation technique and Brown and Harvey (1969) applied the finite difference procedure to solve the governing differential equations of the related problem.

The Finite Element Method (FEM) to solve non-linear plate problems has also been employed by many investigators; most notable among them are Kawai and Yoshimura (1969), Murray and Wilson (1969), Yang (1970, 1971), Roberts and Ashwell (1971), Colville et. al. (1973), Shye and Colville (1979), Yang and Han (1983), Carnoy and Hughes (1983) and Szilard (1985). While some

of these investigators (Kawai and Yoshimura, 1969; Colville et. al., 1973 and Shye and Colville, 1979) have used the direct iteration procedure to solve the resulting finite element matrix equations, there are some (Yang, 1970, 1971; Yang and Han, 1983) who used the incremental approach. Roberts and Ashwell (1971) made use of the mid-increment stiffness matrix in the incremental method and Szilard applied the energy balancing technique to the problem. The majority of researchers have used the total Lagrangian approach in their formulations, except a few like Murray and Wilson (1969) who adopted the updated Lagrangian approach. The finite element models employed in these analyses vary from simple triangles (Murray and Wilson, 1969) and simple rectangles (Yang, 1970) to isoparametric shell elements (Carnoy and Hughes, 1983) and high-order triangular elements (Yang and Han, 1983). In studying the postbuckling behavior of isotropic plates, some authors have also examined the problem of secondary buckling and of change in the wave-form; these include Stein (1960), Chang and Masur (1965), Rushton (1970), Supple (1966, 1967, 1968; 1970), Shye and Colville (1979), Nakamura and Uetani (1979) and Carnoy and Hughes (1983).

1.4.2 Orthotropic Plates Under Edge Compression

A very early attempt in this regard is due to Wittrick (1952), who brought out a correlation between some stability problems for orthotropic and isotropic plates under uniaxial and biaxial compression. Basu and Chapman (1966) analysed plates subjected to uniformly distributed lateral load whereas Aalami and Chapman (1969)

included the effect of edge loads as well. Chia (1972) and Niyogi (1973) used the perturbation and the Galerkin techniques respectively, to solve governing equations for the case of uniformly distributed load.

The available work which deals with the postbuckling behavior of orthotropic plates is rather small. Chandra and Raju (1973) and Prabhakara and Chia (1973) used the perturbation method and the double series solution respectively, to investigate this problem. In their investigations, unloaded edges of the plate were maintained straight throughout. Harris (1975) investigated both the buckling and the postbuckling of a class of biaxially loaded laminated plates in the presence of bending-extensional elastic couplings. Stein (1983), in an extension of his earlier work on isotropic plates (Stein, 1960) has analysed simply supported and clamped long rectangular orthotropic plates to study the postbuckling phenomenon.

1.4.3 Plates Under Shear Loading

A review of the work on shear buckling of isotropic and orthotropic plates has been presented by Johns (1970) in a comprehensive style. The problem of postbuckling analysis was first undertaken by Kaminski and Ashton (1971) who presented an experimental study of the post shear-buckling diagonal tension behavior of rectangular laminated boron-epoxy plates clamped on each edge. Kobayashi et. al. (1981) also made an experimental study on graphite-epoxy laminated plates; the ultimate load was

found to be considerably greater than the initial buckling load. Agarwal (1981) examined the postbuckling behavior of multibay composite shear webs to study failure modes typical of composite panels. The investigation of Zhang and Matthews (1984) on the postbuckling analysis of anisotropic plates under combined compressive and shear loading revealed the importance of the direction of the applied shear force in the case of anisotropic plates. Very recently, Stein (1985) has analysed long orthotropic plates in combined shear and compression; the method used is similar to the one developed in his earlier investigations (1960, 1983) dealing with longitudinally compressed plates.

1.5 OBJECT AND SCOPE OF PRESENT INVESTIGATION

From the foregoing literature review, it is clear that much of the work on postbuckling has been for longitudinally compressed isotropic plates. In most of these investigations, an important feature, namely the "change in buckle pattern" beyond the primary buckling, has been overlooked. The resulting curves for the effective width and the maximum longitudinal stress are, therefore, applicable only for the primary mode. All the analyses for orthotropic plates also suffer from the similar drawback. Regarding the consideration of inplane boundary conditions, the unloaded edges of the plates have mostly been assumed to be held straight (SE condition). Some investigators have used stress-free unloaded edges that are free to move in the plane of the plate (ME condition) and a very few have considered the edges rigidly held apart (FE condition). Finally, the

postbuckling behavior of plates under shear loading has received very little attention; the most comprehensive work is due to Stein (1985) which, however, deals with long plates only.

The literature review also reveals that the finite element method has been employed only for isotropic plates under edge compression. The method has, so far, not been extended to include orthotropic plates and the plates loaded in shear. With these points in view, the aim of the present investigation is -

i) to demonstrate the potentiality of the finite element method to handle the problem of postbuckling of plates, taking into consideration the variation in material properties (isotropic and orthotropic), load conditions (compression and shear) and inplane (membrane) boundary conditions (ME and FE conditions).

ii) to explore in detail the behavior of a plate under FE condition (which relatively has received less attention in the literature) and to compare the results with those under ME condition.

iii) to study the phenomena of the change in buckle pattern, beyond the primary buckling.

iv) to arrive at some formula/method to estimate/predict the load at which a changeover from the primary mode may take place.

v) to present the effective width curves which take due consideration of the change in the buckling mode.

vi) to get an insight into the postbuckling behavior of isotropic and orthotropic plates subjected to pure shear.

Thus in brief, the thesis deals with the postbuckling analysis of simply supported thin isotropic and orthotropic rectangular plates subjected to either uniaxial compression or to pure shear. The entire thesis is divided into six main chapters. Chapter 1 is the Introduction. In Chapter 2, complete details of the finite element formulation are given, the governing equations are derived and the solution procedure is discussed. Chapter 3 deals with the analysis of isotropic rectangular plates subjected to longitudinal compression. This analysis has been extended in Chapter 4 to include orthotropic materials; the results presented are for glass-epoxy and boron-epoxy plates. Chapter 5 is devoted to study the postbuckling behavior of both isotropic and orthotropic plates under pure shear. Although, the results are presented and discussed at the end of each chapter, the main results and conclusions have been summarised in Chapter 6 for the sake of completeness.

CHAPTER 2

FINITE ELEMENT FORMULATION AND SOLUTION PROCEDURE

2.1 TOTAL POTENTIAL OF THE FINITE ELEMENT

Consider a rectangular finite element shown in Figure 2.1. The total potential energy π of such an element consists of its strain energy U and the work done V by various forces acting on it, so that

$$\pi = U - V \tag{2.1}$$

2.1.1 Strain Energy of an Isotropic Element

The strain energy U for a thin plate is given by

$$U = \frac{1}{2} \int_V (\sigma_x \varepsilon_x + \sigma_y \varepsilon_y + \tau_{xy} \gamma_{xy}) \, dV \tag{2.2}$$

where σ_x, σ_y, τ_{xy} are the stresses and ε_x, ε_y, γ_{xy} the strains. The stresses associated with the z-direction, being very small, have been neglected.

For an isotropic material, the stress-strain relations are

$$\sigma_x = \frac{E}{1-\nu^2} (\varepsilon_x + \nu \varepsilon_y)$$

$$\sigma_y = \frac{E}{1-\nu^2} (\varepsilon_y + \nu \varepsilon_x) \tag{2.3}$$

$$\tau_{xy} = \frac{E}{2(1+\nu)} \gamma_{xy}$$

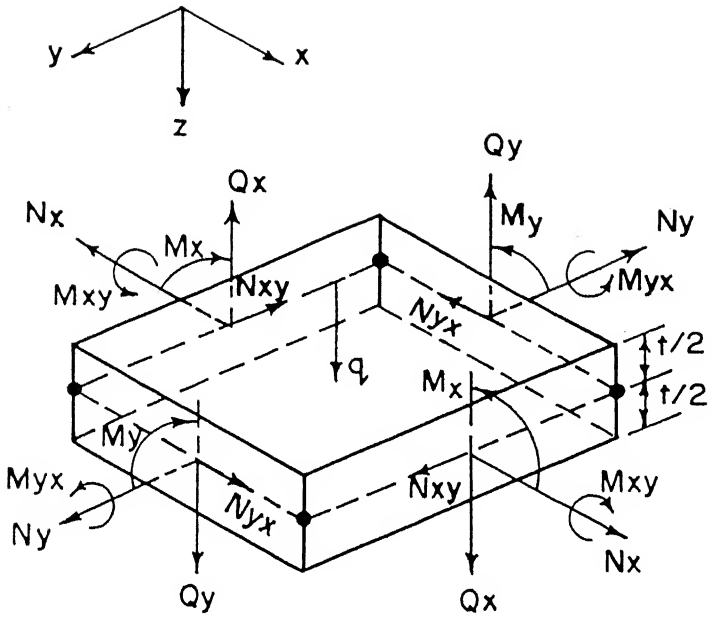

Fig. 2.1 A typical rectangular finite element.

where E is the modulus of elasticity and ν the Poisson's ratio. Substitution of Eqs. (2.3) in Eq. (2.2) yields

$$U = \frac{Et}{2(1-\nu^2)} \iint \left[\varepsilon_x^2 + \varepsilon_y^2 + 2\nu\varepsilon_x \varepsilon_y + \frac{1}{2}(1-\nu)\ \gamma_{xy}^2 \right] dx\, dy \quad (2.4)$$

where t is the plate thickness. At any point, the strain-displacement relations from large deflection theory are,

$$\begin{aligned} \varepsilon_x &= \frac{\partial u}{\partial x} + \frac{1}{2}\left(\frac{\partial w}{\partial x}\right)^2 - z\frac{\partial^2 w}{\partial x^2} \\ \varepsilon_y &= \frac{\partial v}{\partial y} + \frac{1}{2}\left(\frac{\partial w}{\partial y}\right)^2 - z\frac{\partial^2 w}{\partial y^2} \\ \gamma_{xy} &= \frac{\partial u}{\partial y} + \frac{\partial v}{\partial x} + \left(\frac{\partial w}{\partial x}\right)\left(\frac{\partial w}{\partial y}\right) - 2z\frac{\partial^2 w}{\partial x \partial y} \end{aligned} \quad (2.5)$$

in which u,v,w are the displacements in x-,y-,z-directions respectively.

Substituting Eqs. (2.5) into Eq. (2.4), the strain energy expression becomes

$$U = U_o + U_1 + U_2 = U_{o,m} + U_{o,b} + U_1 + U_2 \quad (2.6)$$

where,

$$U_{o,m} = \frac{6D}{t^2} \iint \left\{ \left(\frac{\partial u}{\partial x}\right)^2 + 2\nu \left(\frac{\partial u}{\partial x}\right)\left(\frac{\partial v}{\partial y}\right) + \left(\frac{\partial v}{\partial y}\right)^2 + \frac{1-\nu}{2}\left(\frac{\partial u}{\partial y} + \frac{\partial v}{\partial x}\right)^2 \right\} dx\, dy \quad (2.7)$$

$$U_{o,b} = \frac{D}{2} \iint \left\{ \left(\frac{\partial^2 w}{\partial x^2}\right)^2 + 2\nu \left(\frac{\partial^2 w}{\partial x^2}\right)\left(\frac{\partial^2 w}{\partial y^2}\right) + \left(\frac{\partial^2 w}{\partial y^2}\right)^2 + 2(1-\nu)\left(\frac{\partial^2 w}{\partial x \partial y}\right)^2 \right\} dx\, dy \quad (2.8)$$

$$U_1 = \frac{6D}{t^2} \int\int \{(\frac{\partial u}{\partial x} + \nu \frac{\partial v}{\partial y})(\frac{\partial w}{\partial x})^2 + (\frac{\partial v}{\partial y} + \nu \frac{\partial u}{\partial x})(\frac{\partial w}{\partial y})^2$$

$$+ (1-\nu) (\frac{\partial u}{\partial y} + \frac{\partial v}{\partial x})(\frac{\partial w}{\partial x})(\frac{\partial w}{\partial y})\} \, dx \, dy \qquad (2.9)$$

$$U_2 = \frac{3D}{2t^2} \int\int \{(\frac{\partial w}{\partial x})^2 + (\frac{\partial w}{\partial y})^2\}^2 \, dx \, dy \qquad (2.10)$$

and D is the flexural rigidity of the isotropic plate, given by

$$D = \frac{Et^3}{12(1-\nu^2)} \qquad (2.11)$$

In the above expressions, $U_{o,m}$ represents strain energy due to inplane stretching (membrane) and $U_{o,b}$ due to bending, both being of quadratic order. The part U_1 represents the cubic-order strain energy due to coupling between the stretching and the bending effects. The quantity U_2 is of quartic order representing the effect of rotations due to large deflections.

2.1.2 Strain Energy of an Orthotropic Element

It is assumed that this orthotropic element has its material axes of symmetry parallel to the coordinate axes and thus the following derivations apply to a specially orthotropic element. The expression for strain energy U, Eq. (2.2) is valid for an orthotropic element also. But the stress-strain relations for this case are given by

$$\sigma_x = \frac{E_x}{1 - \nu_x \nu_y} (\varepsilon_x + \nu_y \varepsilon_y)$$

$$\sigma_y = \frac{E_y}{1 - \nu_x \nu_y} (\varepsilon_y + \nu_x \varepsilon_x)$$

$$\tau_{xy} = G_{xy}\,\gamma_{xy} \qquad (2.12)$$

Here E_x, E_y and ν_x, ν_y are, respectively, modulii of elasticity and Poisson ratios associated with x- and y-axes and G_{xy} is the shear modulus associated with x- and y-axes.

The substitution of strain-displacement Eqs. (2.5) in Eqs. (2.12) and then in Eq. (2.2), results in the following expressions for various components of strain energy for the orthotropic element :

$$U_{o,m} = \frac{6}{t^2} \int\int \{D_x(\frac{\partial u}{\partial x})^2 + D_y(\frac{\partial v}{\partial y})^2 + 2\,D_x\,\nu_y(\frac{\partial u}{\partial x})(\frac{\partial v}{\partial y}) + D_{xy}(\frac{\partial u}{\partial y} + \frac{\partial v}{\partial x})^2\}\,dx\,dy \qquad (2.13)$$

$$U_{o,b} = \frac{1}{2} \int\int \{D_x(\frac{\partial^2 w}{\partial x^2})^2 + D_y(\frac{\partial^2 w}{\partial y^2})^2 + 2D_x\,\nu_y\,\frac{\partial^2 w}{\partial x^2}\frac{\partial^2 w}{\partial y^2} + 4\,D_{xy}(\frac{\partial^2 w}{\partial x \partial y})^2\}\,dx\,dy \qquad (2.14)$$

$$U_1 = \frac{6}{t^2} \int\int \{D_x(\frac{\partial u}{\partial x} + \nu_y\,\frac{\partial v}{\partial y})(\frac{\partial w}{\partial x})^2 + D_y(\frac{\partial v}{\partial y} + \nu_x\,\frac{\partial u}{\partial x})(\frac{\partial w}{\partial y})^2 + 2\,D_{xy}(\frac{\partial u}{\partial y} + \frac{\partial v}{\partial x})(\frac{\partial w}{\partial x})(\frac{\partial w}{\partial y})\}\,dx\,dy \qquad (2.15)$$

$$U_2 = \frac{3}{2t^2} \int\int \{D_x(\frac{\partial w}{\partial x})^4 + D_y(\frac{\partial w}{\partial y})^4 + 2D_x\,\nu_y(\frac{\partial w}{\partial x})^2(\frac{\partial w}{\partial y})^2 + 4\,D_{xy}(\frac{\partial w}{\partial x})^2(\frac{\partial w}{\partial y})^2\}\,dx\,dy \qquad (2.16)$$

Here, flexural rigiditives D_x, D_y and shear rigidity D_{xy} are given by

$$D_x = E_x\,t^3/12(1 - \nu_x\nu_y)$$

$$D_y = E_y\, t^3/12(1 - \nu_x \nu_y)$$

$$D_{xy} = G_{xy}\, t^3/12 \qquad (2.17)$$

2.1.3 Work Done by Forces Acting on the Element

Work done by inplane forces N_x, N_y and N_{xy} is

$$V_1 = \oint u(N_x\, n_x + N_{xy}\, n_y)\, dB$$

$$V_2 = \oint v(N_{xy}\, n_x + N_y\, n_y)\, dB \qquad (2.18)$$

where n_x and n_y are the direction cosines of the outer normal and the line integral is along the boundary of the element. The forces N_x, N_y and N_{xy} in terms of displacements for isotropic and orthotropic plates, Chia (1980), are :

$$N_x = \frac{E\,t}{1-\nu^2}\left[\left\{\frac{\partial u}{\partial x} + \frac{1}{2}\left(\frac{\partial w}{\partial x}\right)^2\right\} + \nu\left\{\frac{\partial v}{\partial y} + \frac{1}{2}\left(\frac{\partial w}{\partial y}\right)^2\right\}\right]$$

$$N_y = \frac{E\,t}{1-\nu^2}\left[\left\{\frac{\partial v}{\partial y} + \frac{1}{2}\left(\frac{\partial w}{\partial y}\right)^2\right\} + \nu\left\{\frac{\partial u}{\partial x} + \frac{1}{2}\left(\frac{\partial w}{\partial x}\right)^2\right]\right. \qquad (2.19)$$

$$N_{xy} = \frac{E\,t}{2(1+\nu)}\left[\frac{\partial u}{\partial y} + \frac{\partial v}{\partial x} + \left(\frac{\partial w}{\partial x}\right)\left(\frac{\partial w}{\partial y}\right)\right],$$

and

$$N_x = \frac{E_x\, t}{1-\nu_x \nu_y}\left\{\frac{\partial u}{\partial x} + \frac{1}{2}\left(\frac{\partial w}{\partial x}\right)^2\right\} + \nu_y\left\{\frac{\partial v}{\partial y} + \frac{1}{2}\left(\frac{\partial w}{\partial y}\right)^2\right\}$$

$$N_y = \frac{E_y\, t}{1-\nu_x \nu_y}\left[\left\{\frac{\partial v}{\partial y} + \frac{1}{2}\left(\frac{\partial w}{\partial y}\right)^2\right\} + \nu_x\left\{\frac{\partial u}{\partial x} + \frac{1}{2}\left(\frac{\partial w}{\partial x}\right)^2\right]\right. \qquad (2.20)$$

$$N_{xy} = G_{xy}\, t\left(\frac{\partial u}{\partial y} + \frac{\partial v}{\partial x} + \frac{\partial w}{\partial x}\,\frac{\partial w}{\partial y}\right).$$

The work done by lateral forces Q_x, Q_y and moments M_x, M_y, M_{xy}, is

$$V_3 = \oint w(Q_x\, n_x + Q_y\, n_y)\, dB$$

$$V_4 = \oint \frac{\partial w}{\partial x}(M_x\, n_x + M_{xy}\, n_y)\, dB \qquad (2.21)$$

$$V_5 = \oint \frac{\partial w}{\partial y}(M_{xy}\, n_x + M_y\, n_y)\, dB$$

where the forces and moments, for isotropic and orthotropic cases (Chia, 1980) are :

$$Q_x = -D\left(\frac{\partial^3 w}{\partial x^3} + \frac{\partial^3 w}{\partial x \partial y^2}\right)$$

$$Q_y = -D\left(\frac{\partial^3 w}{\partial y^3} + \frac{\partial^3 w}{\partial y \partial x^2}\right)$$

$$M_x = -D\left(\frac{\partial^2 w}{\partial x^2} + \nu \frac{\partial^2 w}{\partial y^2}\right) \qquad (2.22)$$

$$M_y = -D\left(\frac{\partial^2 w}{\partial y^2} + \nu \frac{\partial^2 w}{\partial x^2}\right)$$

$$M_{xy} = -D(1-\nu)\frac{\partial^2 w}{\partial x \partial y}$$

and

$$Q_x = -D_x \frac{\partial^3 w}{\partial x^3} - (\nu_y D_x + 2 D_{xy}) \frac{\partial^3 w}{\partial x \partial y^2}$$

$$Q_y = -D_y \frac{\partial^3 w}{\partial y^3} - \{\nu_x D_y + 2(1-\nu_x \nu_y) D_{xy}\} \frac{\partial^3 w}{\partial y \partial x^2}$$

$$M_x = -D_x\left(\frac{\partial^2 w}{\partial x^2} + \nu_y \frac{\partial^2 w}{\partial y^2}\right) \qquad (2.23)$$

$$M_y = -D_y\left(\frac{\partial^2 w}{\partial y^2} + \nu_x \frac{\partial^2 w}{\partial x^2}\right)$$

$$M_{xy} = -2\, D_{xy} \frac{\partial^2 w}{\partial x \partial y}$$

Finally the work done by the surface load q is

$$V_6 = \iint qw \, dx \, dy \tag{2.24}$$

2.1.4 Total Potential Energy

Collecting various expressions for strain energy and the work done by loads and then substituting them in Eq. (2.1), the total potential energy π for an isotropic element becomes

$$\pi = \frac{6D}{t^2} \iint \{ (\frac{\partial u}{\partial x})^2 + 2\nu (\frac{\partial u}{\partial x})(\frac{\partial v}{\partial y}) + (\frac{\partial v}{\partial y})^2 + \frac{1-\nu}{2}(\frac{\partial u}{\partial y} + \frac{\partial v}{\partial x})^2 \} \, dx \, dy$$

$$+ \frac{D}{2} \iint \{ (\frac{\partial^2 w}{\partial x^2})^2 + 2\nu (\frac{\partial^2 w}{\partial x^2})(\frac{\partial^2 w}{\partial y^2}) + (\frac{\partial^2 w}{\partial y^2})^2 + 2(1-\nu)(\frac{\partial^2 w}{\partial x \partial y})^2 \} dx \, dy$$

$$+ \frac{6D}{t^2} \iint \{ (\frac{\partial u}{\partial x} + \nu \frac{\partial v}{\partial y})(\frac{\partial w}{\partial x})^2 + (\frac{\partial v}{\partial y} + \nu \frac{\partial u}{\partial x})(\frac{\partial w}{\partial y})^2$$

$$+ (1-\nu)(\frac{\partial u}{\partial y} + \frac{\partial v}{\partial x})(\frac{\partial w}{\partial x})(\frac{\partial w}{\partial y}) \} dx \, dy$$

$$+ \frac{3D}{t^2} \iint \{ (\frac{\partial w}{\partial x})^2 + (\frac{\partial w}{\partial y})^2 \}^2 \, dx \, dy - q \iint w \, dx \, dy$$

$$- \oint u(N_x n_x + N_{xy} n_y) \, dB$$

$$- \oint v(N_{xy} n_x + N_y n_y) \, dB$$

$$- \oint w(Q_x n_x + Q_y n_y) \, dB$$

$$- \oint \frac{\partial w}{\partial x} (M_x n_x + M_{xy} n_y) \, dB$$

$$- \oint \frac{\partial w}{\partial y} (M_{xy} n_x + M_y n_y) \, dB \tag{2.25}$$

The corresponding expression, for the orthotropic element is

$$\pi = \frac{6}{t^2}\iint \{D_x(\frac{\partial u}{\partial x})^2 + D_y(\frac{\partial v}{\partial y})^2 + 2\, D_x\nu_y(\frac{\partial u}{\partial x})(\frac{\partial v}{\partial y}) + D_{xy}(\frac{\partial u}{\partial y}+\frac{\partial v}{\partial x})^2\}\, dx\, dy$$

$$+ \frac{1}{2}\iint \{D_x(\frac{\partial^2 w}{\partial x^2})^2 + D_y(\frac{\partial^2 w}{\partial y^2})^2 + 2\, D_x\nu_y(\frac{\partial^2 w}{\partial x^2})(\frac{\partial^2 w}{\partial y^2}) + 4\, D_{xy}(\frac{\partial^2 w}{\partial x \partial y})^2\}\, dx\, dy$$

$$+ \frac{6}{t^2}\iint \{D_x(\frac{\partial u}{\partial x} + \nu_y \frac{\partial v}{\partial y})(\frac{\partial w}{\partial x})^2 + D_y(\frac{\partial v}{\partial y} + \nu_x \frac{\partial u}{\partial x})(\frac{\partial w}{\partial y})^2$$

$$+ 2\, D_{xy}(\frac{\partial u}{\partial y} + \frac{\partial v}{\partial x})(\frac{\partial w}{\partial x})(\frac{\partial w}{\partial y})\}\, dx\, dy$$

$$+ \frac{3}{2t^2}\iint \{D_x(\frac{\partial w}{\partial x})^4 + D_y(\frac{\partial w}{\partial y})^4 + 2\, D_x\nu_y\, (\frac{\partial w}{\partial x})^2(\frac{\partial w}{\partial y})^2$$

$$+ 4\, D_{xy}(\frac{\partial w}{\partial x})^2\, (\frac{\partial w}{\partial y})^2\}\, dx\, dy$$

$$- q\iint w\, dx\, dy - \oint u\,(N_x\, n_x + N_{xy}\, n_y)\, dB - \oint v(N_{xy} n_x + N_y n_y)\, dB$$

$$- \oint w(Q_x\, n_x + Q_y\, n_y)\, dB - \oint \frac{\partial w}{\partial x}\,(M_x\, n_x + M_{xy}\, n_y)\, dB$$

$$- \oint \frac{\partial w}{\partial y}\,(M_{xy}\, n_x + M_y\, n_y)\, dB. \qquad (2.26)$$

2.2 DISPLACEMENT FUNCTIONS

To guarantee monotonic convergence, the displacement functions chosen should satisfy the compatability and completeness requirements. (Huebner and Thornton, 1982). For compatibility, it is observed from Eq. (2.25), [Eq. (2.26) for orthotropic case], that the highest order of derivatives of displacements u,v and w, under the double integral sign are one, one

and two, respectively. Thus compatibilities of u,v,w, $\partial w/\partial x$ and $\partial w/\partial y$ are needed. For completeness, the complete Eq.(2.25), [Eq. (2.26) for orthotropic case] is viewed. It is found that the highest order of derivatives of u, v and w are one, one and three respectively. Hence, for inplane displacements u and v, the completeness upto first order derivatives, and for the out of plane displacement w, the completeness upto third order derivatives are required.

The requirements of compatibility (of zeroth order derivatives) and completeness (of first order derivatives) of displacements u and v are identical. Thus the approximating polynomial displacements for these will also be identical. The bilinear displacement rectangular C_o element i.e. the four noded rectangular element with u and v as the degrees of freedom will satisfy the above requirements; thus displacement functions are

$$u^{(e)} = \lfloor N_1 \; N_2 \; N_3 \; N_4 \rfloor \{u\}^{(ne)}$$
$$v^{(e)} = \lfloor N_1 \; N_2 \; N_3 \; N_4 \rfloor \{v\}^{(ne)} \qquad (2.27)$$

where the superscript (e) denotes 'over an element' and (ne) denotes 'at the nodes of the element'. Interpolating functions N_1 to N_4 can be found in Zienkiewicz (1977).

The requirements of compatibility and completeness of displacement w are more stringent than those of u and v. Compatibility upto first order derivatives and completeness upto third order derivatives are needed. The bicubic rectangular C_1 element

i.e. the four noded rectangular element with w, $\frac{\partial w}{\partial x}$, $\frac{\partial w}{\partial y}$ and $\frac{\partial^2 w}{\partial x \partial y}$ degrees of freedom at each node will satisfy the above requirement. Thus displacement function w is

$$w^{(e)} = \lfloor M_1 \; M_2 \; \cdots \; M_{16} \rfloor \; \{w\}^{(ne)} \qquad (2.28)$$

Interpolating functions M_1 to M_{16} can be found in Zienkieicz (1977). Thus the rectangular finite element model, Figure 2.1, will have a total of 24 degrees of freedom with 6 at each node viz. u,v,w, $\frac{\partial w}{\partial x}$, $\frac{\partial w}{\partial y}$, $\frac{\partial^2 w}{\partial x \partial y}$.

2.3 BASIC EQUILIBRIUM EQUATIONS

2.3.1 Equilibrium Equations For the Element

Using Eqs. (2.27) and (2.28) the expression for total potential energy [Eq. (2.25) or Eq. (2.26)] , becomes

$$\pi = U_o + U_1 + U_2 - V \qquad (2.29)$$

where, now, U_o, U_1 and U_2 are, respectively, quadratic, cubic and quartic functions of nodal displacements

$$q^{(ne)} \; (\equiv \lfloor u_1, v_1, w_1, \left.\frac{\partial w}{\partial x}\right|_1 , \left.\frac{\partial w}{\partial y}\right|_1 , \left.\frac{\partial^2 w}{\partial x \partial y}\right|_1 , \cdots \left.\frac{\partial^2 w}{\partial x \partial y}\right|_4 \rfloor)$$

The equations of equilibrium are obtained by minimising the above energy :

$$\{\frac{\partial U_o}{\partial \{q\}^{(ne)}}\} + \{\frac{\partial U_1}{\partial \{q\}^{(ne)}}\} + \{\frac{\partial U_2}{\partial \{q\}^{(ne)}}\} = \{Q\}^{(ne)} + \{B\}^{(ne)} \qquad (2.30)$$

where $\{Q\}^{(ne)}$ is the load matrix of external loads and $\{B\}^{(ne)}$ is the boundary force matrix.

Equations (2.30) can be put in the form

$$([K_o]^{(e)} + \tfrac{1}{2}[N_1]^{(e)} + \tfrac{1}{3}[N_2]^{(e)})\{q\}^{(ne)} = \{Q\}^{(ne)} + \{B\}^{(ne)} \tag{2.31}$$

where

$$[K_o]^{(e)}_{ij} = \frac{\partial^2 U_o}{\partial q_i \partial q_j}$$

$$[N_1]^{(e)}_{ij} = \frac{\partial^2 U_1}{\partial q_i \partial q_j} \tag{2.32}$$

$$[N_2]^{(e)}_{ij} = \frac{\partial^2 U_2}{\partial q_i \partial q_j} .$$

It may be noted that the stiffness matrices $[K_o]^{(e)}$, $[N_1]^{(e)}$ and $[N_2]^{(e)}$ are all symmetric. The matrix $[K_o]^{(e)}$ is the conventional linear stiffness matrix and $[N_1]$ and $[N_2]$ are non-linear stiffness matrices which are respectively linear and quadratic functions of nodal displacements. Many a times Eq. (2.31) is also written as

$$[K_S]^{(e)}\{q\}^{(ne)} = \{Q\}^{(ne)} + \{B\}^{(ne)} \tag{2.33}$$

where

$$[K_S]^{(e)} = [K_o]^{(e)} + \tfrac{1}{2}[N_1]^{(e)} + \tfrac{1}{3}[N_2]^{(e)} \tag{2.34}$$

The matrix $[K_S]$ is called the <u>secant stiffness matrix</u>.

2.3.2 Evaluation of Matrices $[K_o]^{(e)}$, $[N_1]^{(e)}$ and $[N_2]^{(e)}$

<u>Case I : Isotropic Plate</u>

For convenience in evaluating these matrices, the vector $\{q\}^{(ne)}$ is rearranged as

$$\{q\}^{(ne)} = \begin{Bmatrix} \{u\}^{(ne)} \\ \{v\}^{(ne)} \\ \{w\}^{(ne)} \end{Bmatrix} \qquad (2.35)$$

With this in view, the matrix $[K_o]^{(e)}$ can be expressed as

$$[K_o]^{(e)} = \begin{bmatrix} [k_{11}] & [k_{12}] & 0 \\ [k_{12}]^T & [k_{22}] & 0 \\ 0 & 0 & [k_{33}] \end{bmatrix} \qquad (2.36)$$

Various submatrices of Eq. (2.36) are given by

$$k_{11} = \frac{\partial^2 U_{o,m}}{\partial \{u\}^{(ne)} \partial \{u\}^{(ne)}}$$

$$= \frac{6D}{t^2} \int\int \left[2\{N,x\} \llcorner N,x \lrcorner + (1-\nu)\{N,y\} \llcorner N,y \lrcorner \right] dx\, dy \qquad (2.37)$$

$$k_{12} = \frac{\partial^2 U_{o,m}}{\partial \{u\}^{(ne)} \partial \{v\}^{(ne)}}$$

$$= \frac{6D}{t^2} \int\int \left[2\nu \{N,x\} \llcorner N,y \lrcorner + (1-\nu)\{N,y\} \llcorner N,x \lrcorner \right] dx\, dy \qquad (2.38)$$

$$k_{22} = \frac{\partial^2 U_{o,m}}{\partial \{v\}^{(ne)} \partial \{v\}^{(ne)}}$$

$$= \frac{6D}{t^2} \int\int \left[2\{N,y\} \llcorner N,y \lrcorner + (1-\nu)\{N,x\} \llcorner N,x \lrcorner \right] dx\, dy \qquad (2.39)$$

$$k_{33} = \frac{\partial^2 U_{o,b}}{\partial \{w\}^{(ne)} \partial \{w\}^{(ne)}}$$

$$= D \int\int \left[\{M,xx\} \llcorner M,xx \lrcorner + \{M,yy\} \llcorner M,yy \lrcorner + \nu \{M,xx\} \llcorner M,yy \lrcorner \right.$$

$$\left. + \nu \{M,yy\} \llcorner M,xx \lrcorner + 2(1-\nu)\{M,xy\} \llcorner M,xy \lrcorner \right] dx\, dy \qquad (2.40)$$

In the derivation of above expressions, Eqs. (2.7), (2.8), (2.27) and (2.28) have been used.

The non-linear matrix $[N_1]^{(e)}$ is similarly expressed as

$$[N_1]^{(e)} = \begin{bmatrix} 0 & 0 & [n_{1,13}] \\ 0 & 0 & [n_{1,23}] \\ [n_{1,13}]^T & [n_{1,23}]^T & [n_{1,33}] \end{bmatrix} \tag{2.41}$$

where

$$n_{1,13} = \frac{\partial^2 U_1}{\partial \{u\}^{(ne)} \partial \{w\}^{(ne)}}$$

$$= \frac{6D}{t^2} \int\int \left[2\{N,x\} \lfloor M,x \rfloor \{w\}^{(ne)} \lfloor M,x \rfloor \right.$$

$$+ 2\nu \{N,x\} \lfloor M,y \rfloor \{w\}^{(ne)} \lfloor M,y \rfloor$$

$$\left. + 2(1-\nu) \{N,y\} \lfloor M,x \rfloor \{w\}^{(ne)} \lfloor M,y \rfloor \right] dx\, dy \tag{2.42}$$

$$n_{1,23} = \frac{\partial^2 U_1}{\partial \{v\}^{(ne)} \partial \{w\}^{(ne)}}$$

$$= \frac{6D}{t^2} \int\int \left[2\nu \{N,y\} \lfloor M,x \rfloor \{w\}^{(ne)} \lfloor M,x \rfloor \right.$$

$$+ 2\{N,y\} \lfloor M,y \rfloor \{w\}^{(ne)} \lfloor M,y \rfloor$$

$$\left. + 2(1-\nu) \{N,x\} \lfloor M,y \rfloor \{w\}^{(ne)} \lfloor M,x \rfloor \right] dx\, dy \tag{2.43}$$

$$n_{1,33} = \frac{\partial^2 U_1}{\partial \{w\}^{(ne)} \partial \{w\}^{(ne)}}$$

$$= \frac{6D}{t^2} \int\int \Big[2\{M,x\} \lfloor N,x \rfloor \{u\}^{(ne)} \lfloor M,x \rfloor$$

$$+ 2\nu \{M,x\} \lfloor N,y \rfloor \{v\}^{(ne)} \lfloor M,x \rfloor$$

$$+ 2\{M,y\} \lfloor N,y \rfloor \{v\}^{(ne)} \lfloor M,y \rfloor$$

$$+ 2\nu \{M,y\} \lfloor N,x \rfloor \{u\}^{(ne)} \lfloor M,y \rfloor$$

$$+ (1-\nu)\{M,x\} \lfloor N,x \rfloor \{v\}^{(ne)} \lfloor M,y \rfloor$$

$$+ (1-\nu)\{M,y\} \lfloor N,x \rfloor \{v\}^{(ne)} \lfloor M,x \rfloor$$

$$+ (1-\nu)\{M,x\} \lfloor N,y \rfloor \{u\}^{(ne)} \lfloor M,y \rfloor$$

$$+ (1-\nu)\{M,y\} \lfloor N,y \rfloor \{u\}^{(ne)} \lfloor M,x \rfloor \Big] \, dx \, dy \qquad (2.44)$$

In the derivation of above relations, Eqs. (2.9), (2.27) and (2.28) have been used. Finally, the second non-linear matrix $[N_2]^{(e)}$ is expressed as

$$[N_2]^{(e)} = \begin{bmatrix} 0 & 0 & 0 \\ 0 & 0 & 0 \\ 0 & 0 & [n_{2,33}] \end{bmatrix} \qquad (2.45)$$

where

$$n_{2,33} = \frac{\partial^2 U_2}{\partial \{w\}^{(ne)} \, \partial \{w\}^{(ne)}}$$

$$= \frac{18D}{t^2} \int\int \Big[\{M,x\} \lfloor M,x \rfloor \{w\}^{(ne)} \lfloor M,x \rfloor \{w\}^{(ne)} \lfloor M,x \rfloor$$

$$+ \{M,y\} \lfloor M,y \rfloor \{w\}^{(ne)} \lfloor M,y \rfloor \{w\}^{(ne)} \lfloor M,y \rfloor$$

$$+ \{M,x\} \lfloor M,x \rfloor \{w\}^{(ne)} \lfloor M,y \rfloor \{w\}^{(ne)} \lfloor M,y \rfloor$$

$$+ \{M,y\} \lfloor M,x \rfloor \{w\}^{(ne)} \lfloor M,y \rfloor \{w\}^{(ne)} \lfloor M,x \rfloor] \, dx \, dy \qquad (2.46)$$

Equations (2.10) and (2.28) have been used to derive the above matrix equation.

Case II : Orthotropic Plate

Submatrices of $[K_o]^{(e)}$, $[N_1]^{(e)}$ and $[N_2]^{(e)}$ for the orthotropic case are similarly derived using the corresponding expressions of strain energy [Eqs. (2.13) - (2.16)] and are

$$k_{11} = \frac{6}{t^2} \int\int (2D_x \{N,x\} \lfloor N,x \rfloor + 2 D_{xy} \{N,y\} \lfloor N,y \rfloor) \, dx \, dy \qquad (2.47)$$

$$k_{12} = \frac{6}{t^2} \int\int (2D_x \nu_y \{N,x\} \lfloor N,y \rfloor + 2 D_{xy} \{N,y\} \lfloor N,x \rfloor) \, dx \, dy \qquad (2.48)$$

$$k_{22} = \frac{6}{t^2} \int\int (2D_y \{N,y\} \lfloor N,y \rfloor + 2 D_{xy} \{N,x\} \lfloor N,x \rfloor) \, dx \, dy \qquad (2.49)$$

$$k_{33} = \int\int (D_x \{M,xx\} \lfloor M,xx \rfloor + D_y \{M,yy\} \lfloor M,yy \rfloor$$

$$+ D_x \nu_y \{M,xx\} \lfloor M,yy \rfloor + D_y \nu_x \{M,yy\} \lfloor M,xx \rfloor$$

$$+ 4 D_{xy} \{M,xy\} \lfloor M,xy \rfloor) \, dx \, dy \qquad (2.50)$$

$$n_{1,13} = \frac{6}{t^2} \int\int (2 D_x \{N,x\} \lfloor M,x \rfloor \{w\}^{(ne)} \lfloor M,x \rfloor$$

$$+ 2 D_x \nu_y \{N,x\} \lfloor M,y \rfloor \{w\}^{(ne)} \lfloor M,y \rfloor$$

$$+ 4 D_{xy} \{N,y\} \lfloor M,x \rfloor \{w\}^{(ne)} \lfloor M,y \rfloor) \, dx \, dy \qquad (2.51)$$

$$n_{1,23} = \frac{6}{t^2} \int\int (2\, D_y \nu_x \{N,y\} \lfloor M,x \rfloor \{w\}^{(ne)} \lfloor M,x \rfloor$$

$$+ 2\, D_y \{N,y\} \lfloor M,y \rfloor \{w\}^{(ne)} \lfloor M,y \rfloor$$

$$+ 4\, D_{xy} \{N,x\} \lfloor M,y \rfloor \{w\}^{(ne)} \lfloor M,x \rfloor)\, dx\, dy \qquad (2.52)$$

$$n_{1,33} = \frac{6}{t^2} \int\int (2\, D_x \{M,x\} \lfloor N,x \rfloor \{u\}^{(ne)} \lfloor M,x \rfloor$$

$$+ 2\, D_x \nu_y \{M,x\} \lfloor N,y \rfloor \{v\}^{(ne)} \lfloor M,x \rfloor$$

$$+ 2\, D_y \{M,y\} \lfloor N,y \rfloor \{v\}^{(ne)} \lfloor M,y \rfloor$$

$$+ 2\, D_y \nu_x \{M,y\} \lfloor N,x \rfloor \{u\}^{(ne)} \lfloor M,y \rfloor$$

$$+ 2\, D_{xy} \{M,x\} \lfloor N,x \rfloor \{v\}^{(ne)} \lfloor M,y \rfloor$$

$$+ 2\, D_{xy} \{M,y\} \lfloor N,x \rfloor \{v\}^{(ne)} \lfloor M,x \rfloor$$

$$+ 2\, D_{xy} \{M,x\} \lfloor N,y \rfloor \{u\}^{(ne)} \lfloor M,y \rfloor$$

$$+ 2\, D_{xy} \{M,y\} \lfloor N,y \rfloor \{u\}^{(ne)} \lfloor M,x \rfloor)\, dx\, dy \qquad (2.53)$$

$$n_{2,33} = \frac{18}{t^2} \int\int (D_x \{M,x\} \lfloor M,x \rfloor \{w\}^{(ne)} \lfloor M,x \rfloor \{w\}^{(ne)} \lfloor M,x \rfloor$$

$$+ D_y \{M,y\} \lfloor M,y \rfloor \{w\}^{(ne)} \lfloor M,y \rfloor \{w\}^{(ne)} \lfloor M,y \rfloor$$

$$+ 2\, D_x \nu_y \{M,x\} \lfloor M,x \rfloor \{w\}^{(ne)} \lfloor M,y \rfloor \{w\}^{(ne)} \lfloor M,y \rfloor$$

$$+ 4\, D_{xy} \{M,y\} \lfloor M,x \rfloor \{w\}^{(ne)} \lfloor M,y \rfloor \{w\}^{(ne)} \lfloor M,x \rfloor)\, dx\, dy$$

$$(2.54)$$

2.3.3 Equilibrium Equations for the Plate

Elemental equations (2.31) are assembled in the usual way, and on application of boundary conditions, take the following form

$$([K_o] + \frac{1}{2}[N_1] + \frac{1}{3}[N_2])\{q\}^{(n)} = \{Q\}^{(n)} \qquad (2.55)$$

or

$$[K_S]\{q\}^{(n)} = \{Q\}^{(n)} \qquad (2.56)$$

and are simply the simultaneous non-linear, algebraic equations. Here the superscript (n) denotes 'at all the nodes of the plate'; n thus represents total number of nodal displacements.

2.4 SOLUTION PROCEDURES

The equilibrium equation (2.56) is a set of non-linear, simultaneous, algebraic equations for the complete plate, which must be solved. Mainly, three methods, viz. the direct iteration, the Newton-Raphson and the incremental method are used to solve these equations (Zienkiewicz, 1977; Cook, 1981; Yang,1970; Stricklin et. al, 1971).

In the direct iteration method the full load is applied in one step. To start with, some solution is guessed (typically $\{q\}_o = \{0\}$), and Eq. (2.56) is used to find $\{q\}_1$. Then $\{q\}_1$ is used to update $[K_S]$, and $\{q\}_2$ is determined, and so on till the convergence is obtained. The main drawback of this method is that for the problems involving high non-linearity, the solution converges very slowly or may even diverge. Morever, the method is computationally expensive.

In the Newton-Raphson method when an approximate solution $\{q_o\}$ for a given load $\{Q\}$ is reached, Eq. (2.56) is not satisfied,

$$[K_S]\{q_o\} \neq \{Q\} \tag{2.57}$$

Let the improved solution $\{q_o + \Delta q\}$ makes the above inequality to vanish,

$$[K_S(q_o + \Delta q)]\{q_o + \Delta q\} - \{Q\} = \{0\} \tag{2.58}$$

Using first order Taylor expansion, this yields

$$[K_S]\{q_o\} + \frac{\partial}{\partial\{q\}}([K_S]\{q\})\Big|_{q_o}\{\Delta q\} - \{Q\} = \{0\}$$

or $$[K_T]\{\Delta q\} = \{Q\} - [K_S]\{q_o\} \tag{2.59}$$

where $$K_T = \frac{\partial}{\partial\{q\}}([K_S]\{q\})\Big|_{q_o} = ([K_o] + [N_1] + [N_2])\Big|_{q_o} \tag{2.60}$$

and is called tangent stiffness matrix. The right hand side of Eq. (2.59) may be interpreted as the unbalanced force vector, say $\{g\}$. This equation is solved for $\{\Delta q\}$ and then using $\{q_1 = q_o + \Delta q\}$, the iterations are carried until $\{\Delta q\}$ is sufficiently small.

This method will converge slowly if the initial guess is not close to the exact solution. The method can also diverge for highly non-linear problems.

In the incremental method, it is assumed that the exact solution $\{q_o\}$ of Eq. (2.56) is known for load $\{Q_o\}$, and a solution $\{q_o + \Delta q\}$ is now desired for $\{Q_o + \Delta Q\}$; Eqn. (2.56) becomes

$$K_S(q_o + \Delta q) \{q_o + \Delta q\} = \{Q_o + \Delta Q\} \quad (2.61)$$

Using a first order Taylor's expansion, one gets

$$[K_S]\{q\}|_{q_o} + \frac{\partial}{\partial\{q\}}([K_S]\{q\}|_{q_o}\{\Delta q\} = \{Q_o\} + \{\Delta Q\}$$

or $$[K_T]\{\Delta q\} = \{\Delta Q\} \quad (2.62)$$

where $[K_T]$ is the tangent stiffness matrix given by Eq. (2.60). Thus in this method the load is applied in increments and corresponding displacements are found using the latest value of the tangent stiffness matrix. It is claimed (Zienkiewicz, 1977) that by using suitably small increments of load the method guarantees to converge. However, the method has a disadvantage that no real estimate of solution accuracy is known since, in general, the equilibrium is not satisfied at any given load level.

To overcome the above difficulty the incremental method is usually supplemented with the Newton-Raphson method; in this combined form, it is known as the incremental-cum-iterative method and the same has been used in the present work. The load is applied in small steps of size $\{\Delta Q\}$ and the corresponding incremental displacements $\{\Delta q\}$ is obtained from Eq. (2.62). After a few steps, the updated (approximate) displacements $\{q_o\}$ and load $\{Q\}$ are used in the Newton-Raphson equation. Then the Eq. (2.59) is solved for $\{\Delta q\}$, and iterations are carried till $\{\Delta q\}$ is reduced to zero or to a prescribed tolerance. In this way, almost an exact solution is obtained. The process is repeated till the full load is reached.

Stress Calculations

Membrane strains and stresses (at the middle surface of the plate) are calculated from Eqs. (2.5) and (2.3). It is well known that the stresses calculated at the nodes are usually in error, (Zienkiewicz, 1977, Cheung and Yeo, 1979). Further, it is also known that for linear C_o elements, stresses are accurately determined at the centroids of the elements. Similarly for C_1 elements, best results are obtained at the Gauss points. For non-linear strain-displacement relations (Eqs. 2.5), the linear parts, therefore, need to be evaluated at centres and the non-linear parts at the Gauss points for obtaining accurate results. However, it is found that if both the terms (first two terms of Eqs. 2.5; the third term being zero at the middle surface) are evaluated at the centre of the element, the stresses are accurate enough. Hence, the strains (and stresses) are found at the centres of the elements and then extrapolated to the nodal points by bilinear extrapolation.

Some Computational Aspects

For the solution procedure adopted, in the present work, the $[K_T]$ and $[K_S]$ matrices are obtained by numerical integration (Gauss quadrature) technique. Number of Gauss points used to evaluate $[K_o]$ is 3 and for $[N_1]$ and $[N_2]$ it is 4. In the analysis, $[K_o]$ is calculated only once, whereas $[N_1]$ and $[N_2]$ are updated for the latest displacements.

A small lateral load is applied to initiate buckling. The order of this load is 0.1% to 1.0% of the critical load.

The lateral load is maintained constant while the inplane load is varied (increased) to study the postbuckling behavior. In the prebuckling range, a load slightly less than the critical is applied in just one step. The convergence for this load is easily obtained in 2-3 iterations. Near the critical load, on either side, the size of incremental load step is kept very small to obtain easy convergence. Once the critical load is passed, the larger step size is used. The convergence is considered achieved when the error

$$\{e\} = \{q\}_{i+1} - \{q\}_i \tag{2.63}$$

satisfies either of the following norms for the absolute error and the relative error, viz.

$$|e_j| \leq .00001 \qquad j = 1,2,\ldots,n \tag{2.64}$$

$$\left|\frac{e_j}{q_j}\right| \leq .001 \qquad j = 1,2,\ldots,n \tag{2.65}$$

where n is the total number of nodal displacements.

To accelerate the convergence in Newton-Raphson iterative method, a technique proposed by Crisfield (1979) is used. In this method the usual correction $\{\Delta q\}_i$, corresponding to the current unbalanced force $\{g\}_i$, obtained in the i^{th} iteration (Eq. 2.59), is modified to $\{\delta\}_i$ and then added to the current displacements $\{q\}_i$ to get the next (updated) displacements $\{q\}_{i+1}$ as,

$$\{q\}_{i+1} = \{q\}_i + \{\delta\}_i \tag{2.66}$$

The accelerated displacement vector $\{\delta\}_i$ is given by

$$\{\delta\}_i = e_i \{\delta\}_{i-1} + f_i \{\Delta q\}_i \qquad (2.67)$$

where $\{\delta\}_{i-1}$ is the previous accelerated displacement vector and e_i and f_i are scalar multipliers (Initially $e_1 = 0$ and $f_1 = 1$), given by

$$f_i = - a_i/b_i$$
$$e_i = f_i (1 - c_i/b_i) - 1 \qquad (2.68)$$

where a_i , b_i and c_i are scalar inner products expressed as

$$a_i = \lfloor \delta \rfloor_{i-1} \{g\}_{i-1}$$
$$b_i = \lfloor \delta \rfloor_{i-1} (\{g\}_i - \{g\}_{i-1}) \qquad (2.69)$$
$$c_i = \lfloor \Delta q \rfloor_i (\{g\}_i - \{g\}_{i-1})$$

in which $\{g\}_{i-1}$ is previous unbalanced force vector.

2.5 TEST PROBLEM

The computer program developed for the present study, is first tested for an isotropic square plate (with side a = 1.0 m, thickness t = 10.0 mm, modulus of elasticity E = 200 GPa and Poisson's ratio ν = 0.316), subjected to uniform lateral pressure p, per unit of area, when the edges of the plate are (a) simply supported and (b) clamped. Further, the edges are held immovable i.e. no inplane movement normal to the edge is allowed. The boundary conditions, thus, are (Eqs. 1.4 and 1.5)

$u = w = M_x = 0$ along the pair of edges parallel to y-axis

$v = w = M_y = 0$ along the pair of edges parallel to x-axis (2.70)

for simply supported edges, and

$u = w = \frac{\partial w}{\partial x} = 0$ along the pair of edges parallel to y-axis

$v = w = \frac{\partial w}{\partial y} = 0$ along the pair of edges parallel to x-axis (2.71)

for clamped edges.

Due to symmetry, only one quadrant of the plate is analysed, which is discretized into 16 rectangular elements of the same size (4-noded elements with 24 degrees of freedom). The consistent load matrix is used in the analysis. Load-deflection values are compared with those of Levy (1942), based on the analytical solution, and with those of Yang and Han (1983) who used FEM employing high-order triangular elements with 54 degrees of freedom. The agreement amongst three results is found to be extremely good, as can be seen in Figure 2.2.

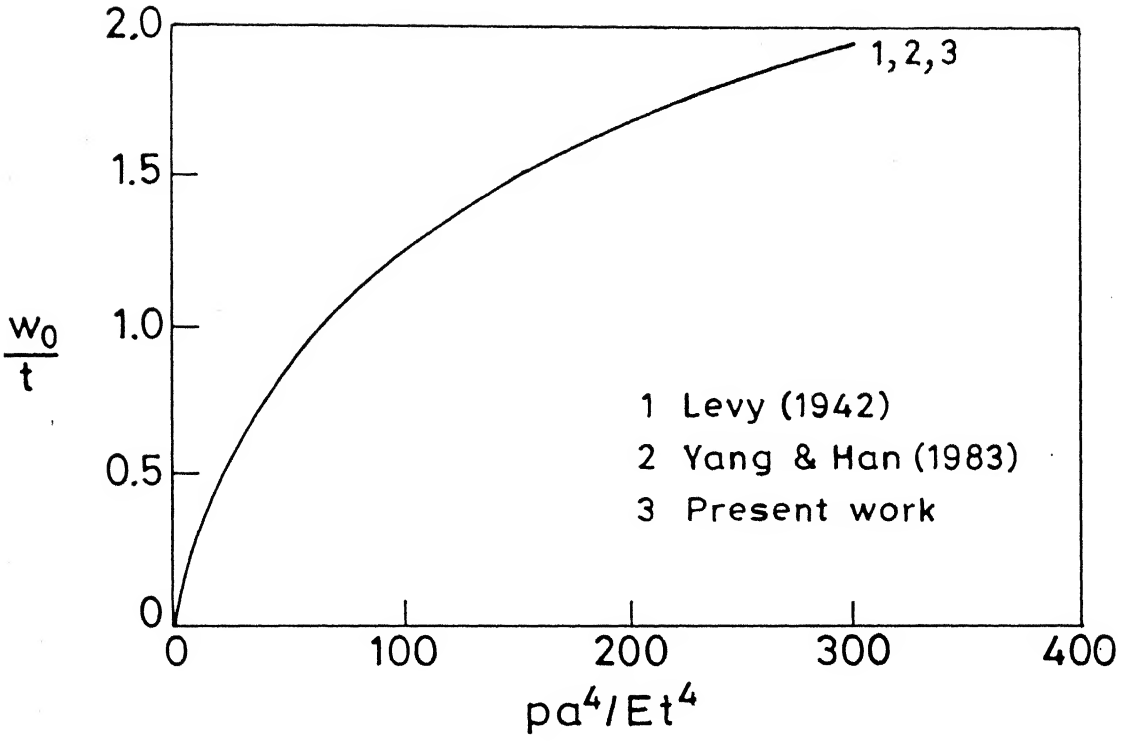

(a) Simply supported edges

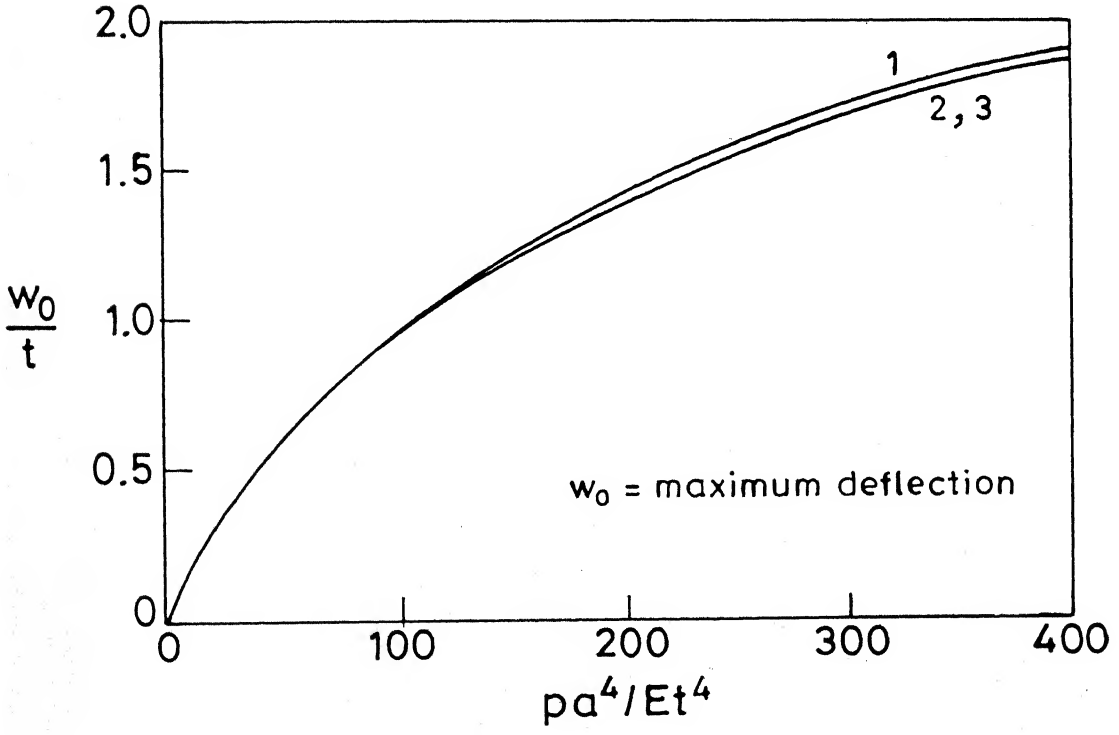

(b) Clamped edges

Fig. 2.2 Load-deflection curves for isotropic square plate under uniform pressure.

CHAPTER 3

ISOTROPIC PLATES SUBJECTED TO LONGITUDINAL COMPRESSION

The postbuckling behavior of isotropic plates subjected to longitudinal compression has been investigated by many researchers, as has been reviewed in Chapter 1. Most of these investigations suffer from a basic drawback that the phenomenon of change in buckling patterns has not been incorporated. In this chapter, this aspect has been properly accounted for in studying the postbuckling behavior of isotropic plates under longitudinal compression.

3.1 ANALYSIS DETAILS

The plate considered is rectangular, of size a x b and with symmetric boundary conditions, and is compressed axially along the edges AD and BC, Figure 3.1(a). Due to symmetry, only one quadrant is analysed; the details of the quadrant APQS are given in Figure 3.1(b). It is discretized into 16 finite elements of 4-noded rectangles of equal size. The plate is assumed to be simply supported on all the four edges. The appropriate boundary conditions as given by Eq. (1.4), are applied.

Along the unloaded edges, the inplane boundary conditions could be one of the following :

(i) Movable Edges or Stress-free Edges (ME)

$$u \neq 0 \ , \ v \neq 0 \qquad (3.1)$$

(ii) Straight Edges (SE)

This imposes a condition of constant v along edges y = 0, b so that

$$\frac{\partial v}{\partial x} = 0 \qquad (3.2)$$

(iii) Fixed Edges (FE)

This implies that the edges are rigidly held apart; i.e. along y = 0, b one must have

$$v = 0 \qquad (3.3)$$

In this chapter, only two inplane boundary conditions, viz. the ME and the FE, have been studied. Only for the sake of comparison, one problem of a square plate is analysed by applying uniform displacement along x = 0, a, while the edges y = 0, b are kept stress-free. For all other problems uniform load has been applied on the loaded edges.

Buckling Modes

Let a particular mode be designated by (m,n), where m and n are the number of half waves along the x- and y-direction, respectively. Since the applied load is acting only in the x-direction, n will always be one at the critical load.

The buckling mode could be symmetric or antisymmetric about the plate centre lines. The symmetric mode requires an additional condition of zero slope ($\partial w/\partial x = 0$) across the centre line. For an antisymmetric mode, the corresponding condition is of zero deflection ($w = 0$). The various modes investigated are (1,1), (2,1) and 3.1) depending upon the problem.

To initiate a particular mode, a very small lateral load s applied at the appropriate position (node). For example, for he mode (1,1), this load is applied at the centre of the plate .e. at the node 25 (Figure 3.1b). For the mode (2,1), the osition of the load would be at the node 15, whereas to initiate (3,1) mode, three such loads are required to be applied — one t node 25 in some direction and the other two at nodes 10 and 15 ı opposite directions to the previous one. It is worth pointing ıat the disturbing force applied to initiate the desired buckling ıttern is too small to cause any effect on the post-buckling ehavior. It may be maintained on the plate throughout the ıalysis (Murray and Wilson, 1969) or removed once the load has ·ossed its critical value or at some other convenient point pending upon the method used (Colville, et. al., 1973).

rves for Buckling Load

For a simply supported, rectangular isotropic plate, under ge compression, the critical load N_{xcr} (per unit width) is given (Chajes, 1974)

$$N_{xcr} = k_c \frac{\pi^2 D}{b^2} \qquad (3.4)$$

en the unloaded edges are movable (ME condition). Here, k_c is e compressive buckling coefficient and is given by

$$k_c = \left(\frac{m}{\lambda} + n^2 \frac{\lambda}{m}\right)^2 , \quad \lambda = \frac{a}{b} , \quad n = 1 \qquad (3.5)$$

e curves obtained from Eq. (3.5) are shown in Figure 3.2. The ınsition from m to m+1 half waves occurs when

$$\lambda = \sqrt{m(m+1)} \qquad (3.6)$$

i.e. the successive values of λ are $\sqrt{2}$, $\sqrt{6}$, $\sqrt{12}$ ... . The point of intersection of curves of higher modes, i.e. of m = 1 and 3 or of m = 2 and 4, is obtained from

$$\lambda = \sqrt{m(m+2)} \qquad (3.7)$$

the successive values being $\sqrt{3}$, $\sqrt{8}$, $\sqrt{15}$ ... .

When the unloaded edges are held rigidly apart (i.e. the FE condition implying v = 0 along y = 0,b), the problem becomes similar to the case of a biaxially loaded plate except that the ratio of the loads N_y and N_x is a constant and is equal to the Poisson's ratio ν . The buckling coefficient k_c, now is given by (Szilard, 1974)

$$k_c = \frac{\left(\frac{m}{\lambda} + \frac{\lambda n^2}{m}\right)^2}{\left(1 + \nu \frac{\lambda^2 n^2}{m^2}\right)} , \quad n = 1 \qquad (3.8)$$

The curves obtained using Eq. (3.8) are shown in Figure 3.3. It can be seen that the transition from m = 1 to m = 2 and from m = 2 to m = 3 occurs at λ = 2.48, 4.12 respectively (Nakamura and Uetani, 1979).

A comparison of curves in Figures 3.2 and 3.3 leads to the following observations :

i) For a particular aspect ratio, k_c is smaller for FE than for ME condition.

ii) The absolute minimum value of k_c is 4.00 for ME (or SE condition) and is 2.80 for FE conditions.

iii) A plate of fixed aspect ratio may have different primary modes under the two membrane boundary conditions. For example, for $\lambda = 2.0$, the plate buckles in (2,1) mode for ME conditions but in (1,1) mode under FE condition.

3.2 ILLUSTRATIVE EXAMPLES

Plates with aspect ratios 1.0, 1.7 and 1.9 are considered for the analysis. These ratios have been so selected as to lie in the range of (i) upto $\sqrt{2}$, (ii) between $\sqrt{2}$ and $\sqrt{3}$ and (iii) between $\sqrt{3}$ and $\sqrt{6}$, of the curves in Figure 3.2 for ME inplane boundary conditions. It is expected that this range of aspect ratio will cover all the salient features of the post-buckling behavior of rectangular plates. With this in view, the following examples are taken up in detail :

I Square plate ($\lambda = 1.0$), 1.0m x 1.0m and 10 mm thick, $E = 200$ GPa, $\nu = .316$.

(i) Unloaded edges free to move (ME condition) – (1,1) and (2,1) modes

(ii) Unloaded edges rigidly held apart (FE condition) (1,1) and (2,1) modes.

II Rectangular plate ($\lambda = 1.7$), 1.7m x 1.0m and 10 mm thick, $E = 200$ GPa , $\nu = .316$

(i) Unloaded edges free to move (ME) – (1,1), (2,1) and (3,1) modes

(ii) Unloaded edges rigidly held apart (FE) – (1,1) and (2,1) modes.

III Rectangular plate ($\lambda = 1.9$), 1.9m x 1.0m and 10mm thick,

$E = 200$ GPa, $\nu = .316$

(i) Unloaded edges free to move (ME)- (1,1), (2,1) and (3,1) modes

(ii) Unloaded edges rigidly held apart (FE) (1,1) and (2,1) modes.

3.3 NUMERICAL RESULTS

3.3.1 Critical Loads

The results are reported in terms of non-dimensional parameters in the form of curves and tables. Wherever possible they are compared with the results available in literature.

In each case of the illustrative example, the critical load is determined as the point of inflexion on the load-deflection curve or as the point of intersection between the pre-buckled line (the portion of the load-shortening curve, before buckling) and the post-buckled line (portion, after buckling). Table 3.1 lists all such values in terms of buckling coefficients, for different cases. For the sake of comparison, the exact values, as obtained from Eqs. (3.5) and (3.8) are also reported. As can be seen, the two set of values match beautifully. The small difference in the two values is due to the error in reading the inflexion point of the load-deflection curve.

3.3.2 Load-Deflection/Shortening Curves

Figure 3.4 shows the graph between the non-dimensional load $\bar{N}_x$ ($= N_x b^2/\pi^2 D$) and the non-dimensional lateral deflection

Table 3.1 Comparison of k_c values for isotropic plates

Aspect ratio $\lambda (= \frac{a}{b})$	Buckling mode (m,n)	Value of k_c			
		ME Condition		FE Condition	
		Exact	Present Work	Exact	Present Work
1.0	(1,1)	4.00	4.05	3.04	3.10
	(2,1)	6.25	6.25	5.79	5.90
1.7	(1,1)	5.24	5.28	2.74	2.77
	(2,1)	4.16	4.16	3.34	3.34
	(3,1)	5.44	5.50	4.94	—
1.9	(1,1)	5.89	6.00	2.75	2.79
	(2,1)	4.03	4.03	3.12	3.18
	(3,1)	4.89	4.93	4.34	—

$\bar{w}_o$ (= w_o/t , w_o being the maximum lateral deflection) for a square plate in (1,1) mode. The curves coincide with those of Yang and Han,(1983) and Rushton,(1970) for ME condition and with Shye and Colville,(1979) and Uemura and Byon,(1977) for FE condition. The symmetric and the anti-symmetric buckled configurations, drawn on the longitudinal centre line of the plate, (Figure 3.5), match closely with Shye and Colville (1979) for FE condition. Similar configurations for ME conditions have been drawn in Figure 3.6. The $\bar{N}_x$ - $\bar{w}_o$ curves for aspect ratios 1.7 and 1.9 are presented in Figure 3.7.

Figures 3.8 to 3.11, depict load-shortening curves, drawn between $\bar{N}_x$ and $\bar{\Delta}$ (= $\Delta E\, b^2 t/a\, \pi^2 D$, Δ being the average shortening of the plate at the load $\bar{N}_x$). It is observed from the graphs that the axial stiffness of the plate has reduced to about 50% - 70% of its initial value in changing from a pre-buckled state to a buckled one. This is the primary buckling. A further reduction in the stiffness takes place in passing from the primary mode to the secondary mode, when the stiffness becomes about 40% - 50% of the original (unbuckled) value, (Carnoy and Hughes,1983). Obviously, the magnitude of reduction is greatly influenced by the in-plane boundary conditions at the unloaded edges (the reduction in stiffness being more under ME condition than under FE condition). The nature of the $\bar{N}_x$ - $\bar{\Delta}$ curves is found to be in very good agreement with that of Rushton (1969) for FE conditions and with Rhodes and Harvey (1977) for ME conditions.

3.3.3 Change in Buckling Pattern *

There is a clear point of intersection between the primary and the secondary modes of a square plate, for both the types of in-plane boundary conditions (Figure 3.8). This point of intersection indicates the possibility of a change in the buckling pattern. A similar observation was reported by Stein (1960) who stated that the actual changeover takes place at the load greater than that given by this common point. Chang and Masur, (1965) have differentiated these points (of intersection) from those at which the energy levels in the two modes become equal. They define the point of intersection as the point at which the secondary mode becomes stable, whereas the point at which the two energies become equal, gives lower bound to the secondary critical load. The point of equal energies is usually at higher load than the point of intersection of the two $\bar{N}_x - \bar{\Delta}$ curves.

For the square plate, the intersection points in Figure 3.8 are at $\bar{N}_x = 9.70$ and 7.90 for ME and FE conditions, respectively. Uemura and Byon,(1977) have reported this value to be 8.80 for SE condition; this appears to be in order because the SE condition is somewhere in between the ME and FE conditions.

A similar change in the buckling pattern is also seen in the rectangular plate ($\lambda = 1.9$) under ME condition (Figure 3.10b), and in the rectangular plates ($\lambda = 1.7, 1.9$) under FE condition (Figure 3.11).

---

* For additional comments see page 134.

3.3.4 Effective Width Curves

Effective width is calculated using the expression (Chandra and Raju, 1973)

$$\bar{b}_e = \frac{N_x\, a}{\Delta t\, E} \qquad (3.9)$$

where $\bar{b}_e$ is the non-dimensionalized effective width (= b_e/b). The curves are drawn between $\bar{N}_x$ and $\bar{b}_e$. Curves of Figure 3.12 are for a square plate, with both in-plane boundary conditions, while in Figure 3.13 the curves are for a rectangular plate ($\lambda = 1.9$). When compared with the values of b_e, for the primary mode, obtained from the formulae used in Narayanan and Chow (1985), the values of present analysis (curve saob) are slightly smaller for the same ME condition. The same trend is found for the FE condition as well, when the results are compared with Timoshenko and Gere (1961). This could be due to the fact that in the present analysis the uniform load has been applied as against a uniform displacement.

3.3.5 Stresses

Stresses are calculated at the selected load levels for all the examples considered. Figures 3.15 and 3.16 show, respectively, the stress distribution at load $\bar{N}_x = 7.0$, for a square plate buckling in (1,1) mode for ME and FE conditions. The stresses match with Coan (1951) and Rushton (1970) for ME conditions. The comparison for FE conditions can not be made due to non-availability of results in literature. The variation of $\bar{\sigma}_{max}$ (= $\sigma_{max}\, b^2 t/\pi^2 D$) with load $\bar{N}_x$ is plotted in Figure 3.17 for

a square plate and in Figure 3.18 for rectangular plates.

3.4 DISCUSSIONS

3.4.1 Symmetric and Anti-symmetric Modes

In the postbuckling analysis by FEM, a particular mode is initiated in the plate by applying a very small force at an appropriate position (node), to have either symmetric (m = 1,3, 5 ...) or anti-symmetric (m = 2,4,6 ...) configuration; n in both cases being equal to 1. For the symmetric mode, the condition of zero slope ($\frac{\partial w}{\partial x} = 0$) and for the anti-symmetric mode, the condition of zero deflection (w = 0) is set across the centre line of the plate.

It is observed that if an anti-symmetric mode is initiated, the final converged mode is the same (initiated) antisymmetric mode. However, if a symmetric mode is initiated, it converges to a symmetric mode but not necessarily to the same initiated mode. Thus, a mode starting from either m = 1 or 3 ends up in a symmetric mode, which could be m = 1 or 3 or its combination, at a particular load level. Similar observations were also made by Shye and Colville (1979).

3.4.2 Changes in Buckling Modes

An important conclusion drawn from the results is that one can predict in advance whether or not the change-over from one mode to another is possible. The procedure to do so is outlined as :

1. On the graph of buckling curves (Figures 3.2 or 3.3) draw a vertical line through the point of given aspect ratio .
2. If it first cuts the curve of lower mode, say 'm' and then the next higher, i.e. 'm+1'; then the changeover from mode m to m+1 will always take place. The corresponding load shortening curves would have a definite point of intersection.
3. If the vertical line first meets the curve of higher mode and then the lower one, the changeover cannot take place. The corresponding load-shortening curves in such a case would never meet.

Further comments have been made with regard to each inplane boundary condition.

Movable Edges (ME)

Referring to Figure 3.2, one would thus expect that

i) for values of λ upto $\sqrt{2}$, lines of m = 1 and m = 2 would intersect and therefore changeover from m = 1 to m = 2 mode is possible.

ii) from $\lambda = \sqrt{2}$ to $\sqrt{3}$ point of intersection of corresponding $\bar{N}_x - \bar{\Delta}$ lines is not possible. Rushton (1970) has shown that for $\lambda = 1.5$, the load-shortening lines of m = 1 and m = 2 do not meet, but has not assigned any reason to it. This fact is further supported by Figure 3.10(a), where for $\lambda = 1.7$, lines of m = 1 and m = 2 diverge. However, the changeover from m = 2 to m = 3 mode is possible.

iii) from $\lambda = \sqrt{3}$ to $\sqrt{6}$, again, the changeover (from m = 2 to m = 3) is possible because, in this range, the vertical line through a given λ meets first the lower mode (m = 2) curve and then the higher mode (m = 3) curve.

iv) An interesting point was observed while executing the program for the plate of $\lambda = 1.7$. The vertical line from this value (Figure 3.2) cuts the various curves, such that

$$P_{cr}|_{m=2} < P_{cr}|_{m=1} < P_{cr}|_{m=3} \qquad (3.10)$$

When a (2,1) mode was initiated, there was no problem in executing the program at any load level. However, when a (3,1) mode was initiated, there was no problem in the beginning but as the load P_x approached (increment by increment) the value $P_{cr}|_{m=1}$, the mode changed from (3,1) to (1,1) and continued to remain in it for higher loads. It happened so because the critical load for the first mode is less than that for the third mode while the zero-slope condition is the same for both the modes which are symmetrical.

This type of trouble is of computational nature and is inherent in the incremental method. In direct iteration method (Shye and Colville, 1979), one may apply directly the required (total) load and get the solution by iterations.

However for the plate with $\lambda = 1.9$, the above problem was not encountered because in this case

$$P_{cr}|_{m=2} < P_{cr}|_{m=3} < P_{cr}|_{m=1} \qquad (3.11)$$

Fixed Edges (FE)

A reference to Figure 3.3 reveals that

i) for λ upto 2.48, the vertical line through it meets different curves in a manner such that

$$P_{cr}|_{m=1} < P_{cr}|_{m=2} < P_{cr}|_{m=3} \qquad (3.12)$$

Hence for plates of aspect ratios upto 2.48, the primary mode is (1,1) and the secondary mode is (2,1), and the changeover from a lower to the higher mode will certainly take place. Here, it is worth mentioning that Shye and Colville (1979), while using the same FE inplane boundary conditions have assumed (2,1) and (3,1) as the primary and the secondary modes, respectively, for a plate with $\lambda = 2$, which is incorrect.

ii) for values of λ lying between 2.48 and ~~4.12~~ 3.20, the following holds

$$P_{cr}|_{m=2} < P_{cr}|_{m=1} < P_{cr}|_{m=3} \qquad (3.13)$$

Obviously (2,1) is the primary mode in this case. But if (3,1) mode is initiated first, it will converge to (1,1) mode, as explained for ME condition. The changeover from higher mode to lower is, of course, ruled out.

iii) for $\lambda > 4.12$ the following inequality is valid

$$P_{cr}|_{m=3} < P_{cr}|_{m=2} < P_{cr}|_{m=1} \qquad (3.14)$$

In this case (3,1) is the primary mode but the other two modes, viz. (2,1) or (1,1), being lower, the changeover is

not possible. (However the changeover from (3,1) to (4,1) can take place).

It is thus obvious that inplane boundary conditions on unloaded edges play a very important role in deciding the possibility of the change in the buckling pattern. For example, as it has been mentioned earlier, for a rectangular plate with aspect ratio 1.7, there will be no change of mode, from (1,1) to (2,1), for ME condition but the mode does change for FE condition [from (1,1) to (2,1)].

It is further observed that the load at which the lines corresponding to modes (1,1) and (2,1) intersect, is greater for ME condition than for FE condition for the same plate : For example, for a square plate, the respective values of the load $\bar{N}_x$ are 9.7 and 7.9 (Figures 3.8a,b). This fact is further supported when the value 7.0, as obtained by Rushton (1970) for $\lambda = 2.0$ plate for ME condition is compared with the value 5.6 obtained by Stein (1960) for SE condition.

A more closer examination of results (of points of intersection obtained for plates of various aspect ratios) available in literature reveals that for SE condition the point of intersection of load-shortening curves, N_{xi} lies approximately at the same distance above the critical load N_{xs}, as the later lies above the load N_{xp}, i.e.

$$N_{xi} - N_{xs} = N_{xs} - N_{xp} \qquad (3.15$$

where N_{xs} and N_{xp} are the critical loads corresponding to secondary and primary modes, respectively.

For ME condition, it was observed that the corresponding point of intersection is about 15-25% higher than that for SE condition, the higher percentage being for the larger aspect ratios. On the contrary, for FE condition the points lie at lower values than those given by the above equation. The reduction is small and varies between 8 - 10% only. For higher values of λ, it is observed that the ratio of N_{xi} and N_{xp}, for FE condition, is lower than that for ME condition. This was also reported by Nakamura and Uetani (1979). For example, for a plate with $\lambda = 1.9$, the ratio under ME condition is 1.81 while it is 1.18 only for FE condition.

3.4.3 Effective Width Curves

Many empirical formulae and curves for effective width have been given and used in the past, they are mainly based on experimental work. In such formulae, it is tacitly assumed that the form of the buckle remains same at all stages of loading. However, the buckling pattern does change, (as has been discussed in the previous section), and it must be taken into account.

The effective width curves of Figures 3.12 and 3.13 are, therefore, applicable even after the mode of the buckled plate has changed to the higher one. The enveloping curve saod, (with firm line), is to be used to estimate the effective width. Until buckling starts, the whole width of the plate is effective (shown by horizontal line sa) and thereafter, the immediate curve ao (corresponding to primary mode) gives $\bar{b}_e$. The effective width thus reduces with increase in load. At the point where the

second curve (corresponding to secondary mode) cuts the initial curve (at o), the change in mode takes place. This should be noted that the changeover point has (and should have) the same value as the point of intersection of the corresponding load-shortening lines discussed earlier.

It is interesting to note that for rectangular plate (λ = 1.9), with FE condition the changeover point is rather quick i.e. the mode changes from (1,1) to (2,1) immediately after the buckling has set in. In this case, therefore, it is the secondary mode which mostly dominates. This shows how important it is to consider the change of mode in estimating the effective width.

The results of $\bar{b}_e$ versus load ratio $\bar{N}$, for the square plate under ME condition, loaded with uniform displacements are shown in Figure 3.14(a). It can be seen that the effective width is greater when loaded edges are uniformly displaced than when they are uniformly loaded. This is true for both modes, i.e. (1,1) and (2,1).

3.4.4 Stresses

Following observations are made from the stress results presented in Figures 3.15 - 3.18.

i) In the case of ME condition, the maximum longitudinal stress σ_{max}, always occurs at the crest of the buckle and on the unloaded edges, whereas for the FE condition it develops at the junction of the loaded and the unloaded edge (Figures 3.15 and 3.16).

ii) Beyond the critical load the transverse membrane stresses (which were initially compressive throughout) progressively reduce near the central portion of the unloaded edge and become tensile (Figure 3.16).

iii) The variation (increase) of $\bar{\sigma}_{max}$ with the applied load $\bar{N}_x$ is linear even in postbuckling range, but at an increased rate. (Figures 3.17 and 3.18).

iv) From Figure 3.17, it is easily interpreted that for the same load ratio N_x/N_{xcr}, the stress σ_{max} is greater in the higher (2,1) mode than the lower (1,1) mode.

v) $\bar{\sigma}_{max}$ is slightly greater for a plate with $\lambda = 1.9$ than with $\lambda = 1.7$, buckling in the same mode, under similar conditions, Figures 3.18(a) and (b).

In the present analysis, a uniform load has been applied whereas most of the available results in literature quote stress values for the case when a uniform displacement is applied on the edges. In the case of uniform load, some small shear stresses do develop on the edges and hence the difference in the two results is not surprising. Actually, the uniform load at higher values ($P >> P_{cr}$), causes the loaded edge to bend inplane, with the central portion having moved longitudinally by a maximum distance; this distance reduces towards the corner. Hence the stress values are likely to involve more error on this section (i.e. the loaded edge), than at other transverse sections.

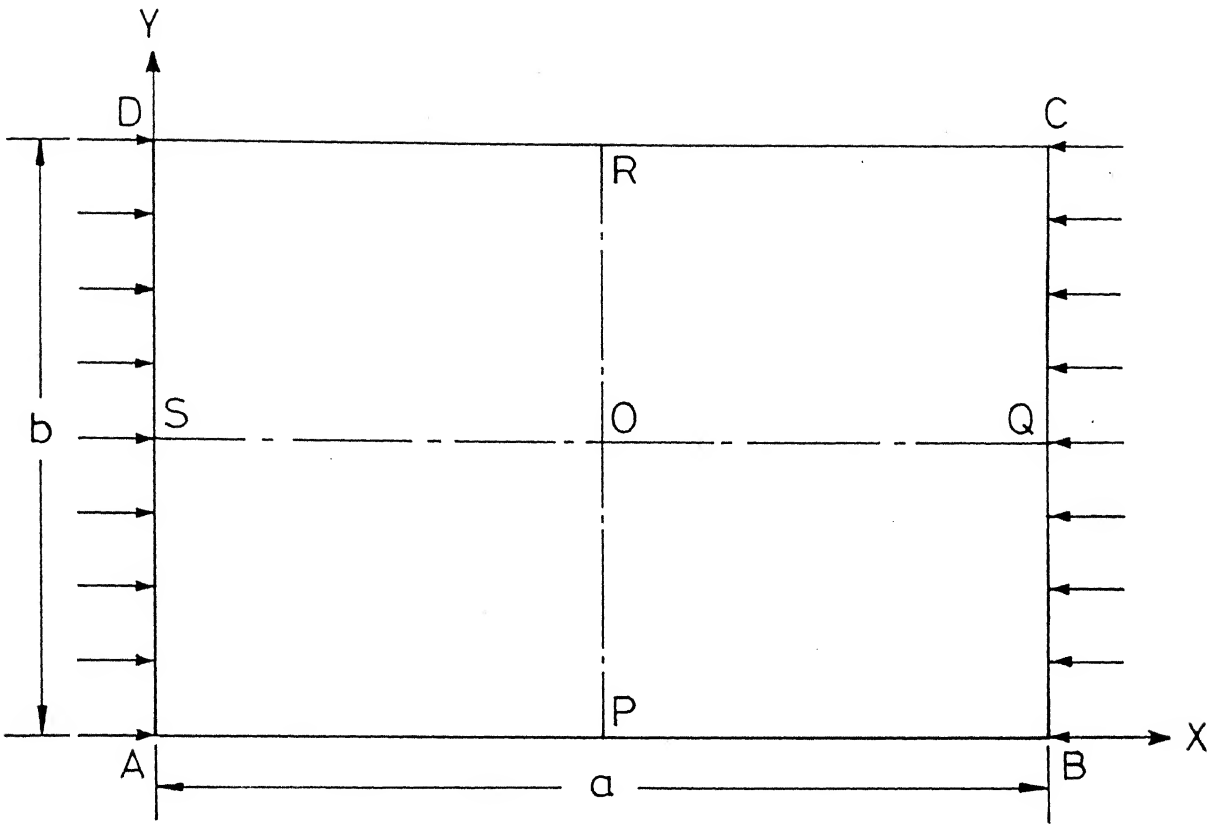

Fig. 3.1(a) Loaded plate with axes of symmetry.

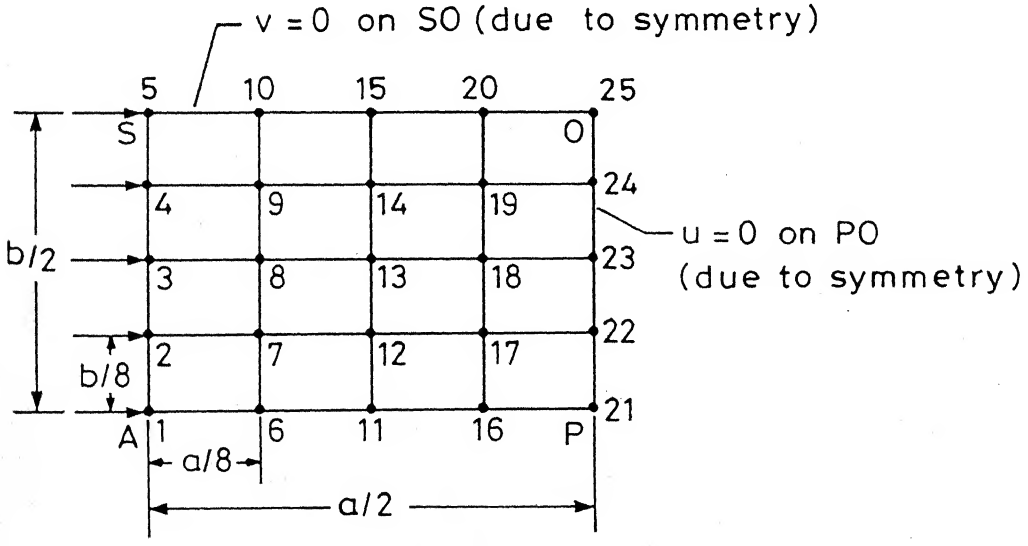

Fig. 3.1(b) Discretization details of a quadrant.

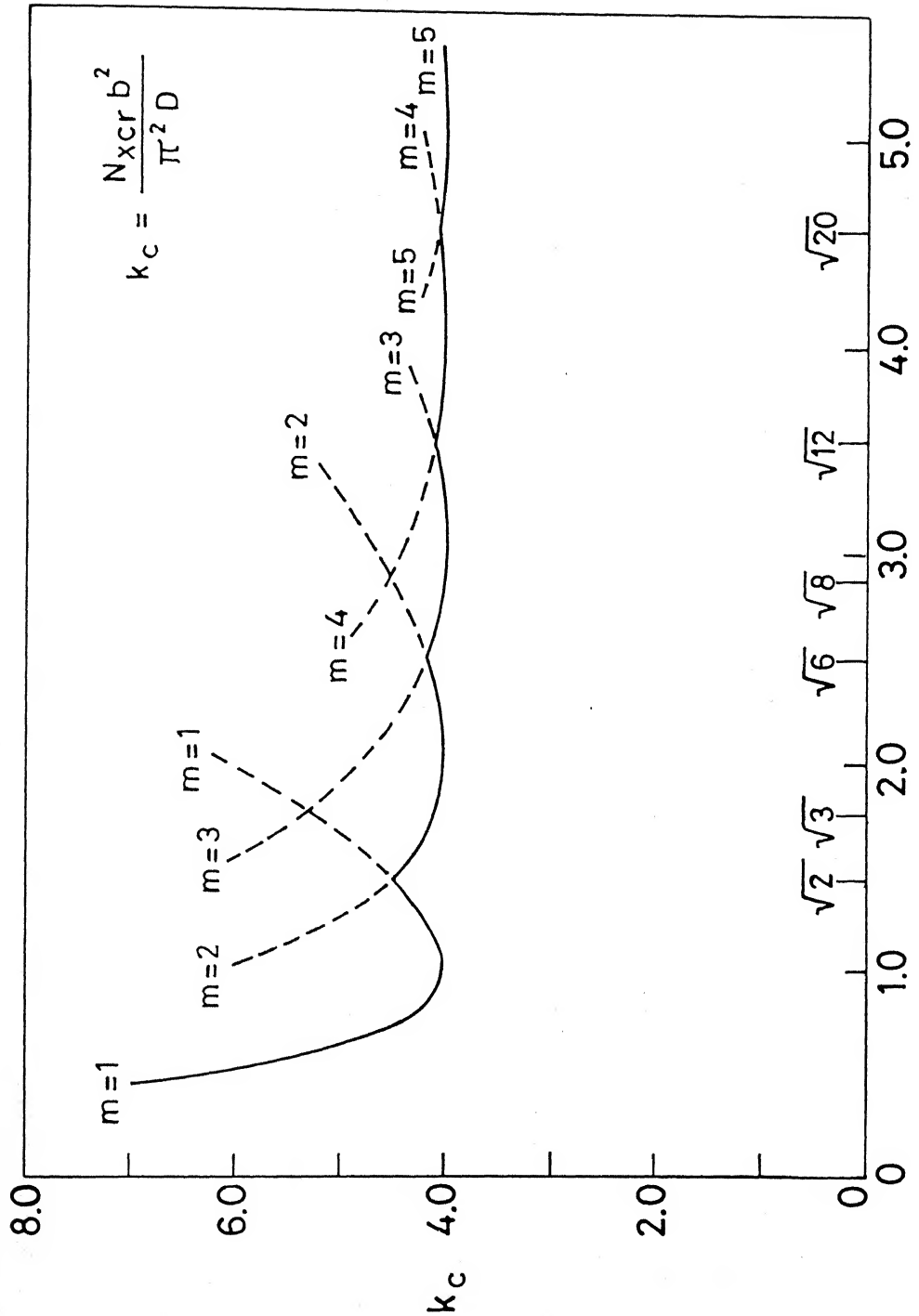

Fig. 3.2 Compressive buckling coefficients for isotropic plates (ME condition)

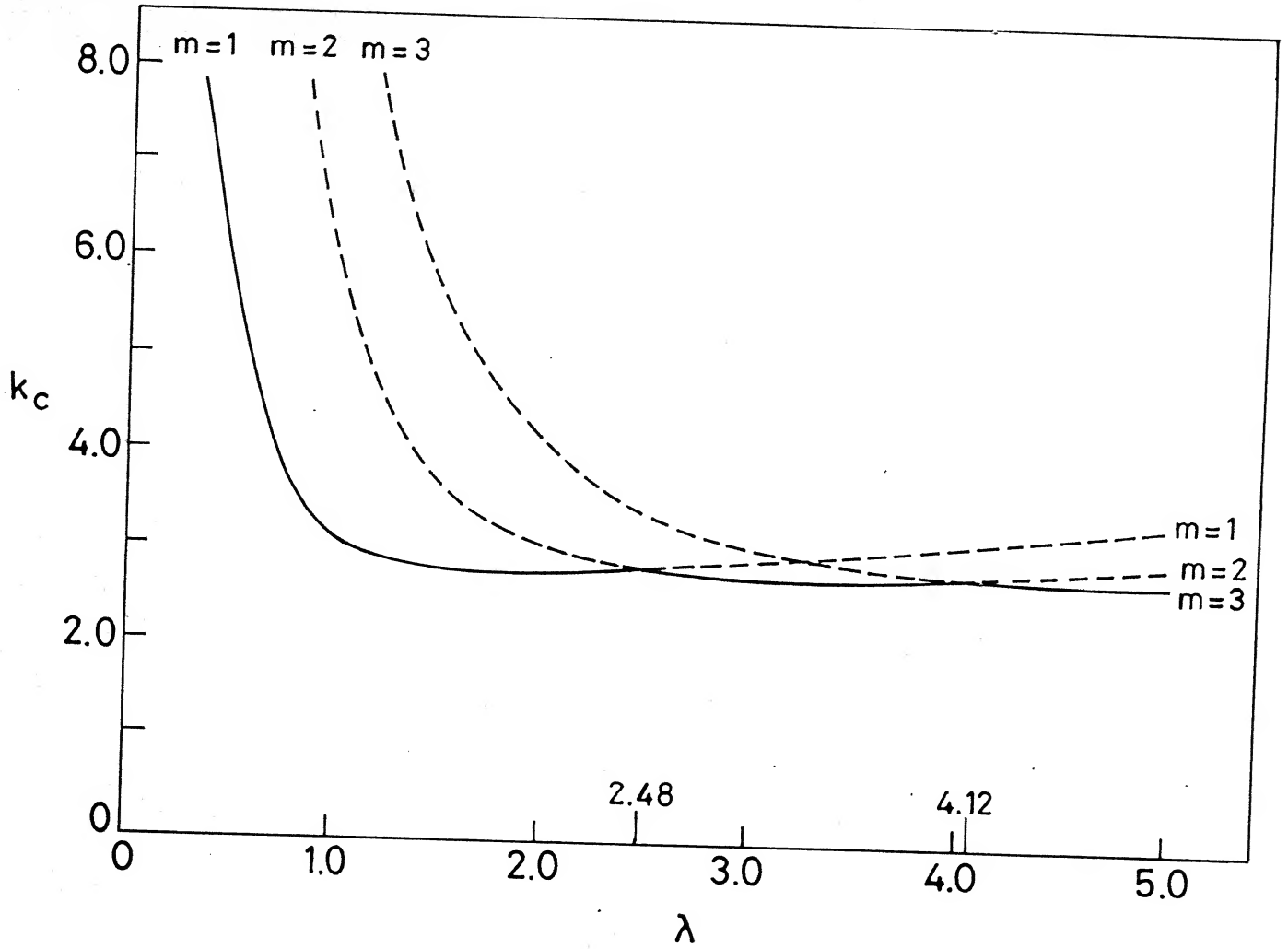

Fig. 3.3 Compressive buckling coefficients for isotropic plates (FE condition).

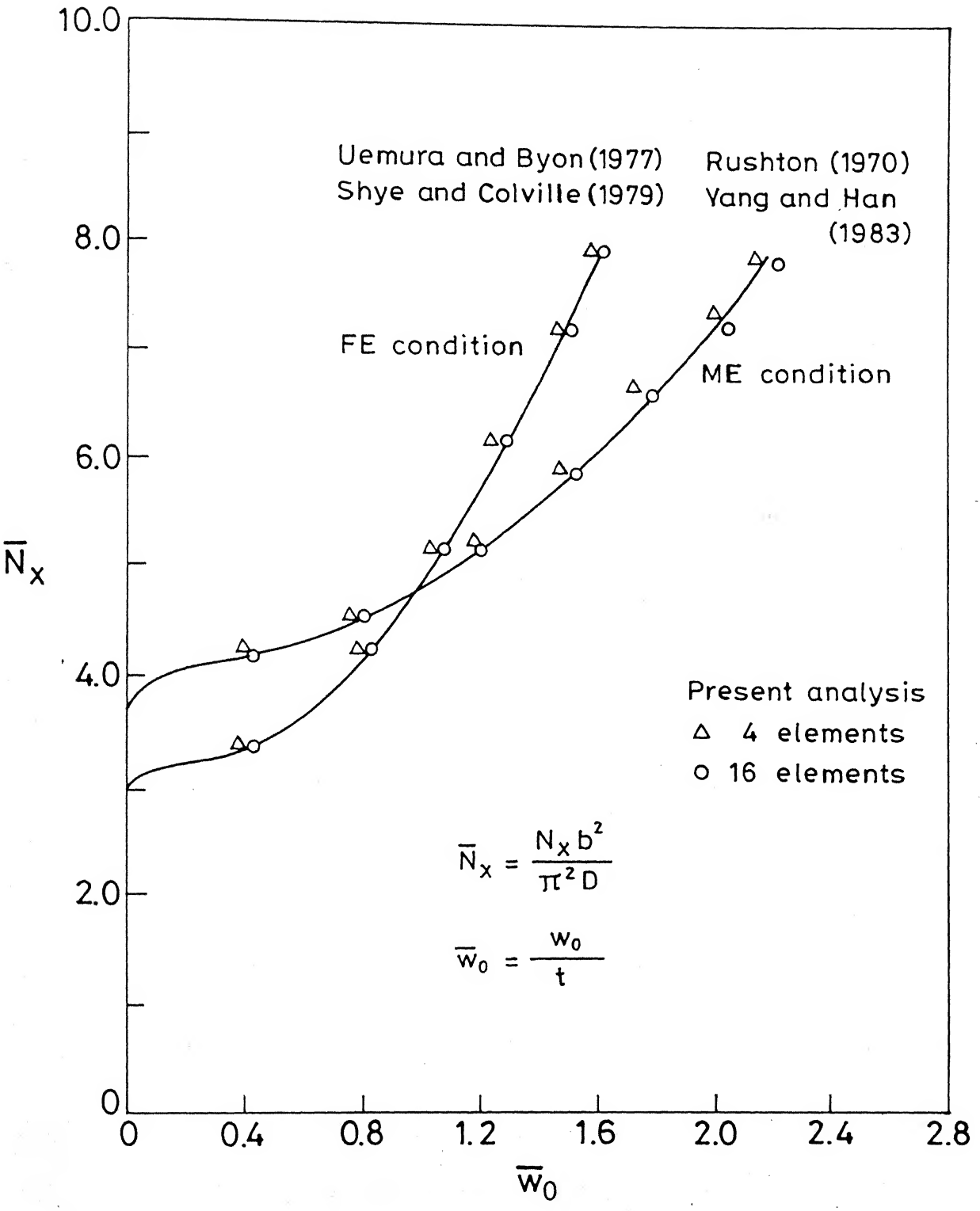

Fig. 3.4 Load-deflection curves for an isotropic square plate, mode (1, 1).

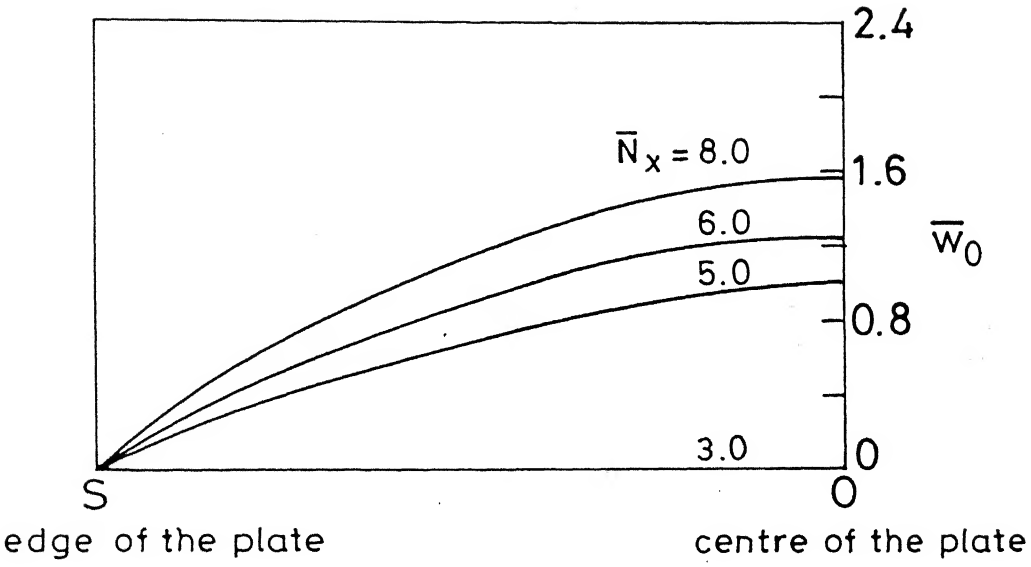

(a) Symmetric configuration, mode (1, 1)

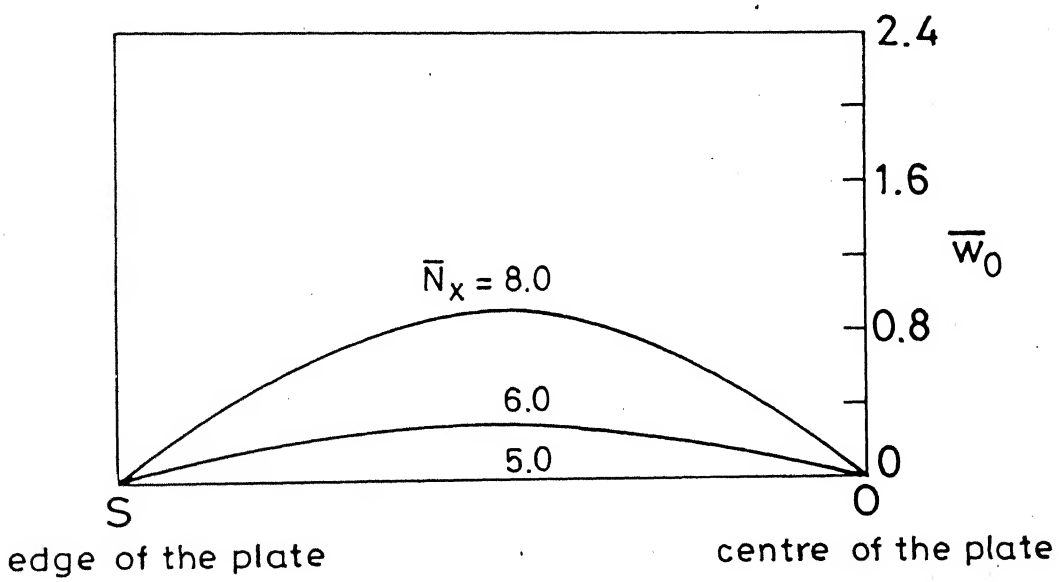

(b) Anti-symmetric configuration, mode (2, 1)

Fig. 3.5 Deflection profiles for an isotropic squre plate, FE condition.

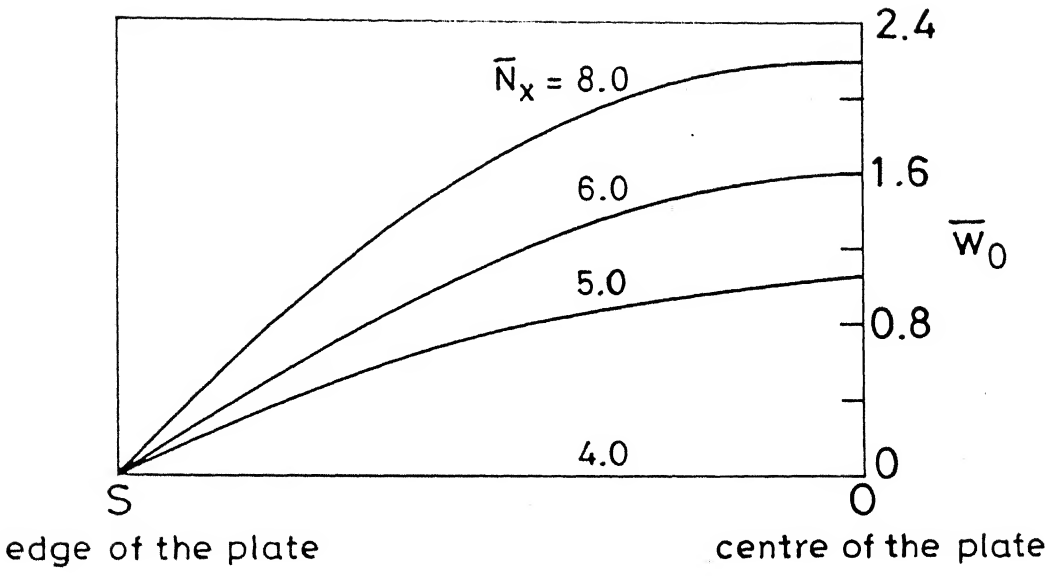

(a) Symmetric configuration, mode (1, 1)

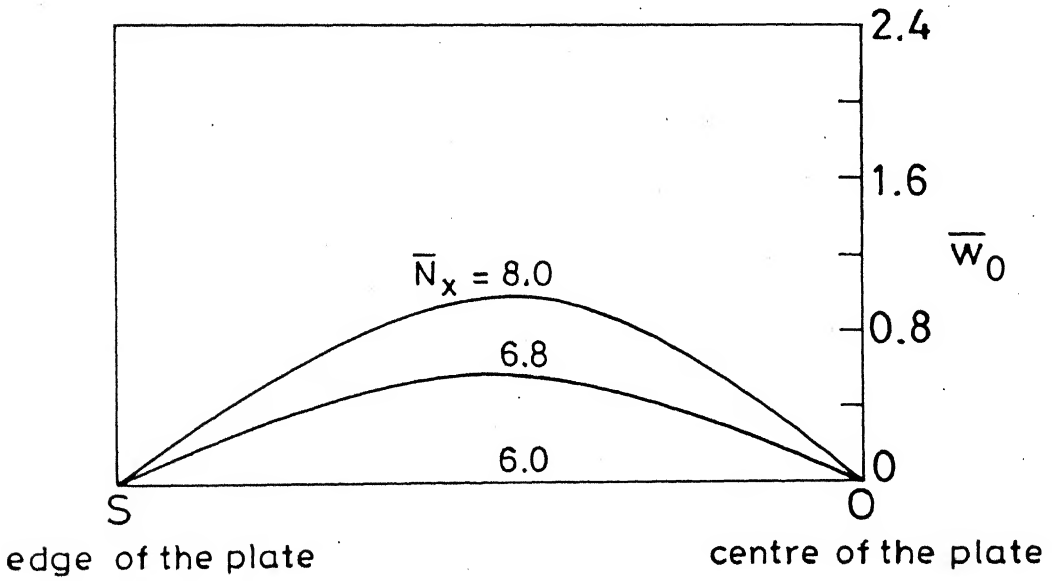

(b) Anti-symmetric configuration, mode (2,1)

Fig. 3.6 Deflection profiles for an isotropic square plate, ME condition.

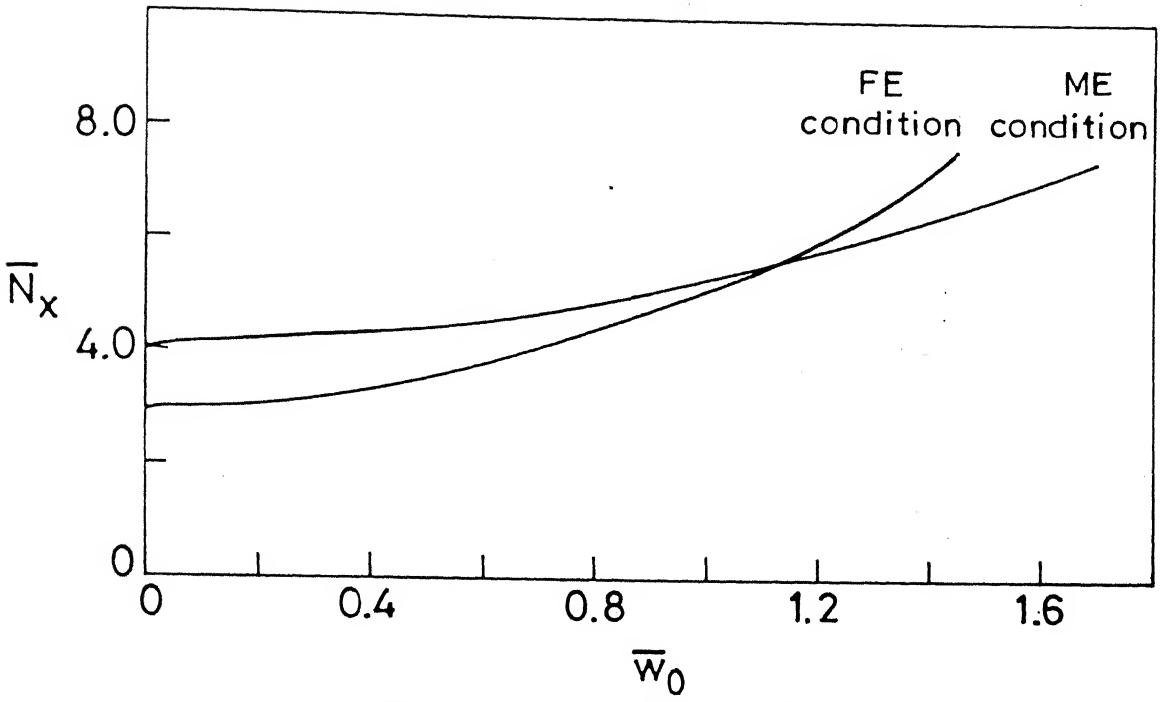

(a) $\lambda = 1.7$, mode (2, 1)

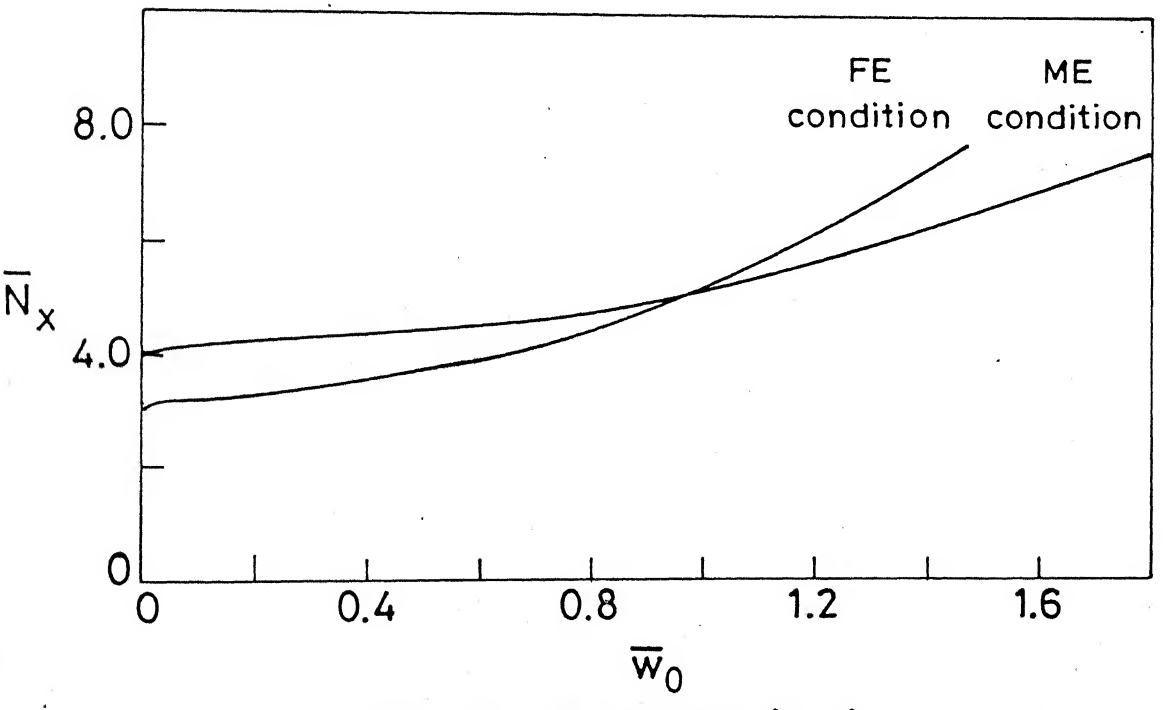

(b) $\lambda = 1.9$, mode (2,1)

Fig. 3.7 Load-deflection curves for isotropic plates.

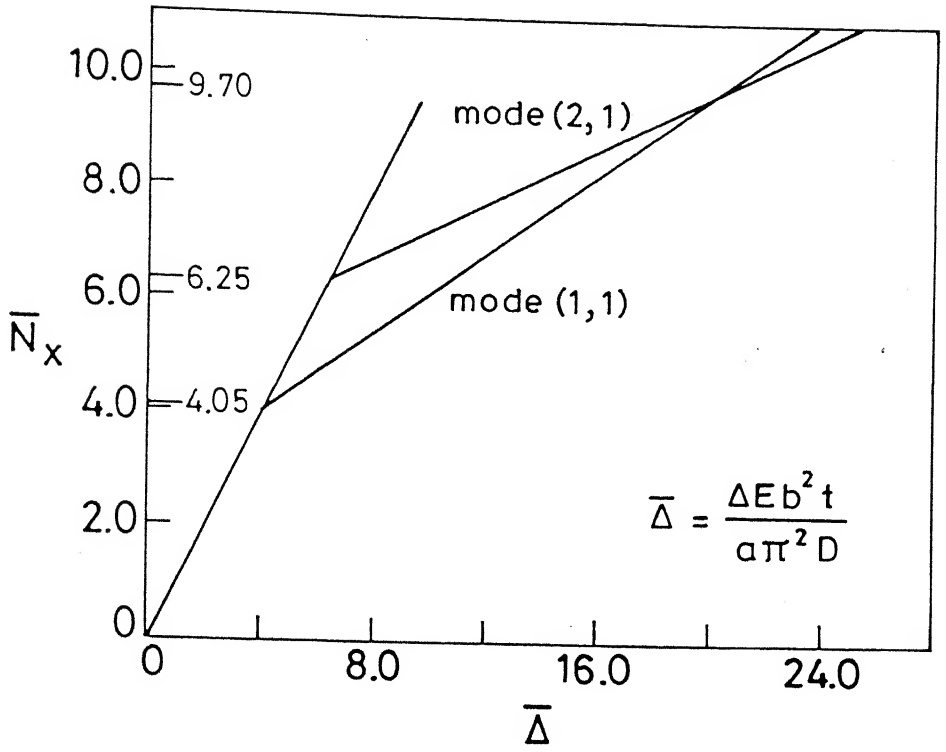

(a) ME condition

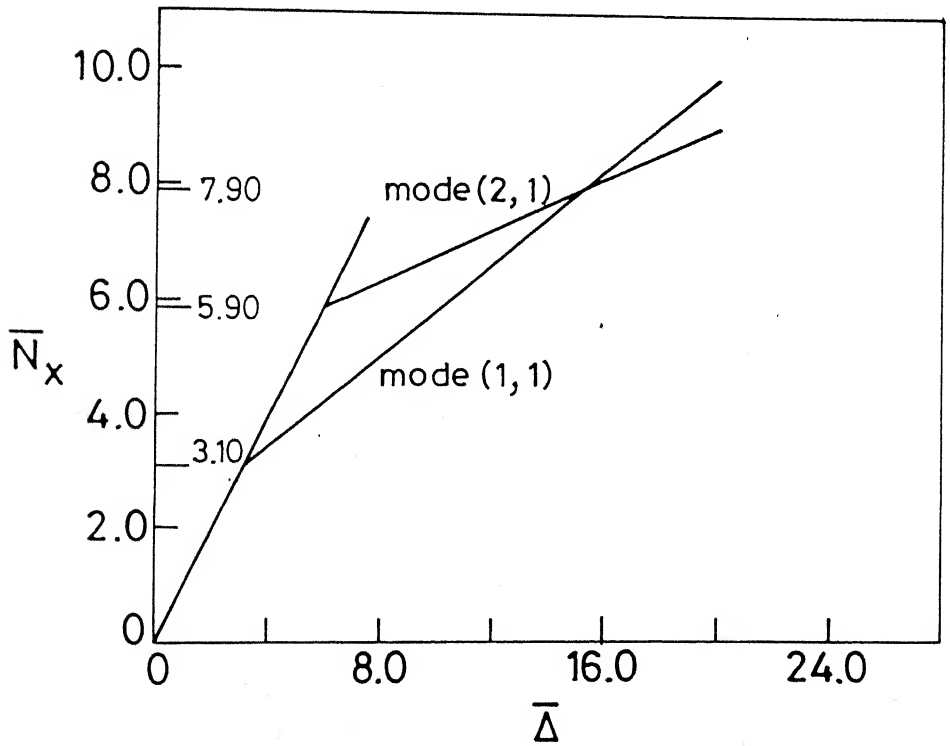

(b) FE condition

Fig. 3.8 Load-shortening curves for an isotropic square plate.

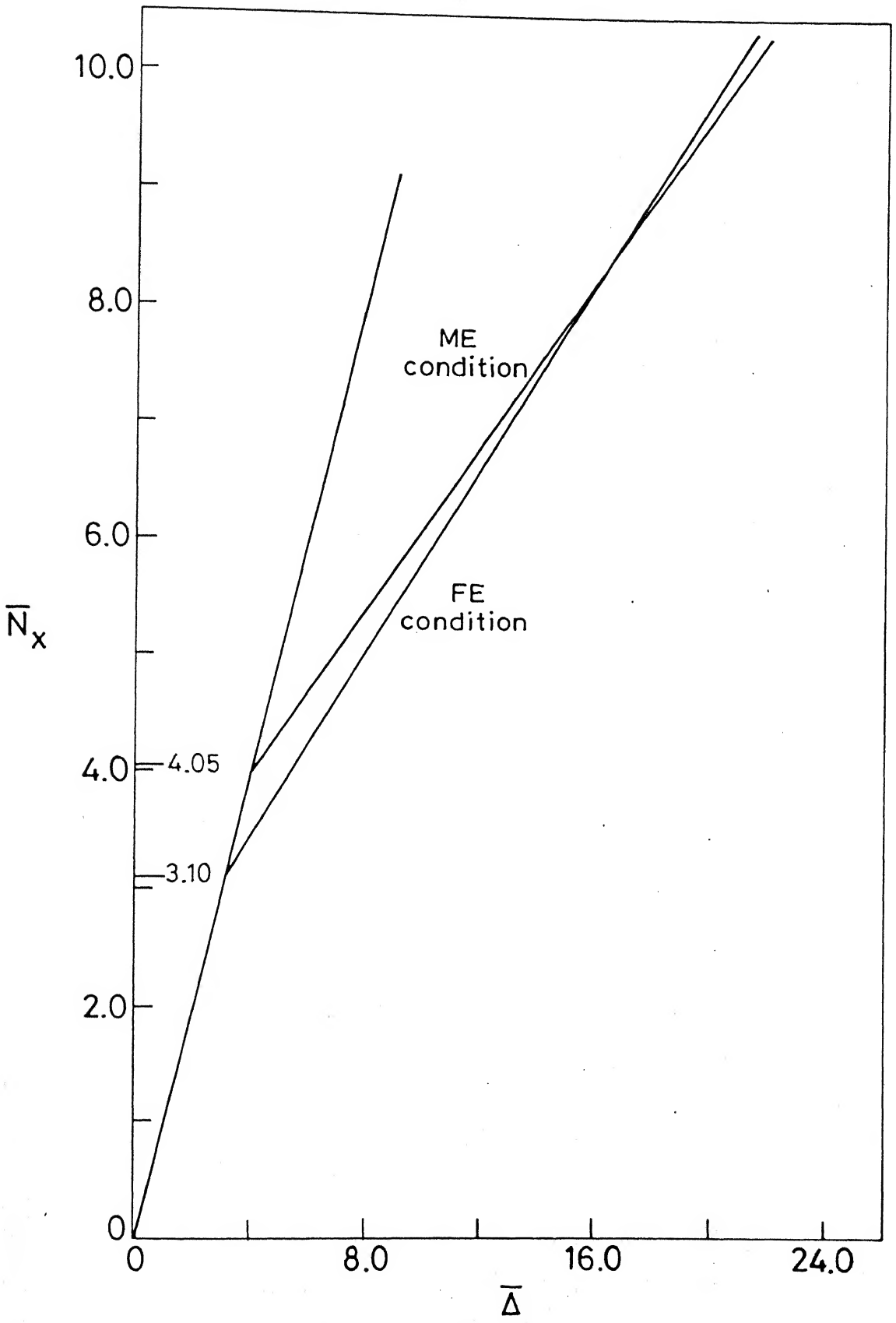

Fig. 3.9 Load-shortening curves for an isotropic square plate, mode (1, 1).

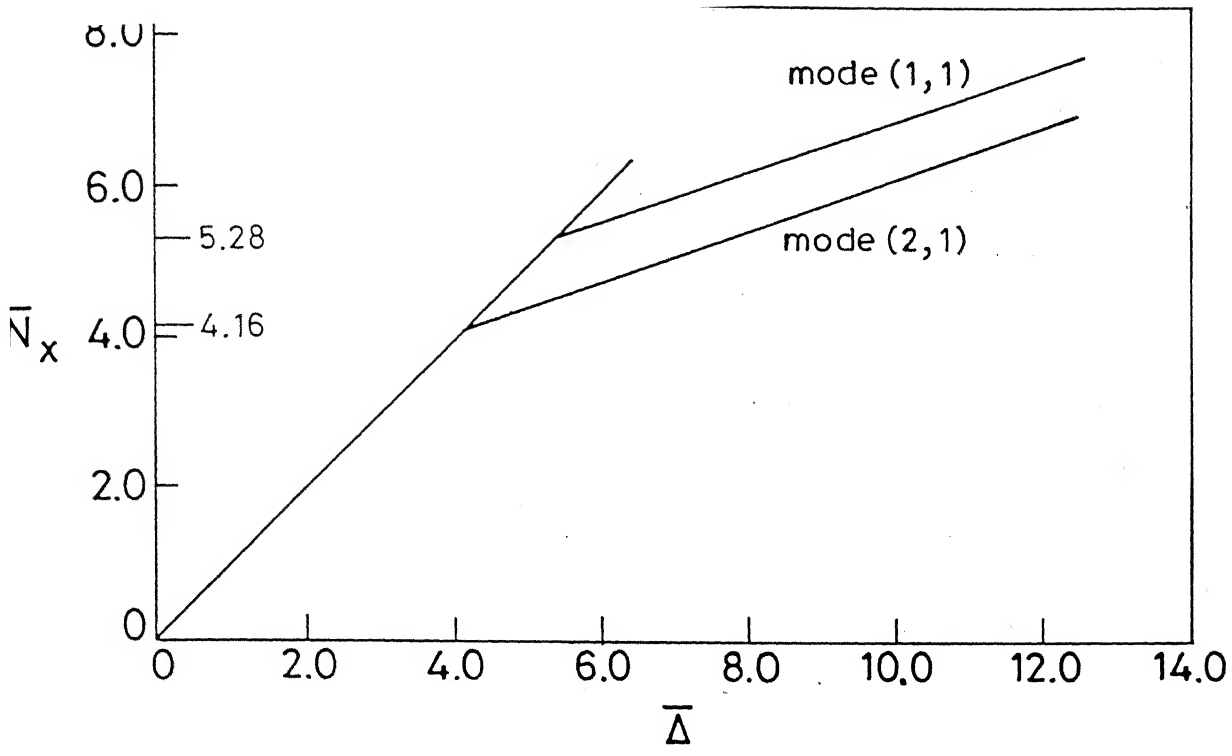

(a) $\lambda = 1.7$, ME condition

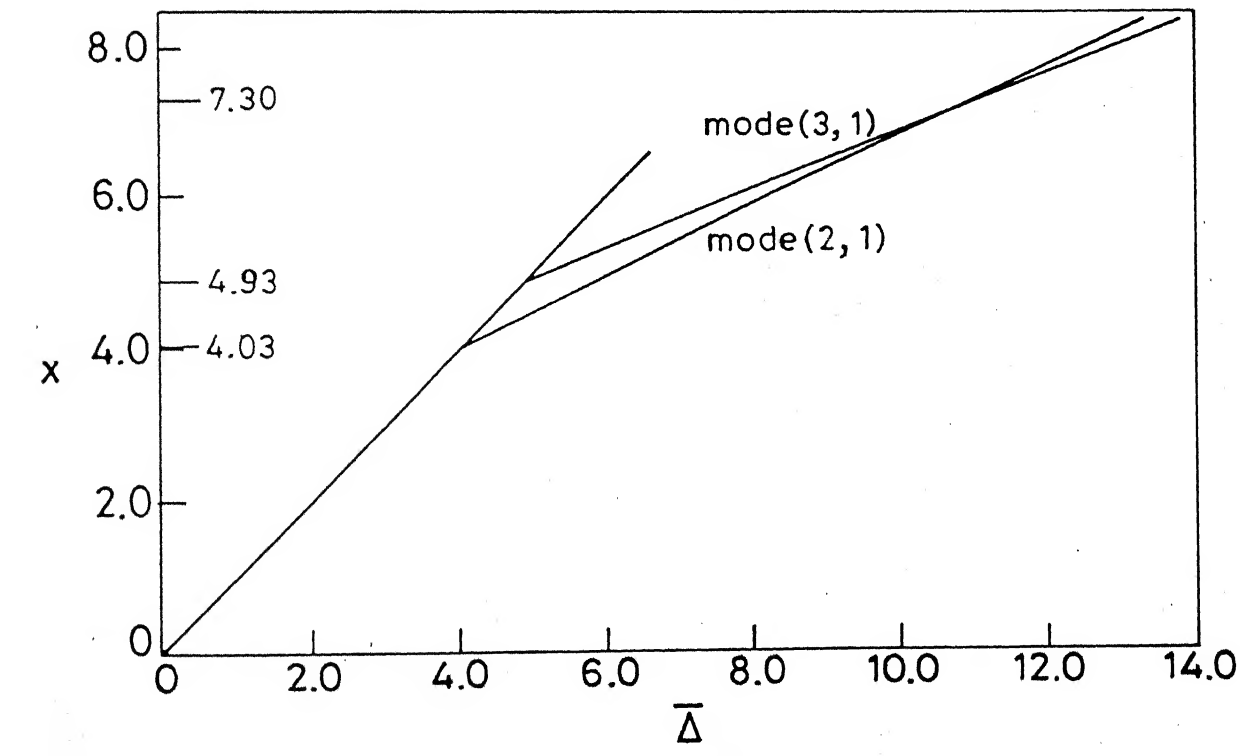

(b) $\lambda = 1.9$, ME condition

Fig. 3.10 Load-shortening curves for isotropic plates.

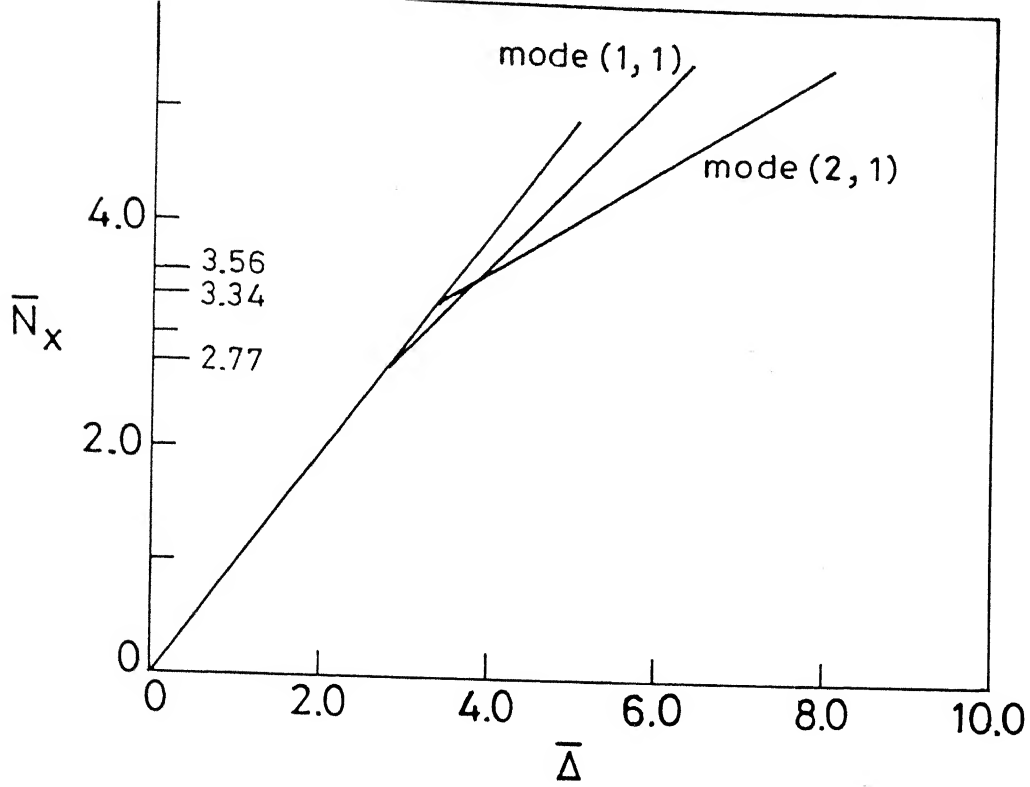

(a) $\lambda = 1.7$, FE condition

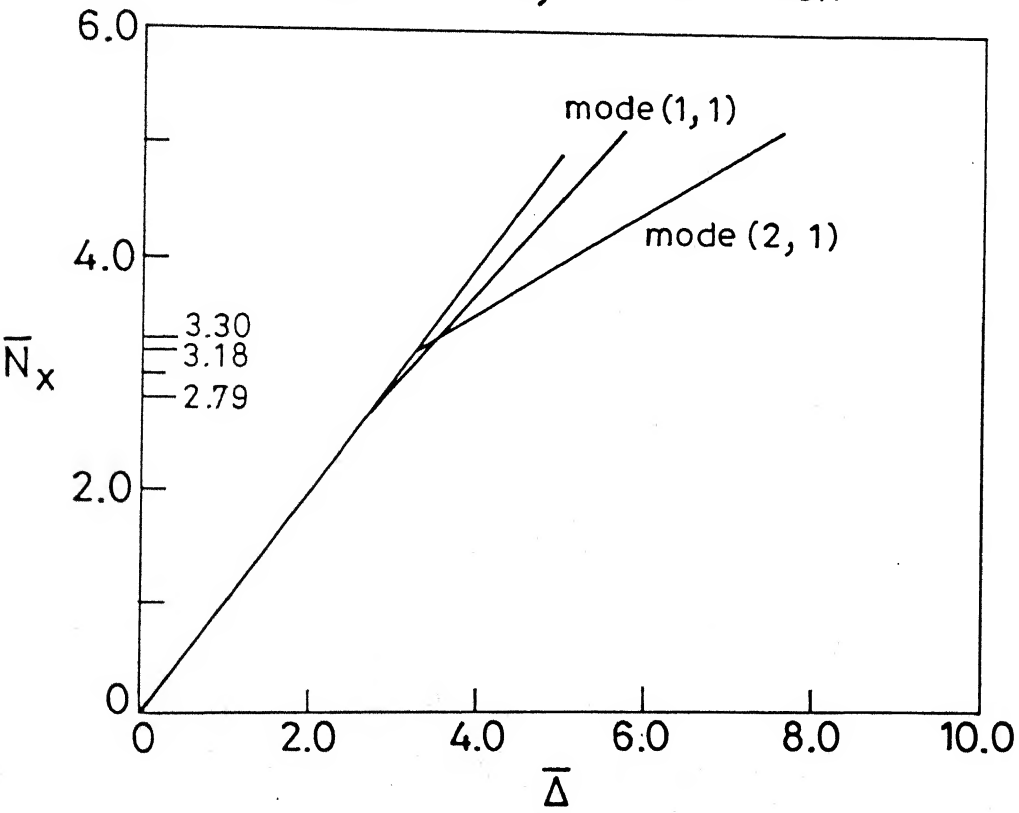

(b) $\lambda = 1.9$, FE condition

Fig. 3.11 Load-shortening curves for isotropic plates.

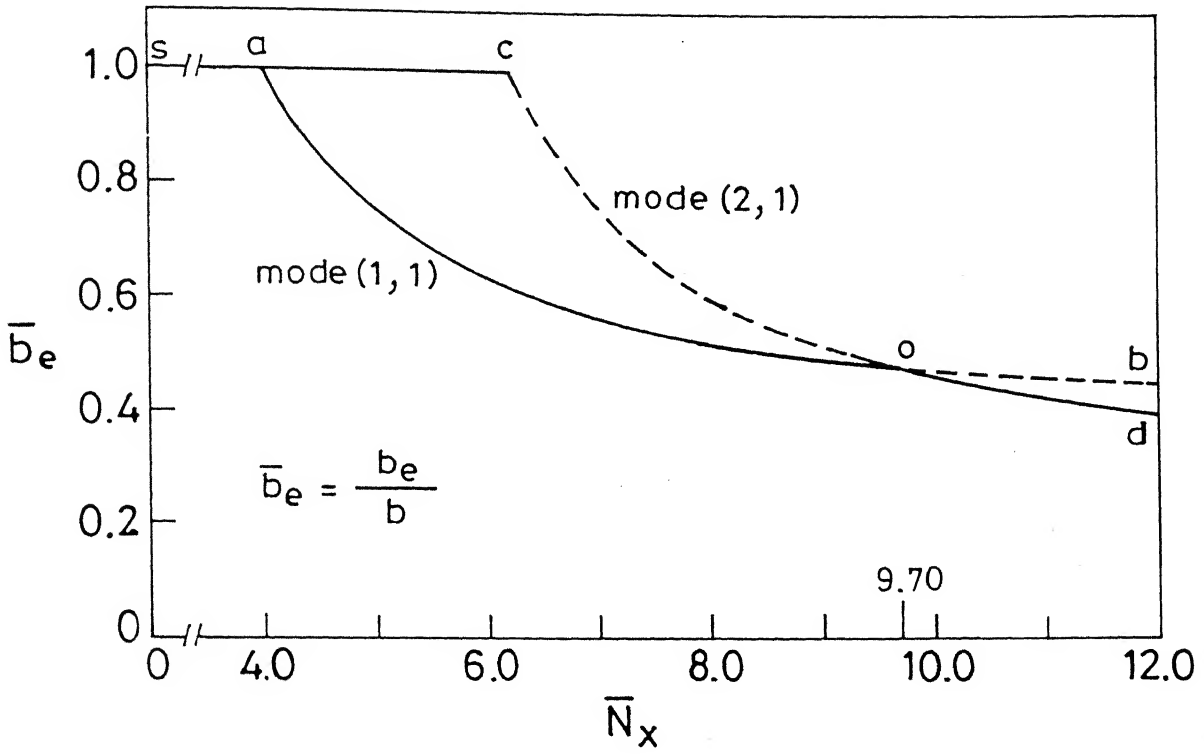

(a) ME condition

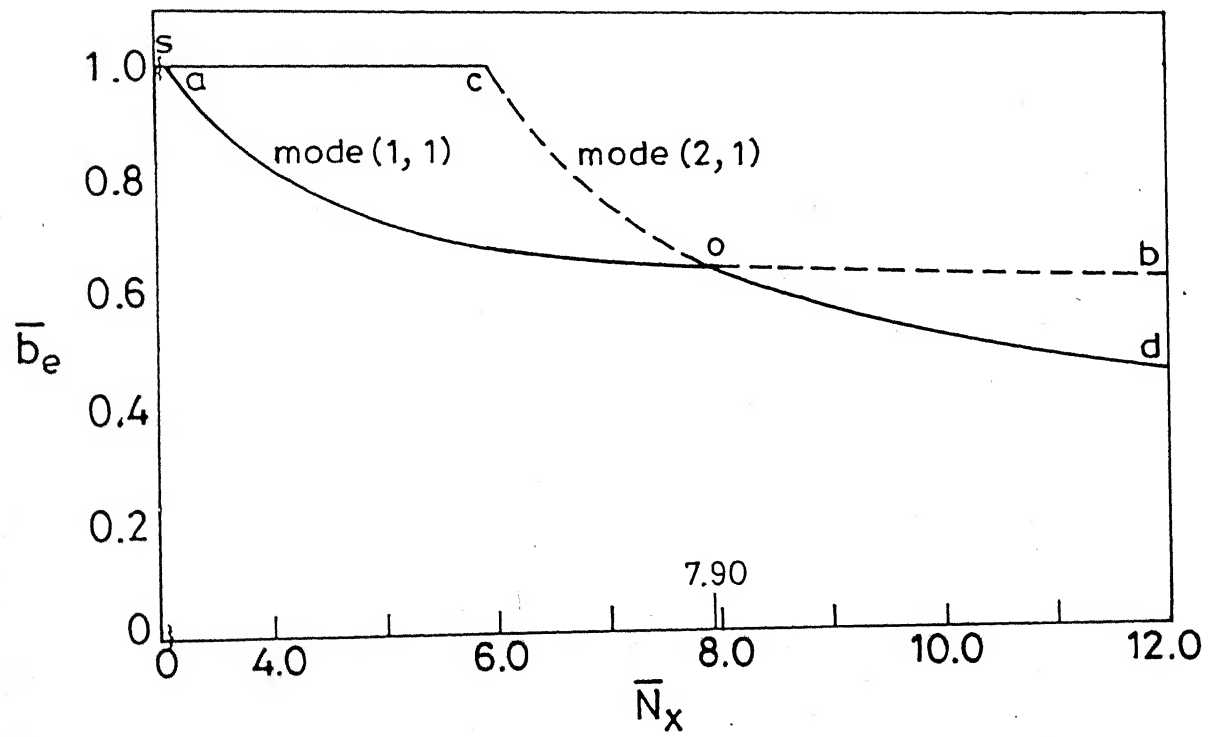

(b) FE condition

Fig. 3.12 Effective width curves for isotropic square plates.

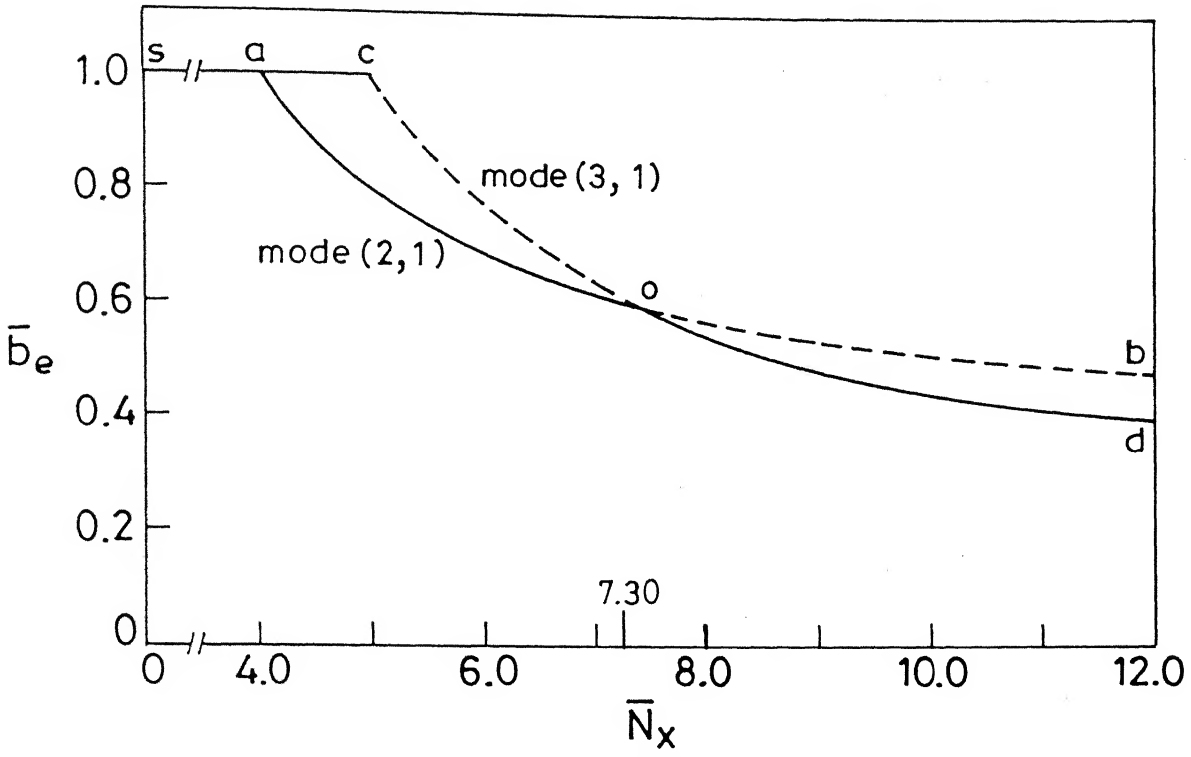

(a) $\lambda = 1.9$, ME condition

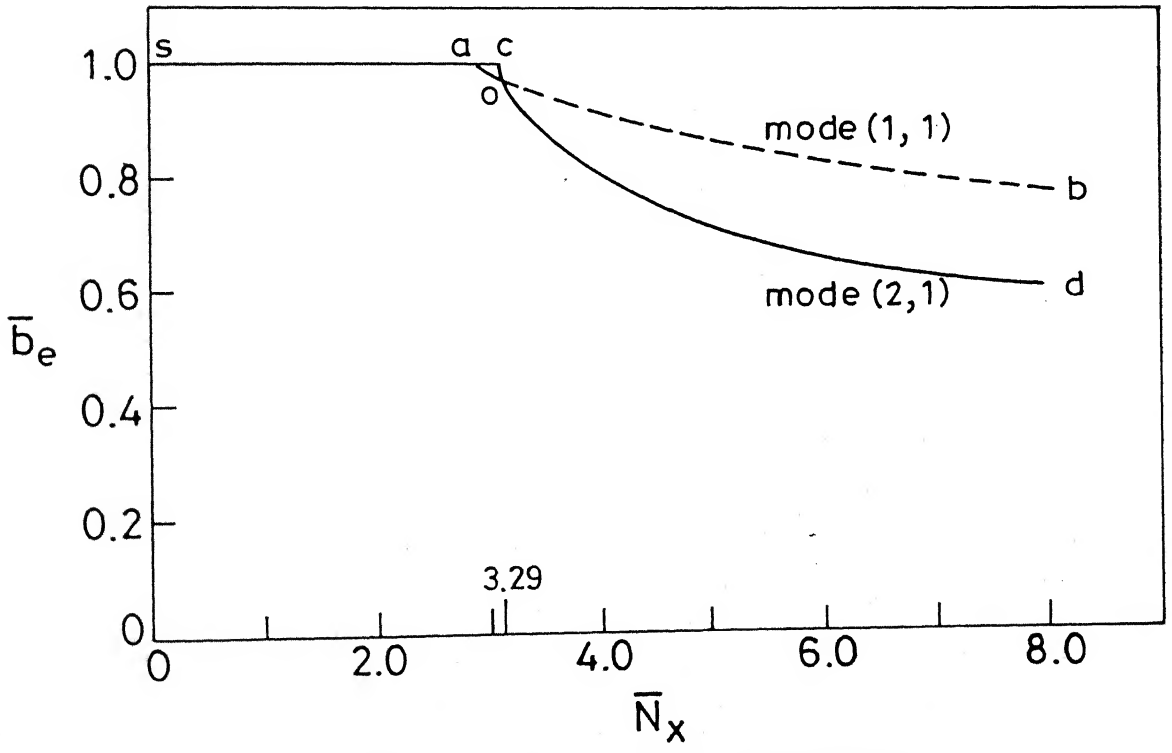

(b) $\lambda = 1.9$, FE condition

Fig. 3.13 Effective width curves for an isotropic plate.

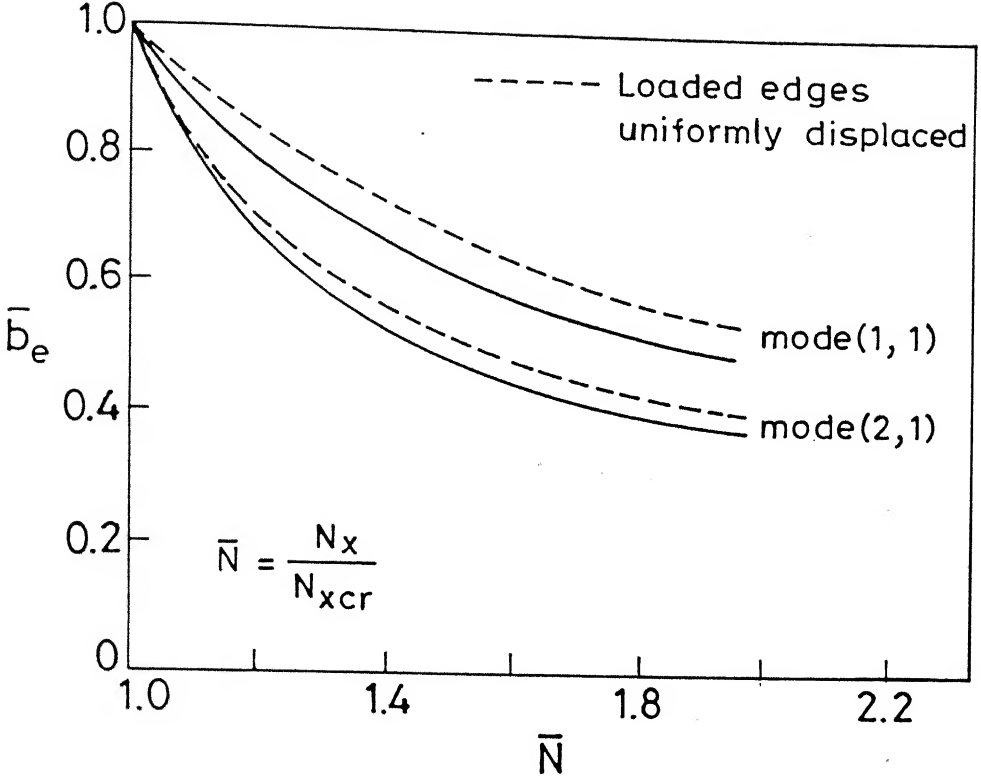

(a) ME condition

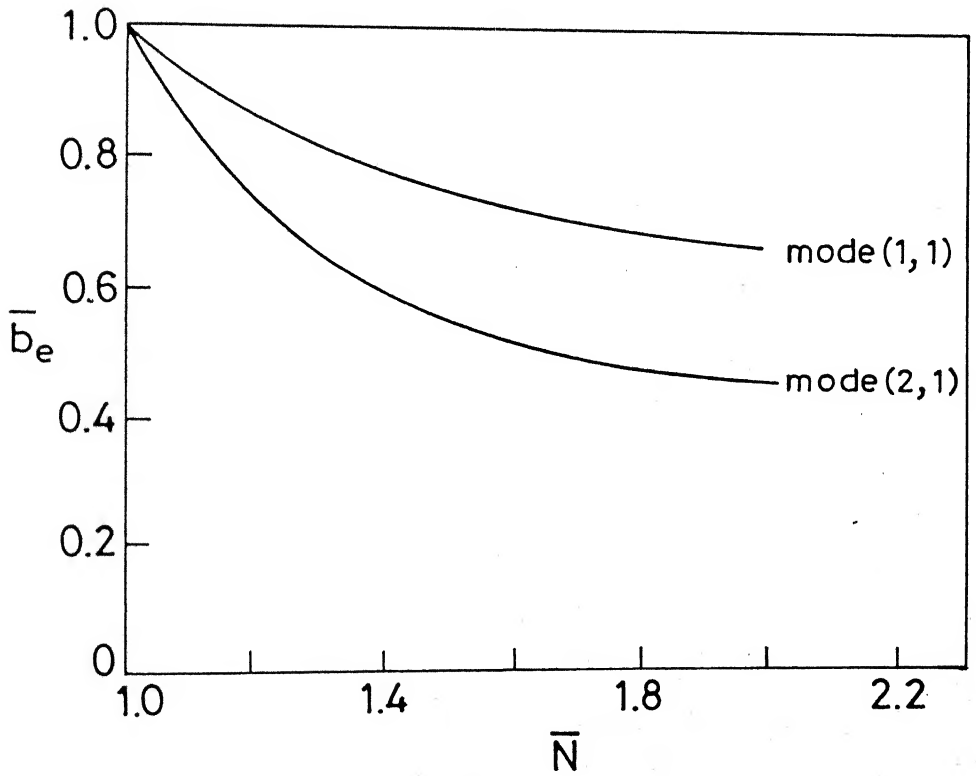

(b) FE condition

Fig.3.14 Effective width curves for an isotropic square plate.

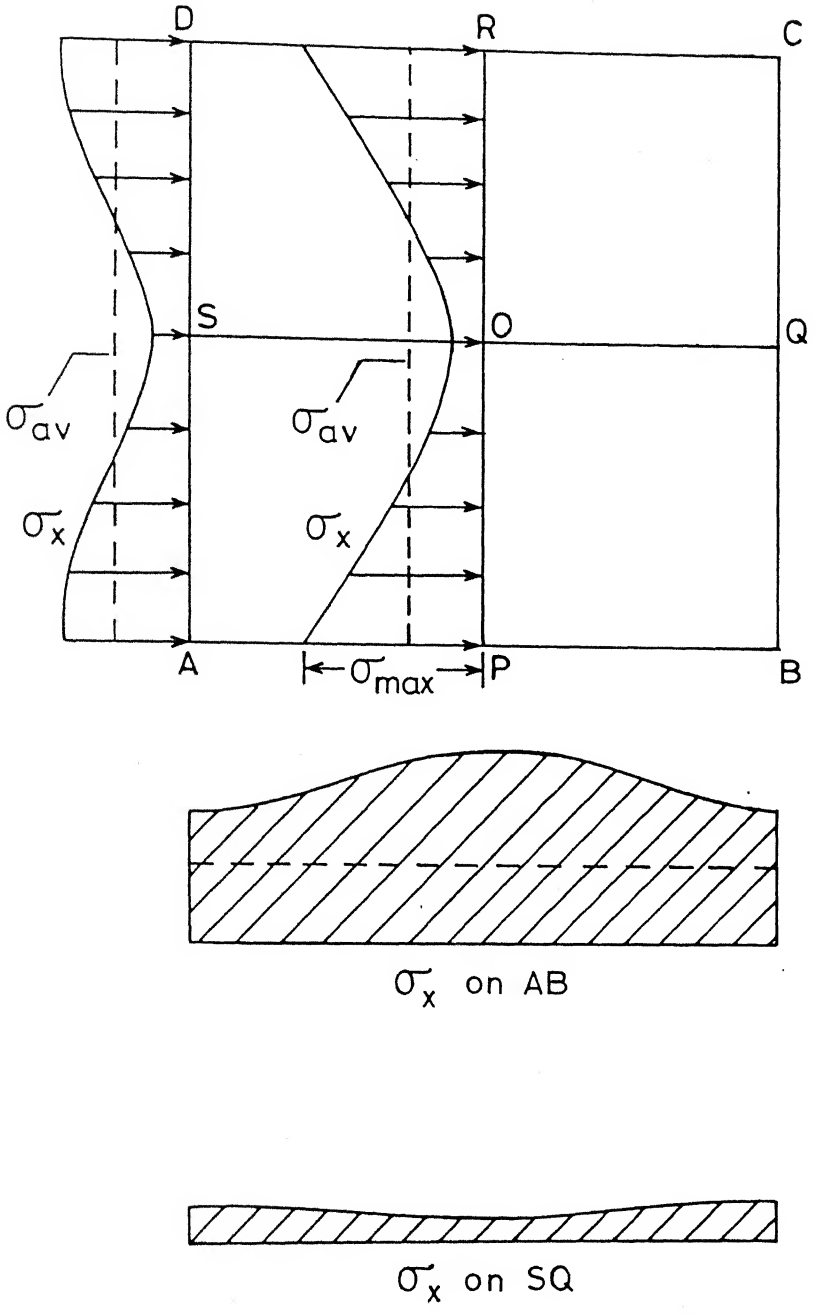

Fig. 3.15 Stress distribution in an isotropic square plate for load $\bar{N}_x = 7.0$, mode (1, 1), ME condition.

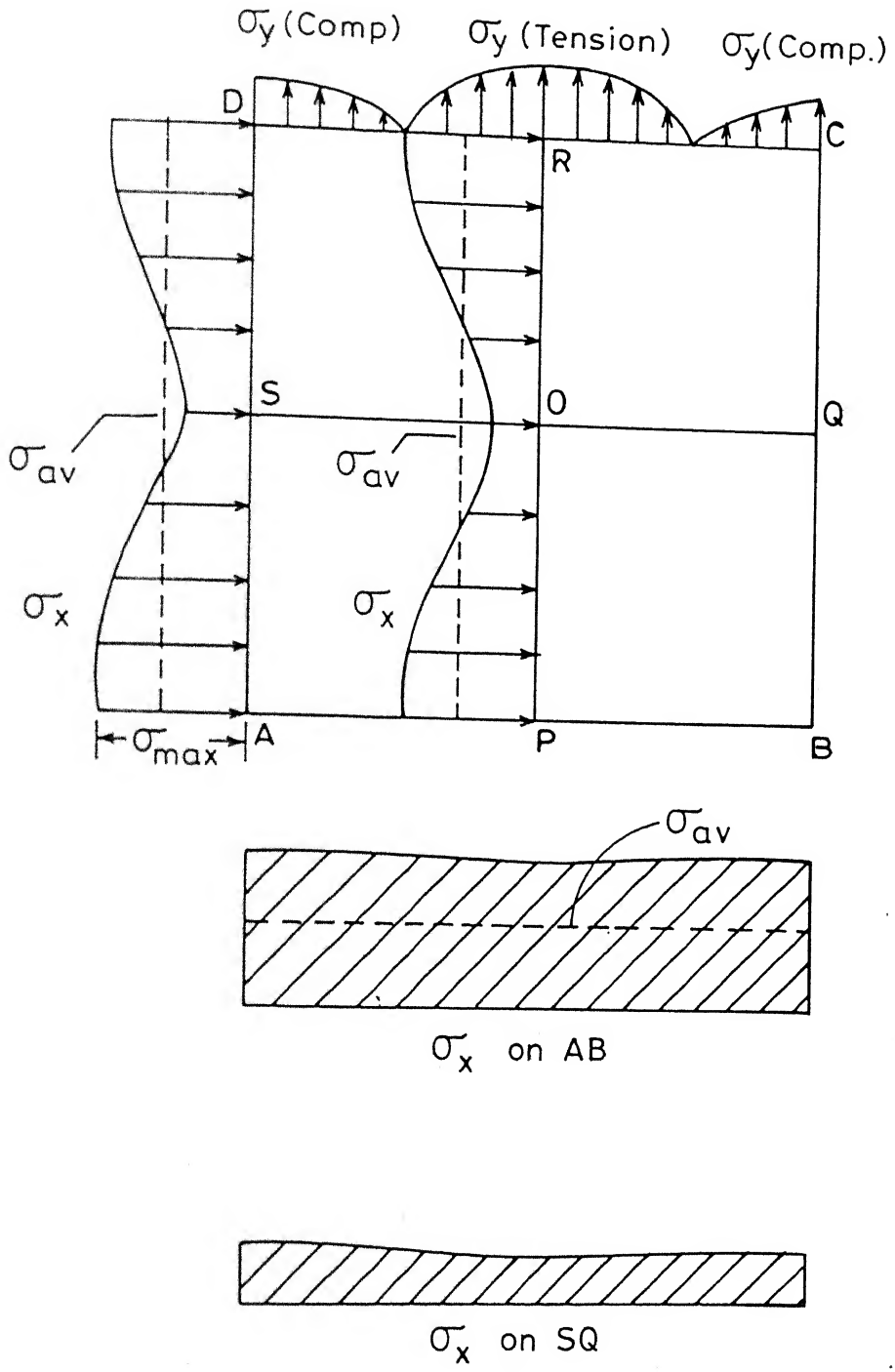

Fig. 3.16 Stress distribution in an isotropic square plate for load $\bar{N}_x = 7.0$, mode (1, 1) FE condition.

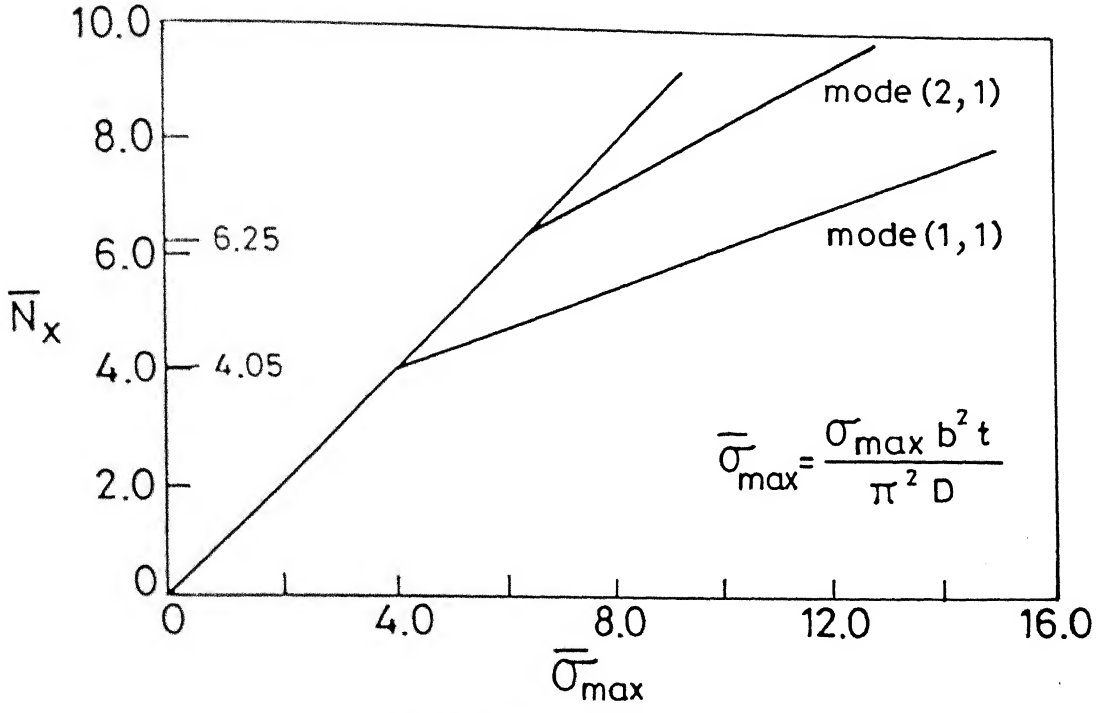

(a) ME condition

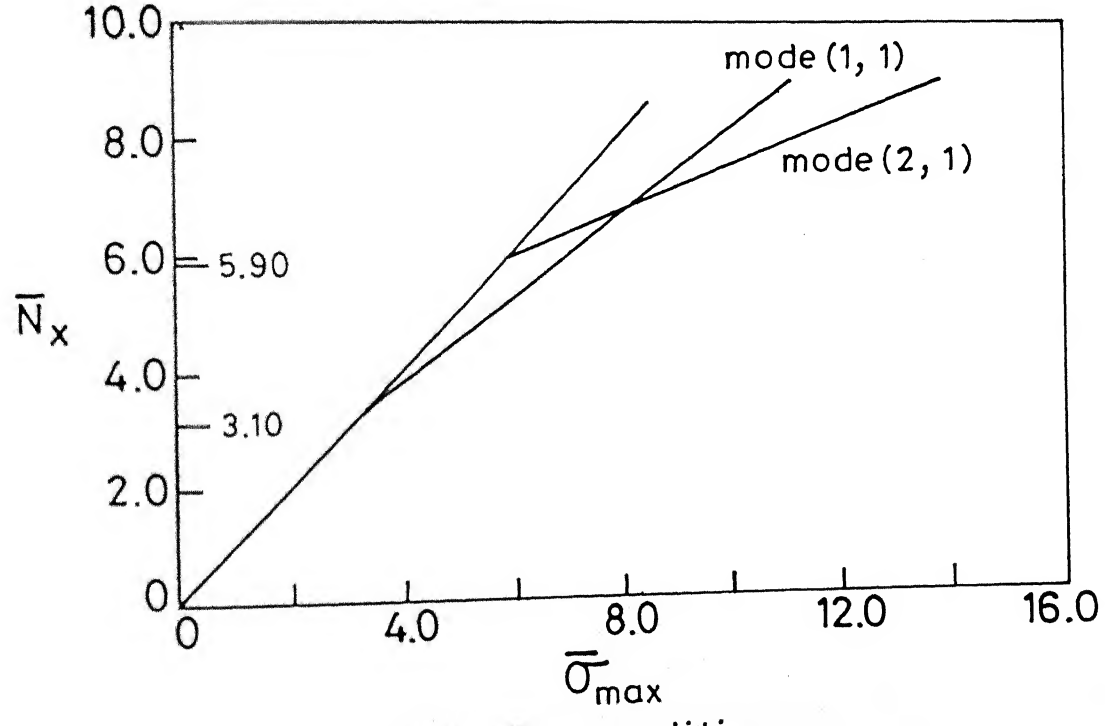

(b) FE condition

Fig. 3.17 Variation of maximum longitudinal stress with the load, for an isotropic square plate.

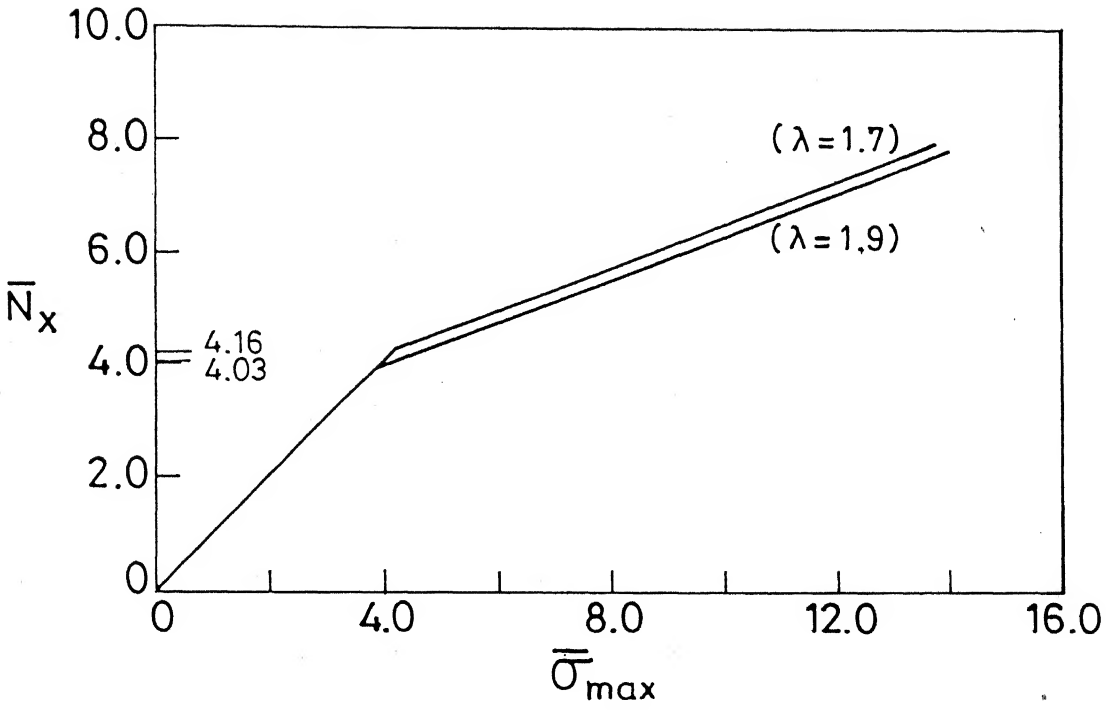

(a) ME condition, mode (2,1)

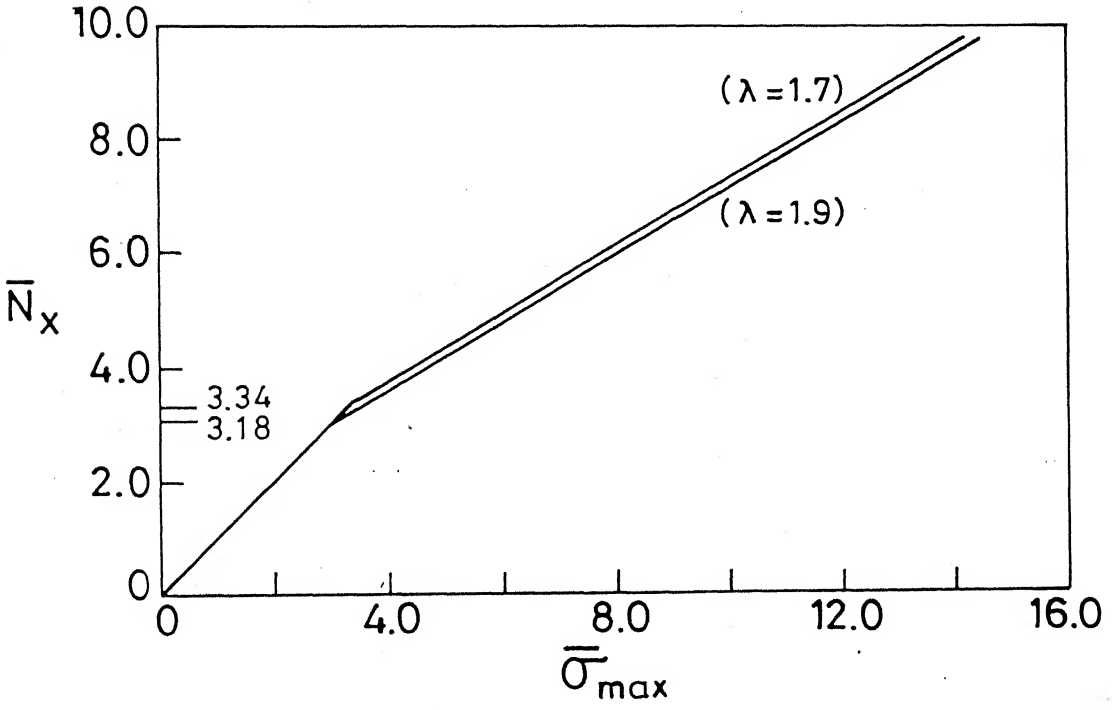

(b) FE condition, mode (2,1)

Fig. 3.18 Variation of maximum longitudinal stress with the load, for isotropic plates.

CHAPTER 4

ORTHOTROPIC PLATES SUBJECTED TO LONGITUDINAL COMPRESSION

4.1 INTRODUCTION

In Chapter 3, the finite element method was applied to study the postbuckling behavior of isotropic plates. In this chapter, the scope of the finite element formulation has been enlarged to include the postbuckling behavior of specially orthotropic plates. Such a plate or a laminate is obtained when orthotropic laminae are symmetrically arranged about the middle surface of the plate.

The details of the analysis are similar to those for isotropic plates (Chapter 3, Section 3.1, Figure 3.1). The boundary conditions used are also the same, i.e. all the four edges are considered simply supported with unloaded edges either unrestrained (ME condition) or fully restrained (FE condition) against the normal (transverse) displacements. The relevant details of FEM have already been presented in Chapter 2; the main difference lies in calculating the element stiffness matrices which are quite involved for orthotropic plates. In order to study the effect of the degree of orthotropy $\bar{E}$ ($= E_x/E_y$) on the postbuckling behavior, two materials are considered: glass-epoxy ($\bar{E} = 3.0$) and boron-epoxy ($\bar{E} = 10.0$). Results like critical loads, load-deflection curves, load-shortening curves, changes in buckle patterns, effective width

curves and stress distribution are reported. Wherever possible, these results are compared with those of other investigators.

4.2 CURVES FOR BUCKLING LOADS

For a simply supported rectangular orthotropic plate, subjected to uniaxial compression, the critical load N_{xcr} (per unit width) is given by (Szilard, 1974)

$$N_{xcr} = k_c \frac{\pi^2 \sqrt{D_x D_y}}{b^2} \tag{4.1}$$

where the compressive buckling coefficient k_c is defined as

$$k_c = (m^2/\lambda^2) \sqrt{(D_x/D_y)} + 2H/\sqrt{(D_x D_y)} + (\lambda^2/m^2) \sqrt{(D_y/D_x)} \tag{4.2}$$

in which $(n = 1)$,

$$H = D_1 + 2D_{xy} \tag{4.3}$$

and $$D_1 = D_x \nu_y = D_y \nu_x \tag{4.4}$$

It is worth noting that the expression (4.2) is valid when the unloaded edges are either movable or are maintained straight (i.e. for ME and SE conditions only). The N_{xcr} (or k_c) thus depends on the relative values of flexural rigidities D_x, D_y and shear rigidity D_{xy}. The k_c-λ curves will, therefore, be different for materials having different degree of orthotropy $\bar{E}$ $(= E_x/E_y$ or $D_x/D_y)$, also called the rigidity ratio. For glass-epoxy $(\bar{E} = 3)$ and boron-epoxy $(\bar{E} = 10)$, the curves are

shown in Figures 4.1(a) and 4.2(a) for ME conditions. The absolute minimum value of the critical load is obtained when

$$\lambda = m\left(\frac{D_x}{D_y}\right)^{1/4} \tag{4.5}$$

The transition from m to m+1 half waves occurs at

$$\lambda = \sqrt{m(m+1)}\ \sqrt{(D_x/D_y)} \tag{4.6}$$

the successive values of λ for glass-epoxy and boron-epoxy are 1.86, 3.22, 4.56, ... and 2.51, 4.35, ... respectively, for ME conditions.

When the unloaded edges are rigidly held apart i.e. for FE condition, the previous expression for k_c gets modified to (Harris, 1975)

$$k_c = \frac{(m^2/\lambda^2)\sqrt{(D_x/D_y)} + 2H/\sqrt{(D_x D_y)} + (\lambda^2/m^2)\sqrt{(D_y/D_x)}}{1 + \nu_y(\lambda^2/m^2)} \tag{4.7}$$

The curves obtained using Eq. (4.7), are shown in Figures 4.1(b) and 4.2(b). It can be seen that the transition from m = 1 to m = 2 and from m = 2 to m = 3 occurs at λ = 2.2, 3.6 for glass-epoxy and at λ = 2.6, 4.5 for boron-epoxy. The following additional points may also be noted as a result of comparison of the curves for the two materials and for the two different inplane boundary conditions:

(i) The statement that for a particular aspect ratio, k_c is smaller for FE than for ME condition, which was valid for isotropic plates, is valid for orthotropic plates as well.

(ii) For same inplane conditions on the unloaded edges and for the same aspect ratio, k_c is smaller for boron-epoxy than for glass-epoxy; thus k_c decreases with the increase in the degree of orthotropy.

(iii) The absolute minimum value of k_c, for a fixed m, occurs at a larger value of λ for materials having greater value of $\bar{E}$. For example for m = 1, λ is 1.316 for glass-epoxy and is 1.778 for boron-epoxy under ME conditions. The corresponding values of k_c are 3.430 and 2.605. Similar trend is also seen for FE condition.

(iv) The transition from one curve to another occurs at different points (λ value) for different inplane boundary conditions; the difference is more for weak orthotropic material (glass-epoxy) and less for strong orthotropic material (boron-epoxy). The difference is maximum for isotropic plates, (Figures 3.2 and 3.3).

(v) Higher the ratio $\bar{E}$, smaller is the critical load for plates of same λ' (= m/λ), under similar inplane boundary conditions. For $\bar{E} > 1$, N_{xcr} is less than that for $\bar{E} = 1$ (i.e. isotropic plate).

(vi) A plate with, $\lambda = 2.0$, and $\bar{E} = 3.0$ (glass-epoxy) buckles in two half waves for ME condition but in a single half wave for FE condition. The same plate with $\bar{E} = 10$ (boron-epoxy) buckles in a single half wave only under either of the inplane boundary conditions on unloaded edges.

4.3 ILLUSTRATIVE EXAMPLES

The two materials considered are glass-epoxy and boron-epoxy whose properties are: (Agarwal and Broutman, 1980)

Glass-Epoxy

E_x = 42 GPa, E_y = 14 GPa, G_{xy} = 7 GPa, ν_x = 0.25, ν_y = 0.0833

Boron-Epoxy

E_x = 210 GPa, E_y = 21 GPa, G_{xy} = 7 GPa, ν_x = 3.0, ν_y = 0.03

For each material, the following illustrative examples are taken:

(i) Square plate (λ = 1.0), 1.0 m x 1.0 m and 10 mm thick – with unloaded edges free to move (ME condition), buckling in (1,1) and (2,1) modes.

(ii) Rectangular plate (λ = 2.0), 2.0 m x 1.0 m and 10 mm thick

(a) unloaded edges rigidly held apart (FE condition), buckling in (1,1) and (2,1) modes

(b) unloaded edges free to move (ME condition), buckling in (1,1) and (2,1) modes (for boron-epoxy only).

(iii) Rectangular plate (λ = 3.0), 3.0 m x 1.0 m and 10 mm thick – with FE condition, buckling in (2,1) and (3,1) modes.

4.4 NUMERICAL RESULTS

4.4.1 Critical Loads

For each illustrative example considered, the critical load is obtained from the load-deflection/shortening curves as explained in Section 3.3.1. The values of the buckling coefficient k_c are tabulated in Table 4.1 wherein the exact values, as obtained from Eqs. (4.2) and (4.7), are also presented. The two sets of value are in very close agreement.

4.4.2 Load-Deflection/Shortening Curves

The load-deflection curves, between the load $\bar{N}_x$ ($= N_x b^2/\pi^2 \sqrt{D_x D_y}$) and the out of plane deflection $\bar{w}_o$ ($= w_o/t$, w_o being the maximum deflection) are drawn in Figures 4.3-4.5. The curves in Figures 4.3(a) and 4.3(b) are for square plates of glass-epoxy and boron-epoxy respectively, buckling in the primary mode (1,1) under ME conditions. The deflection profiles for the symmetric and the anti-symmetric configurations, corresponding to modes (1,1) and (2,1), are given separately in Figures 4.6(a,b). In order to make a direct comparison of the results, the load-deflection curves are presented in Figure 4.7 between the load ratio $\bar{N}$ ($= N_x/N_{xcr}$ or $= \bar{N}_x/k_c$) and $\bar{w}_o$. The results for the corresponding isotropic case are also reproduced. When compared with the results of Prabhakara and Chia (1973), some discrepancy is observed between the two results (Figure 4.7 a); the deflections in the present analysis are on the lower side by about 15-20%, under ME conditions. The reasons for this difference are manifold: first

Table 4.1 Comparison of k_c values for orthotropic plates

Aspect ratio λ $(= \frac{a}{b})$	Buckling mode (m,n)	Glass-Epoxy ($\bar{E}$ = 3.0)				Boron-Epoxy ($\bar{E}$ = 10.0)			
		ME condition		FE condition		ME condition		FE condition	
		Exact	Present work	Exact	Present work	Exact	Present work	Exact	Present work
1.0	(1,1)	3.73	3.90			4.08	4.10		
	(2,1)	8.49	8.50			13.33	13.50		
2.0	(1,1)			3.12	3.15	2.66	2.80	2.38	2.40
	(2,1)			3.44	3.50	4.08	4.20	3.96	4.00
3.0	(2,1)			2.94	3.00			2.55	2.60
	(3,1)			3.44	3.50			3.96	4.00

Prabhakara and Chia (1973) have not specifically mentioned the type of inplane boundary condition used. Secondly, they have applied the condition of zero shear on the edges. Thirdly, the material properties used by them slightly differ from those used in this work.

The load-shortening curves are drawn between the non-dimensional load $\bar{N}_x$ and the non-dimensional shortening $\bar{\Delta}$ ($= \Delta E_x b^2 t/a \pi^2 \sqrt{D_x D_y}$) and are shown in Figures 4.8-4.12. Figure 4.9 shows such curves for glass-epoxy plates with λ = 2.0 and 3.0 under FE conditions. These curves match with those of Chandra and Raju (1973). The small difference is because of different inplane conditions. Figure 4.12 gives a comparison of load-shortening curves for three materials, drawn on the same plot, for a fixed value of λ' = 1 ($\lambda' = m/\lambda$). Again the trend of these curves is very much similar to that reported by Chandra and Raju (1973).

4.4.3 Change in Buckle Pattern *

The possibility of a change in the buckling pattern is indicated by the point of intersection of the corresponding load-shortening curves. Whereas a clear point of intersection is obtained for a glass-epoxy square plate under ME condition (Figure 4.8 a), there is no such phenomenon in the case of boron-epoxy plate (Figure 4.8 b). Figure 4.9 shows results of glass-epoxy rectangular plates of aspect ratios 2.0 and 3.0 under FE conditions. In both cases, the changeover points [for λ = 2.0 from mode (1,1) to (2,1) and for λ = 3.0 from (2,1) to (3,1)] are distinct. Similar curves for boron-epoxy

* For additional comments see page 134.

plates are shown in Figures 4.10 and 4.11; the later figure shows divergence of the two lines corresponding to (1,1) and (2,1) modes.

4.4.4 Effective Width Curves

The effective width formula for isotropic plates, expressed by Eq. (3.9), gets modified to (Chandra and Raju, 1973)

$$\bar{b}_e = \frac{N_x\, a}{\Delta t\, E_x} \tag{4.8}$$

for orthotropic plates. Curves are drawn to represent variation of non-dimensional effective width $\bar{b}_e$ with the non-dimensional load $\bar{N}_x$ as well as with the load ratio $\bar{N}$. Figure 4.13 is for glass-epoxy plates of λ = 2.0 and 3.0 under FE conditions and Figure 4.14 for a boron-epoxy plate of λ = 2.0 with ME and FE conditions. The variation of effective width with the parameter λ' (= m/n) is illustrated in Figures 4.15 and 4.16. For a fixed value of λ' (= 1.0), Figure 4.15 shows the variation under different inplane boundary conditions whereas for a given inplane boundary condition (FE), the variation of $\bar{b}_e$ for different values of λ' is shown in Figure 4.16. Results of Figure 4.15(b), (λ' = 1.0, FE condition) are quite close to those of Chandra and Raju (1973).

4.4.5 Stresses

For the problems analysed, stresses have also been calculated at some load levels. The stress distribution follows a similar pattern as in Figures 3.15 and 3.16 for

isotropic plates, under the two inplane boundary conditions. Figures 4.17-4.19 show the variation of non-dimensional maximum longitudinal stress $\bar{\sigma}_{max}$ ($= \sigma_{max}\, b^2\, t/\pi^2 \sqrt{D_x D_y}$) with the non-dimensional load $\bar{N}_x$. The variation in postbuckling range is also linear, as in an isotropic plate.

4.5 DISCUSSIONS

4.5.1 Load-Deflection/Shortening Curves

From the load-deflection curves in Figures 4.3-4.7, following conclusions are drawn:

(i) For the same load ratio $\bar{N}$, the deflection $\bar{w}_o$ is higher for higher values of the rigidity ratio $\bar{E}$ of the plate (Figure 4.7). It is obvious from these curves that, other parameters remaining same, the deflection of an orthotropic plate is greater than that of an isotropic plate.

(ii) The deflection curve for the glass-epoxy plate ($\bar{E}$ = 3.0) is only marginally different from that of an isotropic plate for ME conditions and the two curves almost coincide for FE conditions (Figures 4.7 c and 4.7 d . This fact is also obvious from Figure 4.12(b), where $\bar{N}_x - \bar{\Delta}$ lines for the isotropic and the glass-epoxy plates for the same λ', are parallel. However the curves of boron-epoxy are quite distinguished from other materials, under both inplane conditions.

(iii) For the same λ' (= m/λ), the deflections are larger for ME conditions than those for FE conditions (Figures 4.7a, d). This is also clear from Figure 4.4, in which $\bar{N}_x - \bar{w}_o$ curves are drawn for boron-epoxy with $\lambda = 2.0$, under ME and FE conditions.

(iv) Whereas for a plate of a fixed aspect ratio, under ME conditions, the tendency for the maximum lateral deflection is to decrease from (1,1) to (2,1) mode (Figures 4.7a, b), the curves of Figures 4.7c, d (for $\lambda = 2.0$, under FE conditions) show just the opposite trend, whereby the maximum deflection in (2,1) mode is greater than that in (1,1) mode.

Further, from the load-shortening curves in Figures 4.8, 4.10 and 4.12, it is observed that:

(v) For a plate of a particular material, size and mode the reduction in the axial stiffness, after primary buckling, is larger for ME condition than for FE condition (Figures 4.10a, b and 4.12a, b).

(vi) The reduction in the axial stiffness increases as the value of $\bar{E}$ increases (Figures 4.8a, b and 4.12a, b).

4.5.2 Change in Buckle Pattern

Following points regarding change in buckle pattern, are observed with reference to the various load-shortening curves shown in Figures 4.8-4.11:

(i) In the case of boron-epoxy with $\lambda = 2.0$ and under FE condition , the load-shortening lines in (1,1) and (2,1)

modes, (Figure 4.10b) intersect at the load $\bar{N}_x = 4.43$, a value slightly higher than the critical load corresponding to the secondary mode (2,1), viz. 4.00. On the other hand under ME condition, (Figure 4.10a), the point of intersection is at 6.40, which is much above the critical load of (2,1) mode, viz. 4.20. Similarly for glass-epoxy plates having $\lambda = 2.0$ and 3.0 (Figures 4.9a, b) the possible changeover appears to be at a load slightly greater than the critical load corresponding to the secondary mode. Thus under FE condition, the change in buckle pattern is rather quick (as observed for isotropic plates also, in Chapter 3).

(ii) Figure 4.11 is the graph of $\bar{N}$ against (Δ/Δ_{cr}) for a boron-epoxy plate with $\lambda = 3.0$. It is clear that (1,1) and (2,1) lines do not meet, implying that the changeover from a higher (2,1) to a lower (1,1) mode is not possible.

(iii) The approximate formula to predict the point of intersection given for isotropic plates, Eq. (3.15), seems to hold good for orthotropic plates, also. However a more rational formula, which takes into account the parameter m as well, is proposed and is valid for ME condition:

$$N_{xi} = \frac{N_{xs}^2}{N_{xp}} \left(\frac{2m^2 - 2m + 1}{m^2}\right) \qquad (4.9)$$

where N_{xs} and N_{xp} are, respectively, the critical loads corresponding to the secondary and the primary modes, N_{xi} is the load point at which the two $\bar{N}_x - \bar{\Delta}$ lines corresponding to the primary mode (= m) and the secondary mode (= m+1) intersect. The value of m, for example, will be 1, for changeover from (1,1) to (2,1) mode and will be 2 for changeover from (2,1) to (3,1) mode.

An interesting observation is made for $\bar{N}_x - \bar{\Delta}$ lines of boron-epoxy square plate under ME condition (Figure 4.8b). The two lines, as per the prediction rule described in Section 3.4.2, should have met whereas they appear to be almost parallel. Actually the two lines do meet but at a very high load which is not of any practical significance.

4.5.3 Effective-Width Curves

Empirical formulae to obtain effective width for orthotropic plates are not many. As in the case of isotropic plate, the formulae are based on the assumption that the mode at the instant of buckling remains unchanged. However in the present investigation, effective width curves, presented in Figures 4.13 and 4.14 incorporate the possibility of the change in buckling pattern.

Following important features can be noted from these curves and those of Figures 4.15 and 4.16:

(i) The changeover from a lower to the next higher mode is quicker under FE condition than under ME condition (Figures 4.14a, b).

(ii) For a particular load ratio $\bar{N}$, the effective width $\bar{b}_e$ reduces with the increase in the value of λ' (Figures 4.16a, b and 4.15 b).

(iii) For the same λ' and under same inplane conditions the effective width $\bar{b}_e$ decreases with the increase in the rigidity ratio $\bar{E}$ (Figures 4.15 and 4.16).

(iv) The reduction in effective width is more in the initial post-buckling range and is very small for the load ratio $\bar{N} > 1.75$ (Figure 4.15). A similar trend was also observed for isotropic plates (Figures 3.12-3.14).

4.5.4 Stresses

Following are some of the general remarks made on various stress results obtained in this analysis. (These also apply to the isotropic plates):

(i) The maximum value of membrane (longitudinal) stress, σ_{max}, occurs at the crest of the buckle on the unloaded edges, under ME condition and at the corners of the loaded edges under FE condition.

(ii) The difference between the values of σ_x at the crest of the buckle and at the edge corner, for a particular load level is very small under FE condition but, is quite large under ME condition.

(iii) Under the FE condition, when the plate buckles in (1,1) mode, the transverse (membrane) stress σ_y develops on

the unloaded edges; this stress is compressive near the sides and tensile in the central part of the edge. Some additional remarks are made with reference to Figures 4.17-4.19:

(iv) The variation of $\bar{\sigma}_{max}$ with the load $\bar{N}_x$ is linear in the postbuckling range as has been the case with isotropic plates also (Figures 4.17-4.19).

(v) The value of $\bar{\sigma}_{max}$ relative to the value at the instant of buckling $\bar{\sigma}_{cr}$ $(= \sigma_{cr}\, b^2\, t/\pi^2 \sqrt{D_x D_y})$, reduces with the increase in degree of orthotropy $\bar{E}$. This is clearly seen in Figures 4.17a, b, where the $\bar{N}_x - \bar{\sigma}_{max}$ line for boron-epoxy ($\bar{E} = 10$) is having greater slope, than that for glass-epoxy ($\bar{E} = 3$) for the same mode.

(vi) When graphs of Figures 4.18 a and b are compared for the same mode (2,1), it is found that, for a given load ratio, the maximum stress ratio σ_{max}/σ_{cr}, (or $\bar{\sigma}_{max}/\bar{\sigma}_{cr}$) reduces with the increase in the aspect ratio.

(vii) From Figure 4.19, it can be interpreted that for a given plate, buckling in a particular mode, the value of $\bar{\sigma}_{max}$, is greater for ME condition than for FE condition, at a specified load ratio.

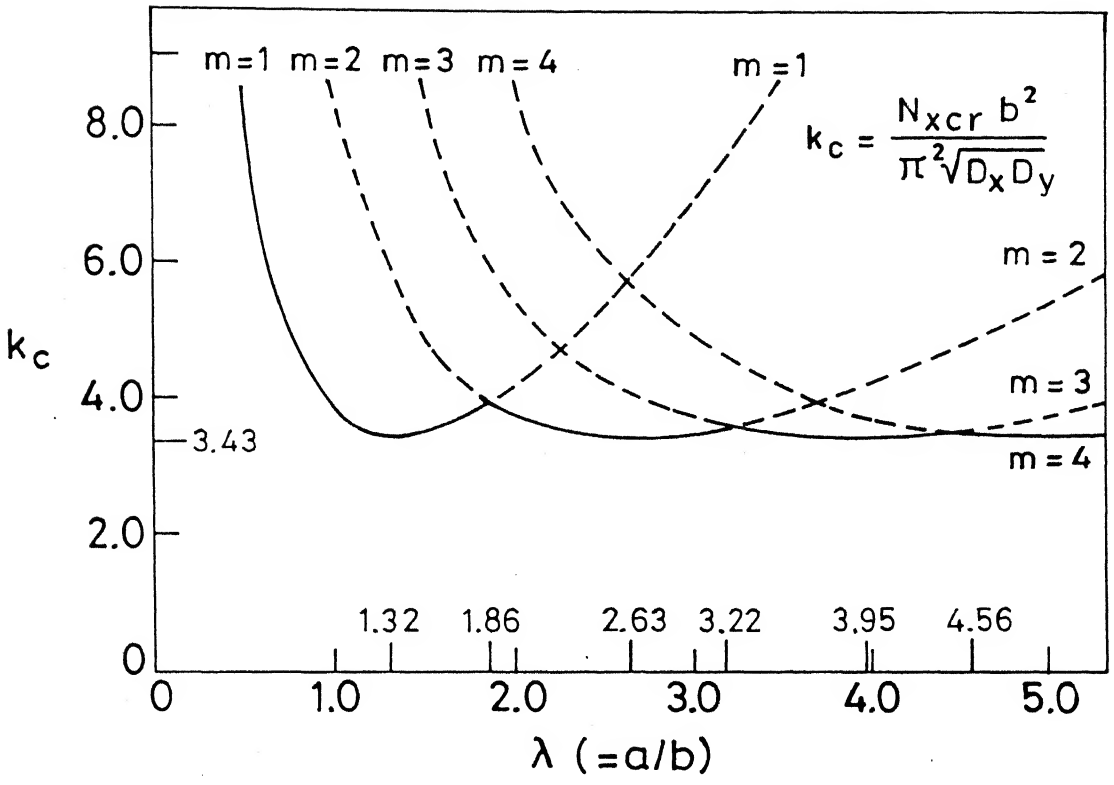

(a) ME condition

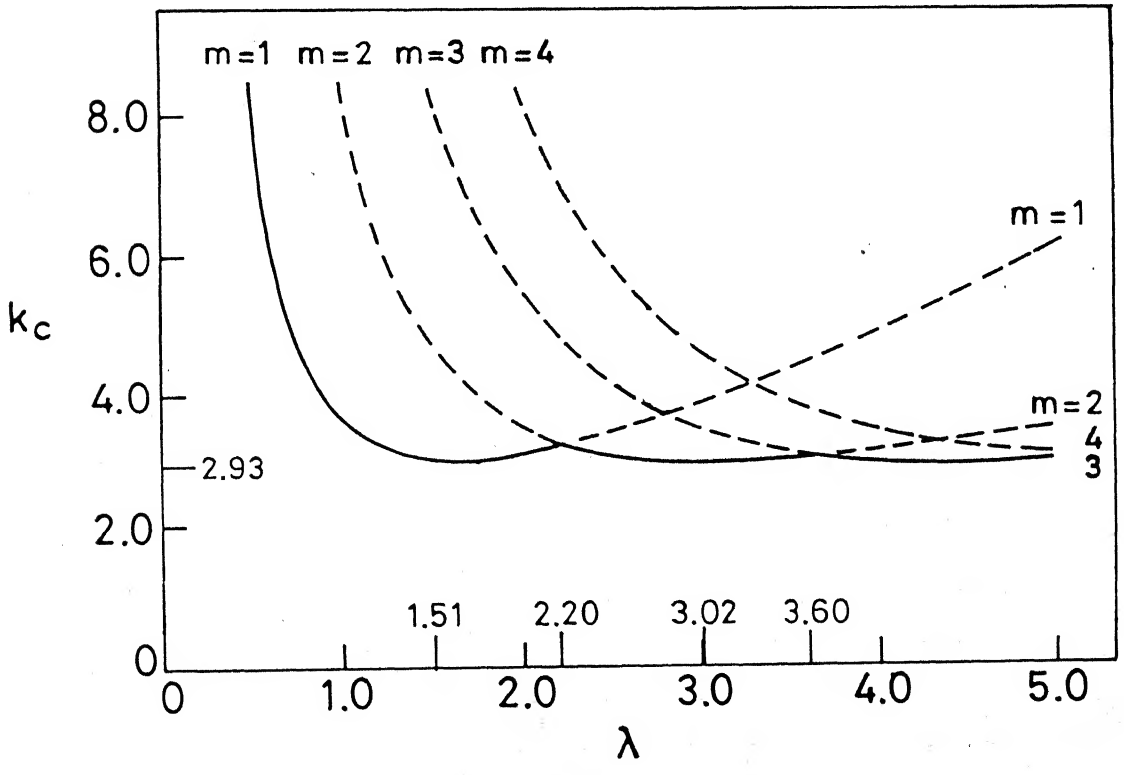

(b) FE condition

Fig. 4.1 Compressive buckling coefficients for glass-epoxy plates.

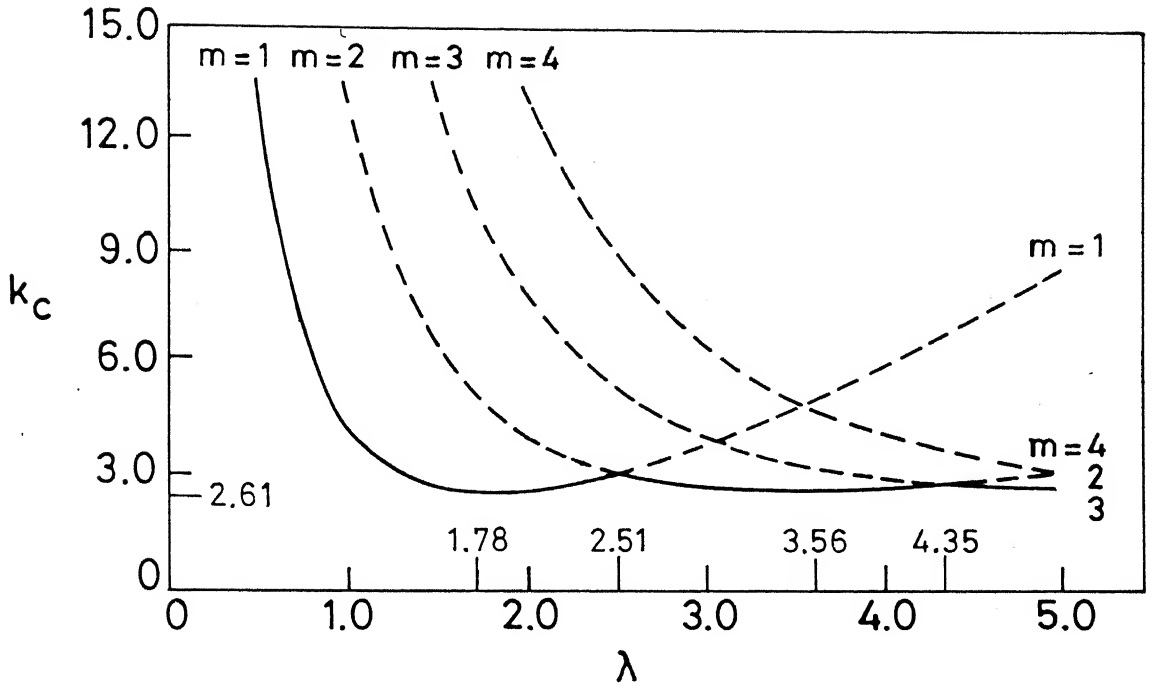

(a) ME condition

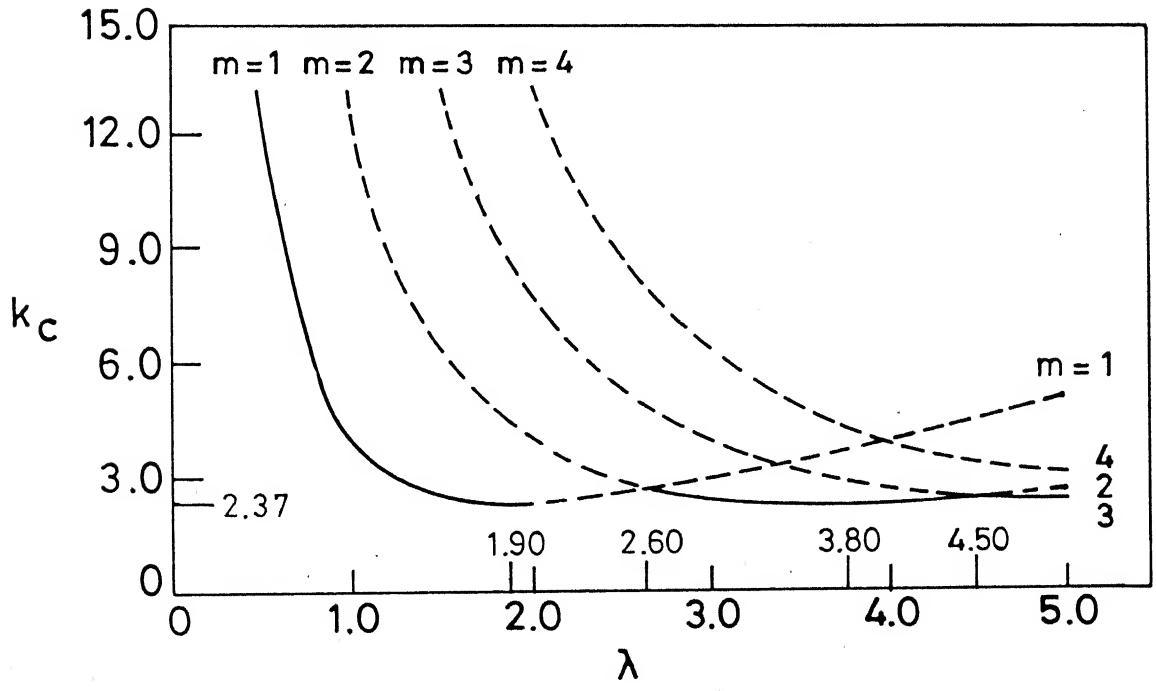

(b) FE condition

Fig. 4.2 Compressive buckling coefficients for boron-epoxy plates.

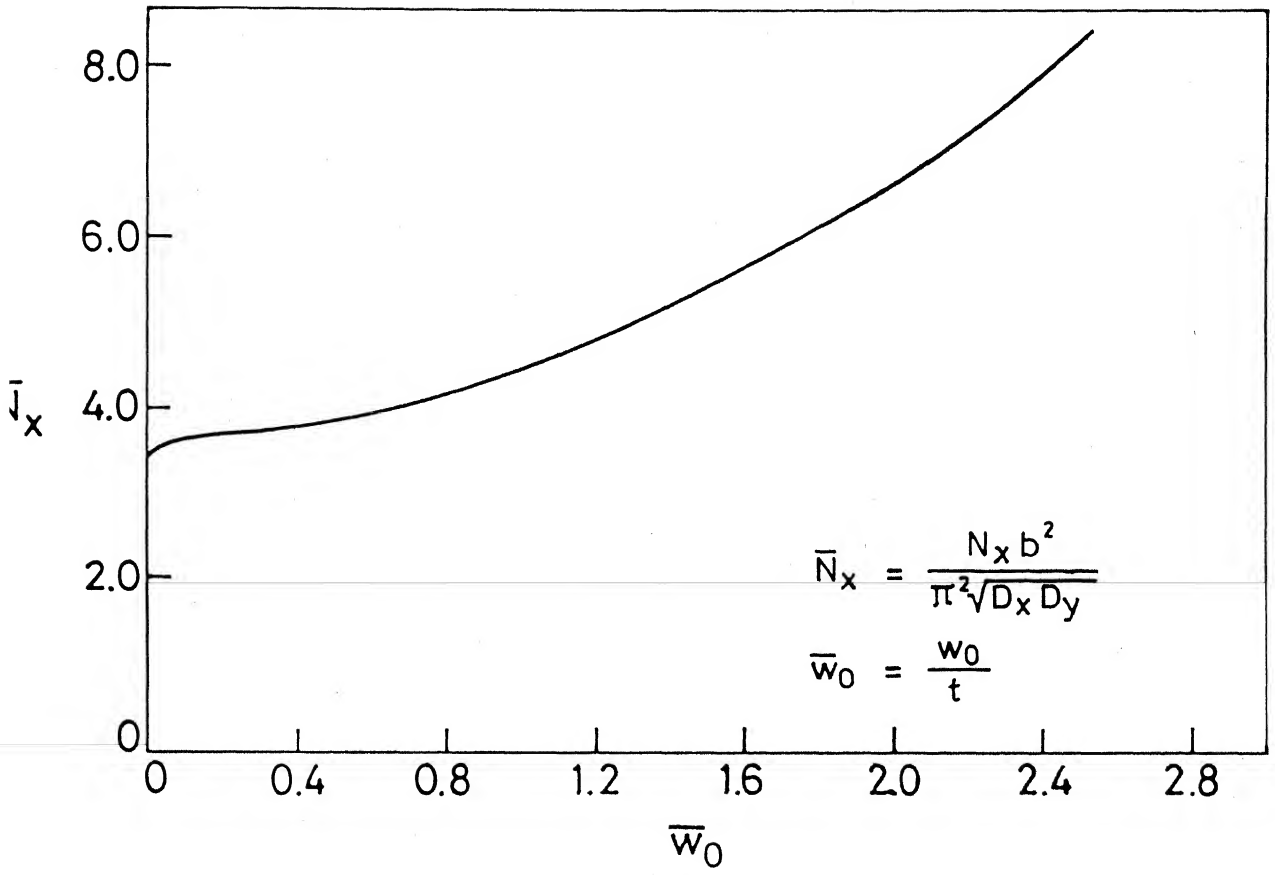

(a) Glass-Epoxy

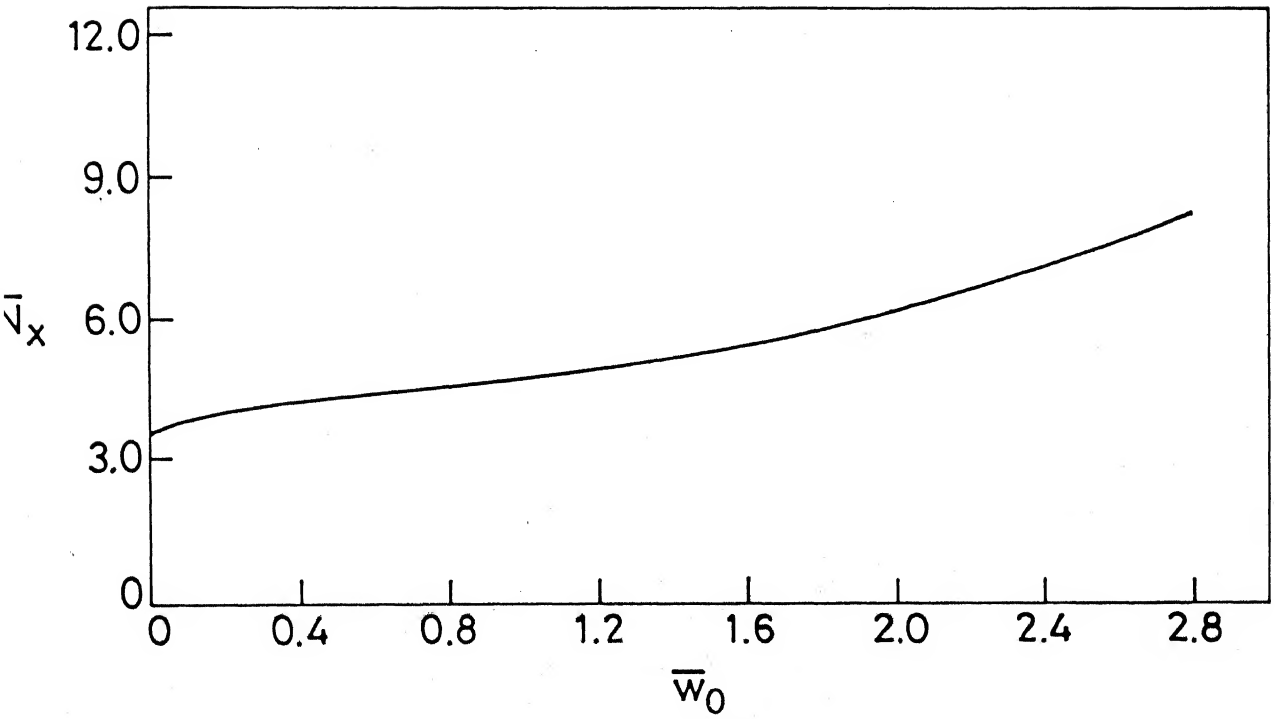

(b) Boron-Epoxy

Fig. 4.3 Load-deflection curves for square plates, ME condition, mode (1, 1).

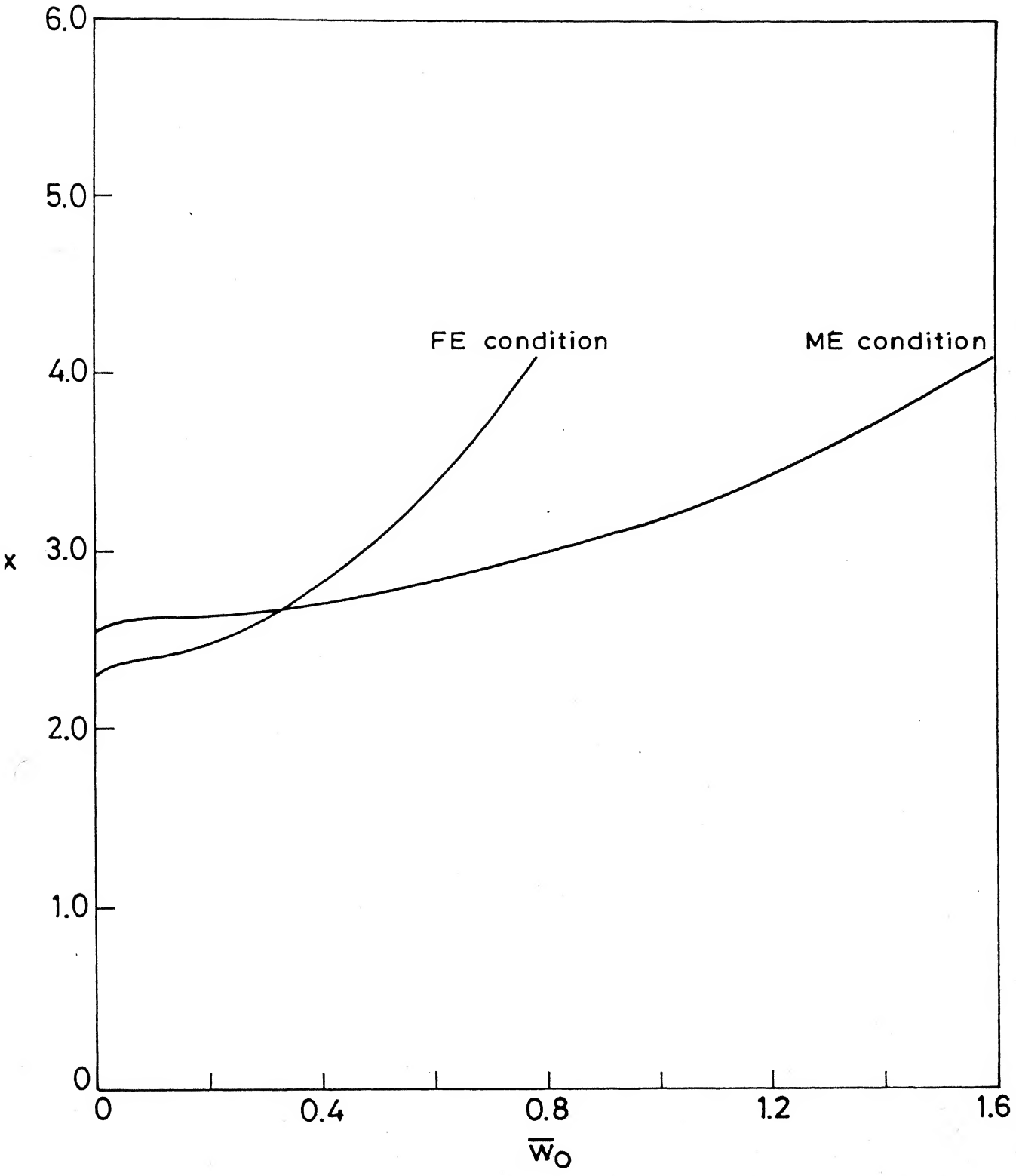

Fig. 4.4 Load-deflection curves for boron-epoxy plate, $\lambda = 2.0$, mode (1, 1).

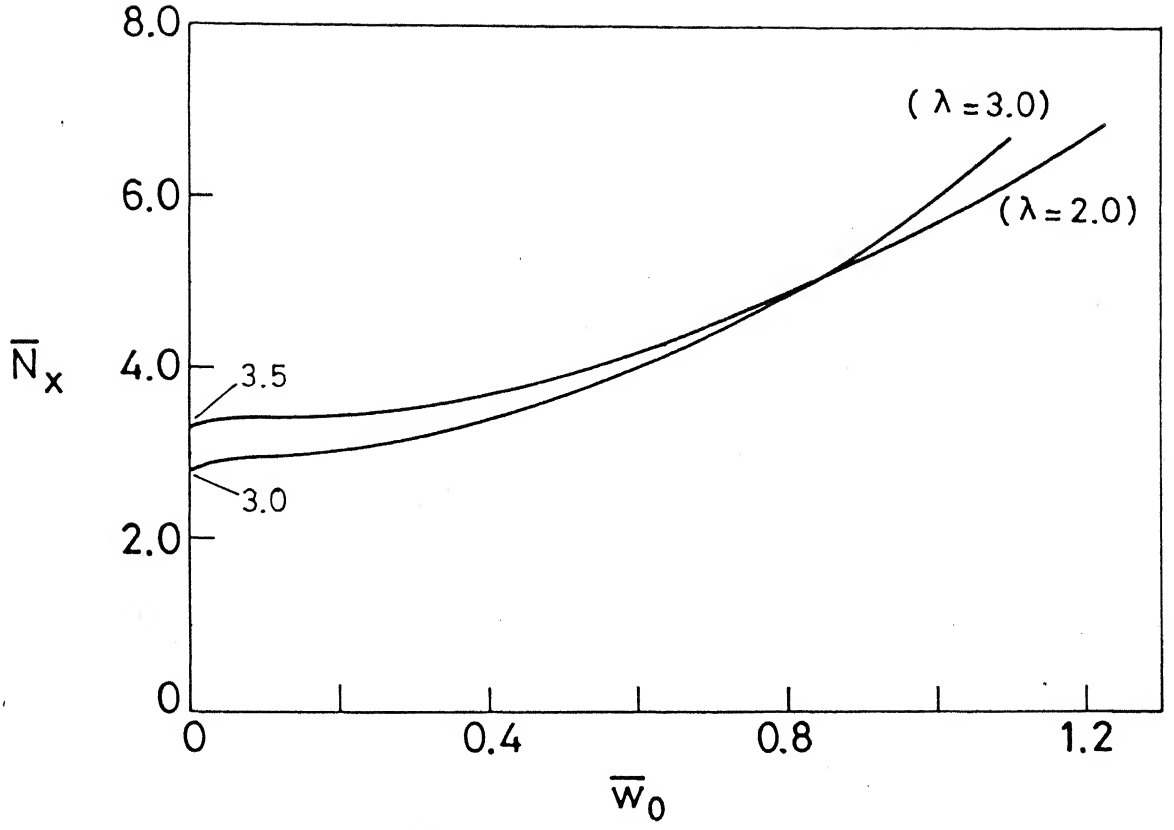

(a) Glass-Epoxy, FE condition, mode (2, 1)

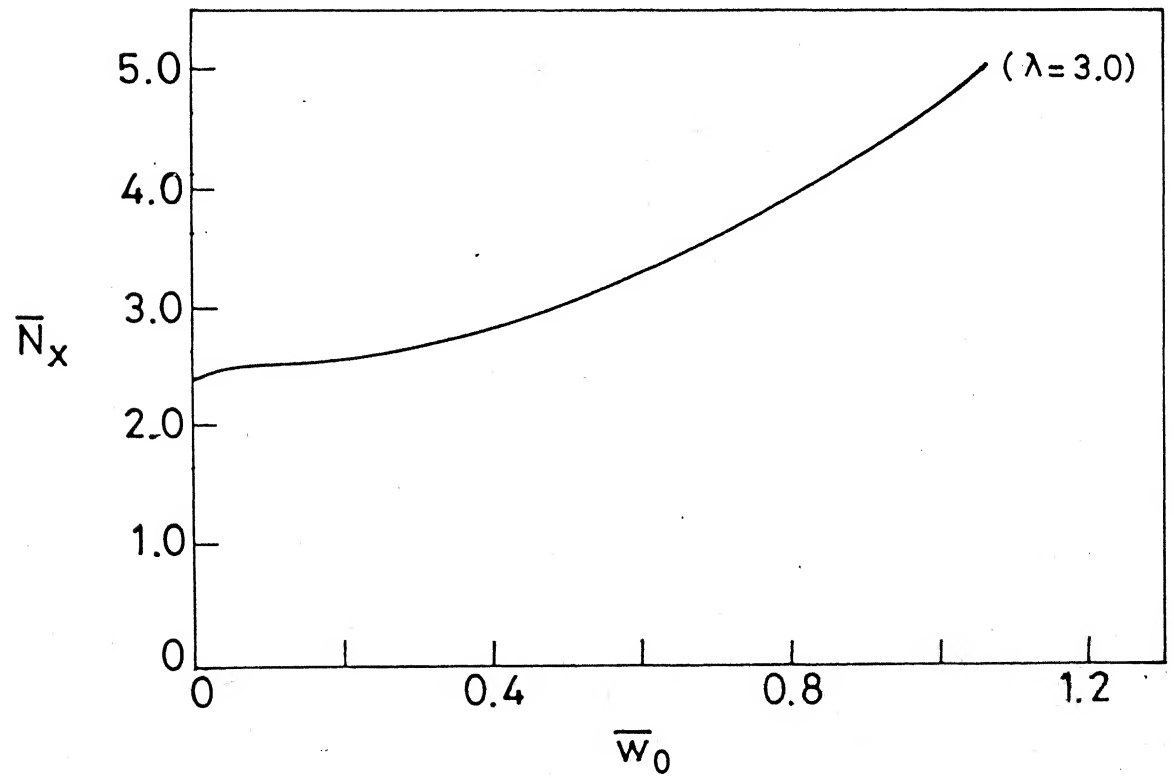

(b) Boron-Epoxy, FE condition, mode (2, 1)

Fig. 4.5 Load-deflection curves.

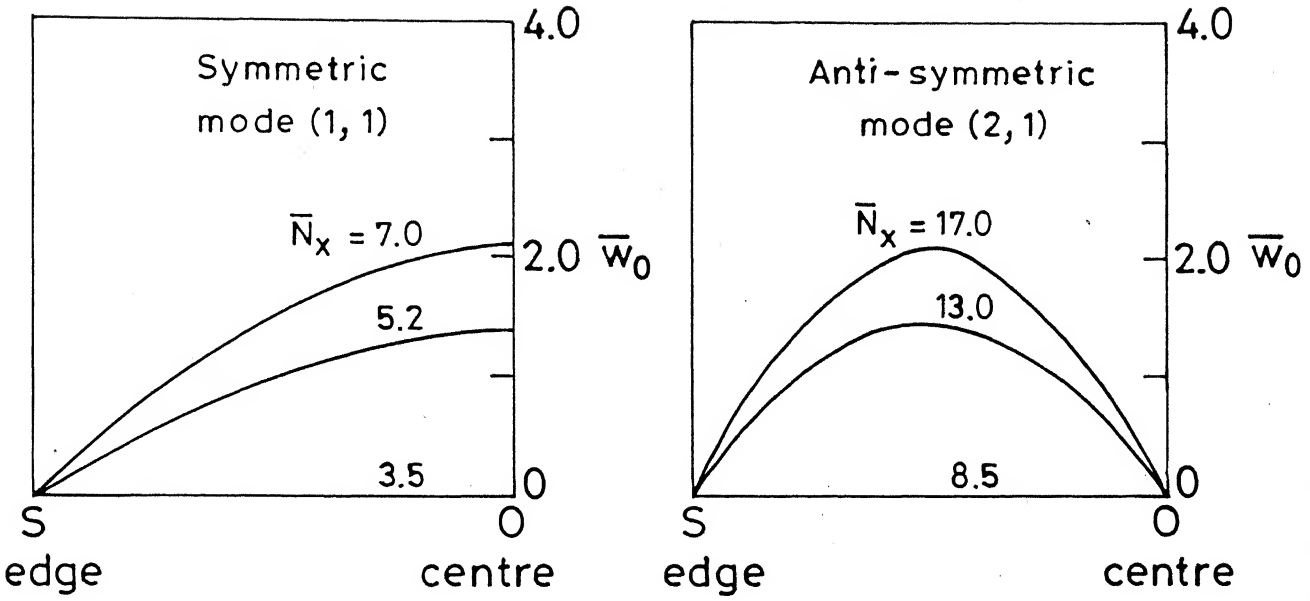

(a) Glass-Epoxy

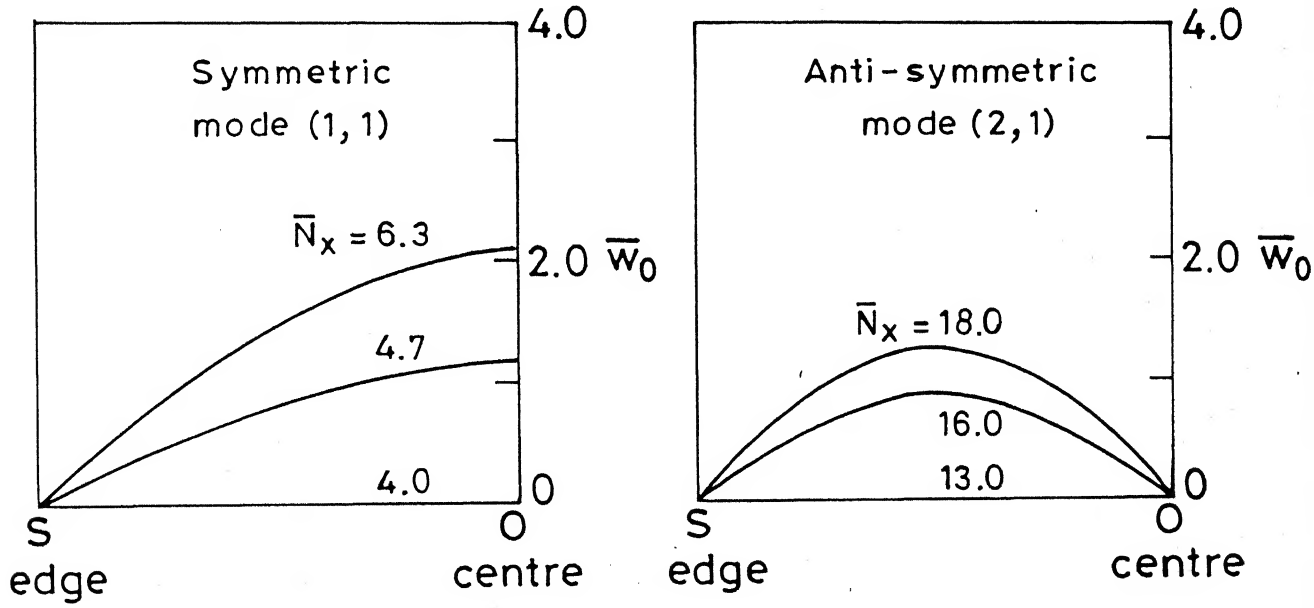

(b) Boron-Epoxy

Fig. 4.6 Deflection profile for a square plate, ME condition.

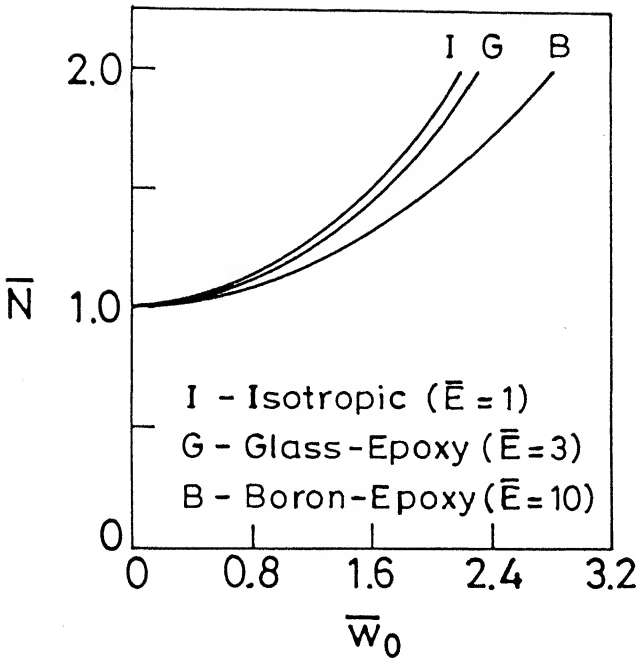

(a) Square plate, ME condition, mode (1, 1), ($\lambda' = 1.0$)

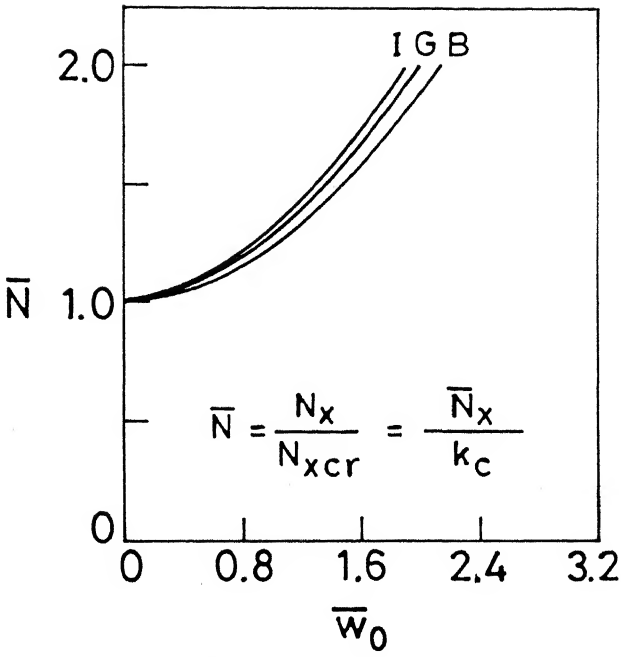

(b) Square plate, ME condition, mode (2, 1), ($\lambda' = 2.0$)

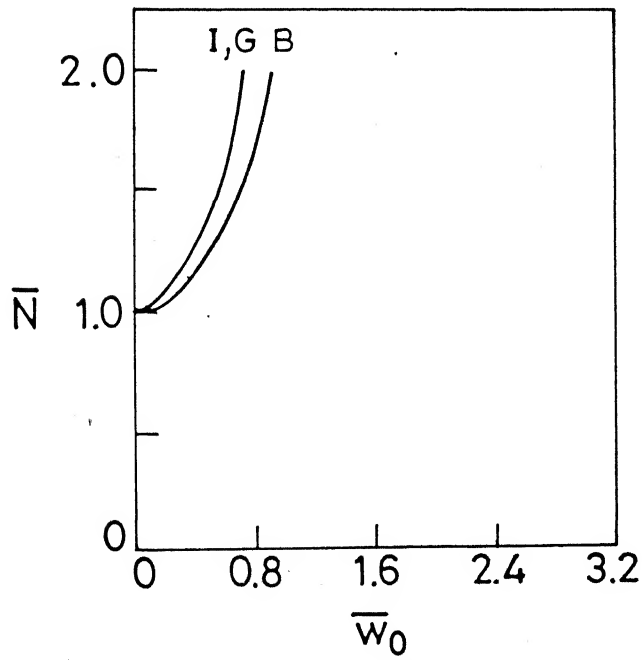

(c) Rectangular plate, $\lambda = 2.0$, FE condition, mode (1, 1) ($\lambda' = 0.5$)

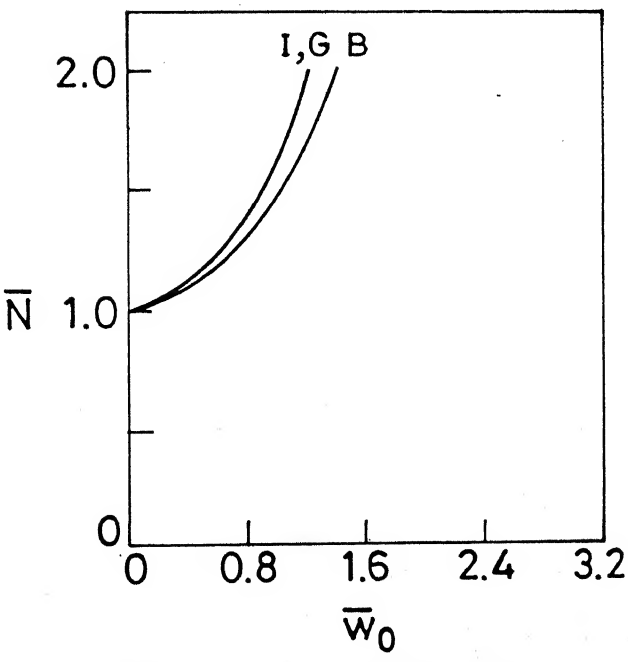

(d) Rectangular plate, $\lambda = 2.0$, FE condition, mode (2, 1) ($\lambda' = 1.0$)

Fig. 4.7 Load-deflection curves between load ratio and maximum deflection.

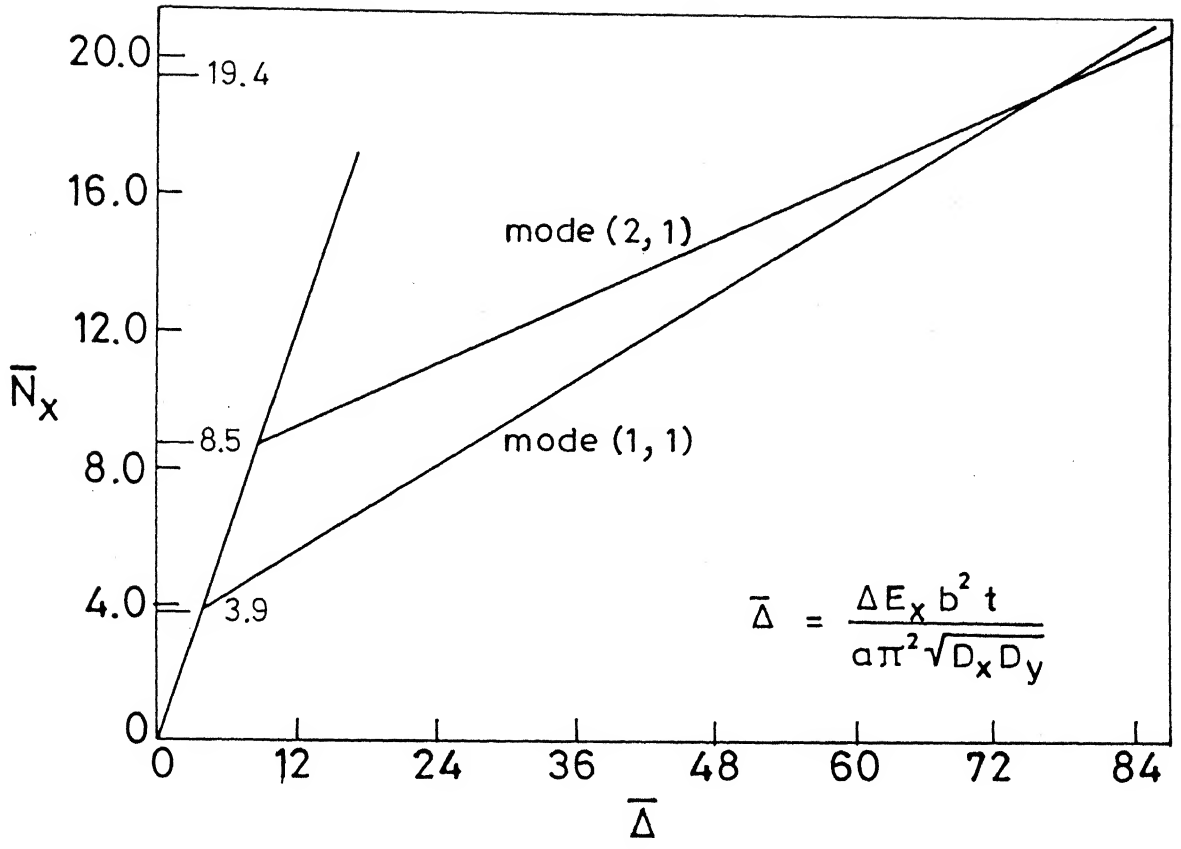

(a) Glass-Epoxy, ME condition

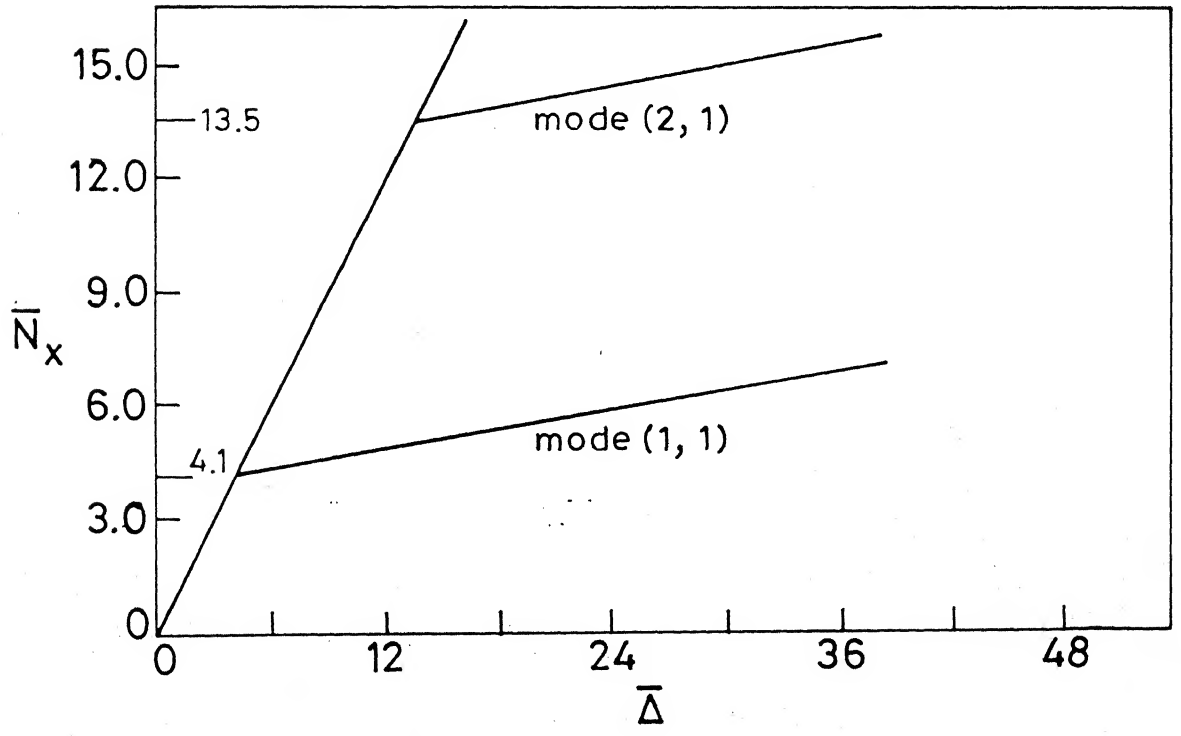

(b) Boron-Epoxy, ME condition

Fig. 4.8 Load-shortening curves for square plates.

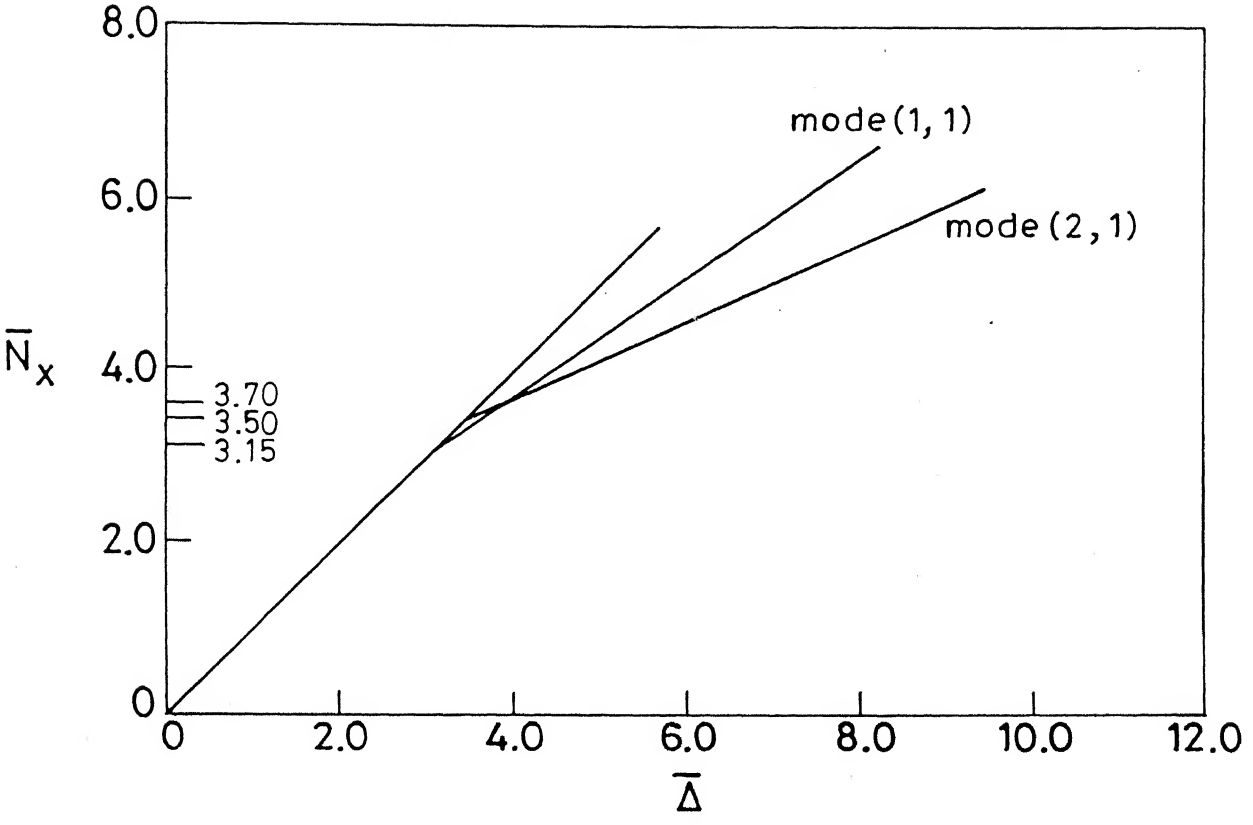

(a) $\lambda = 2.0$, FE condition

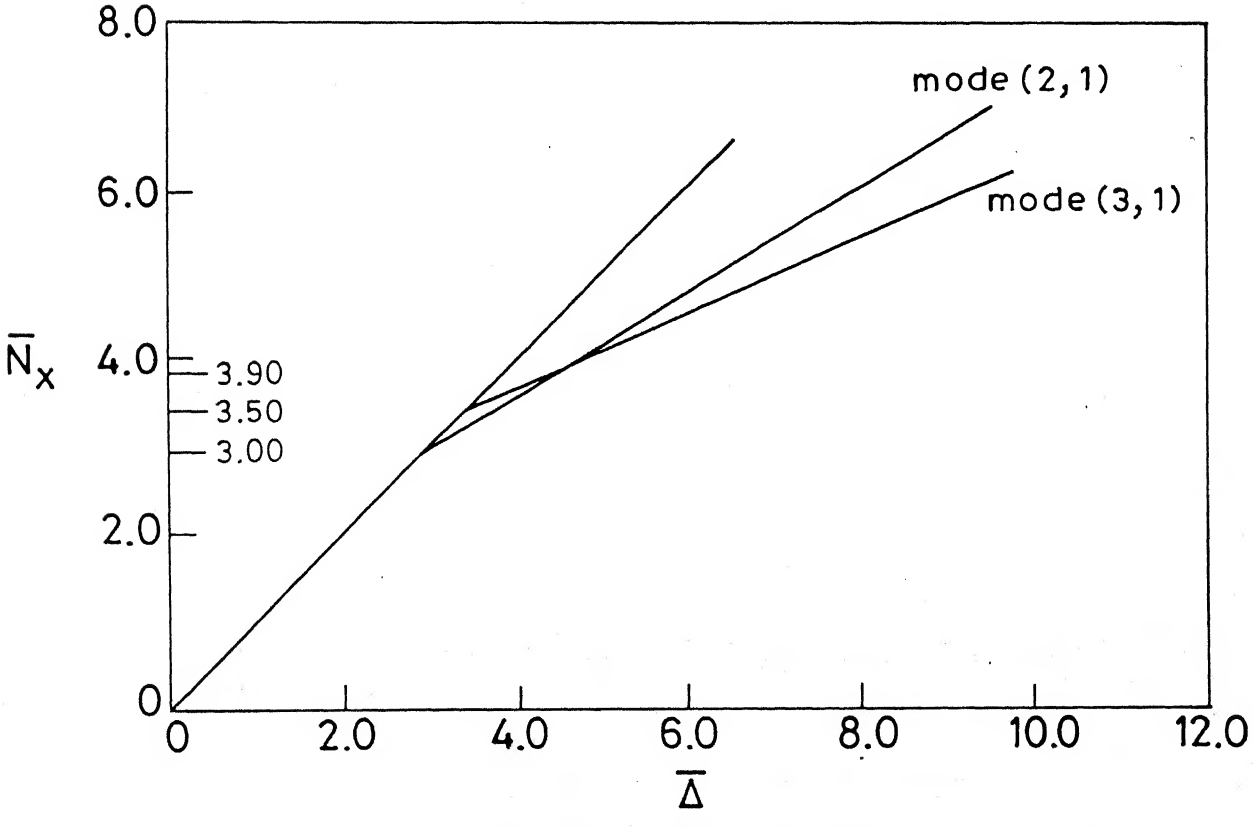

(b) $\lambda = 3.0$, FE condition

Fig. 4.9 Load-shortening curves for glass-epoxy plates.

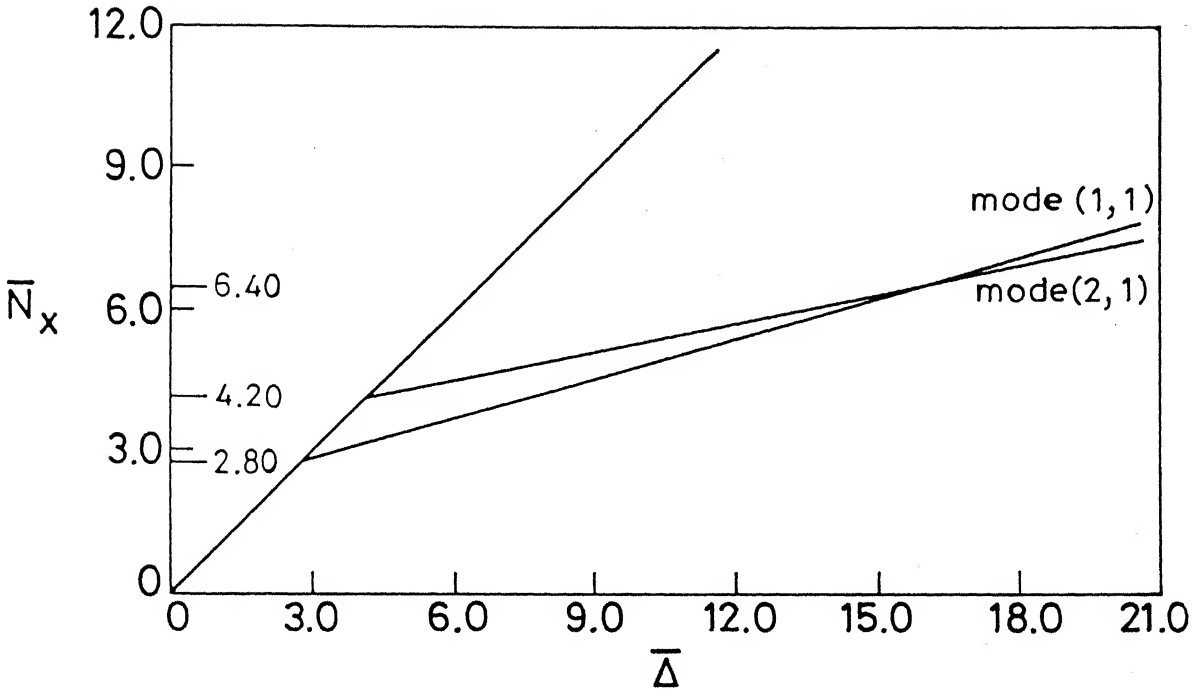

(a) $\lambda = 2.0$, ME condition

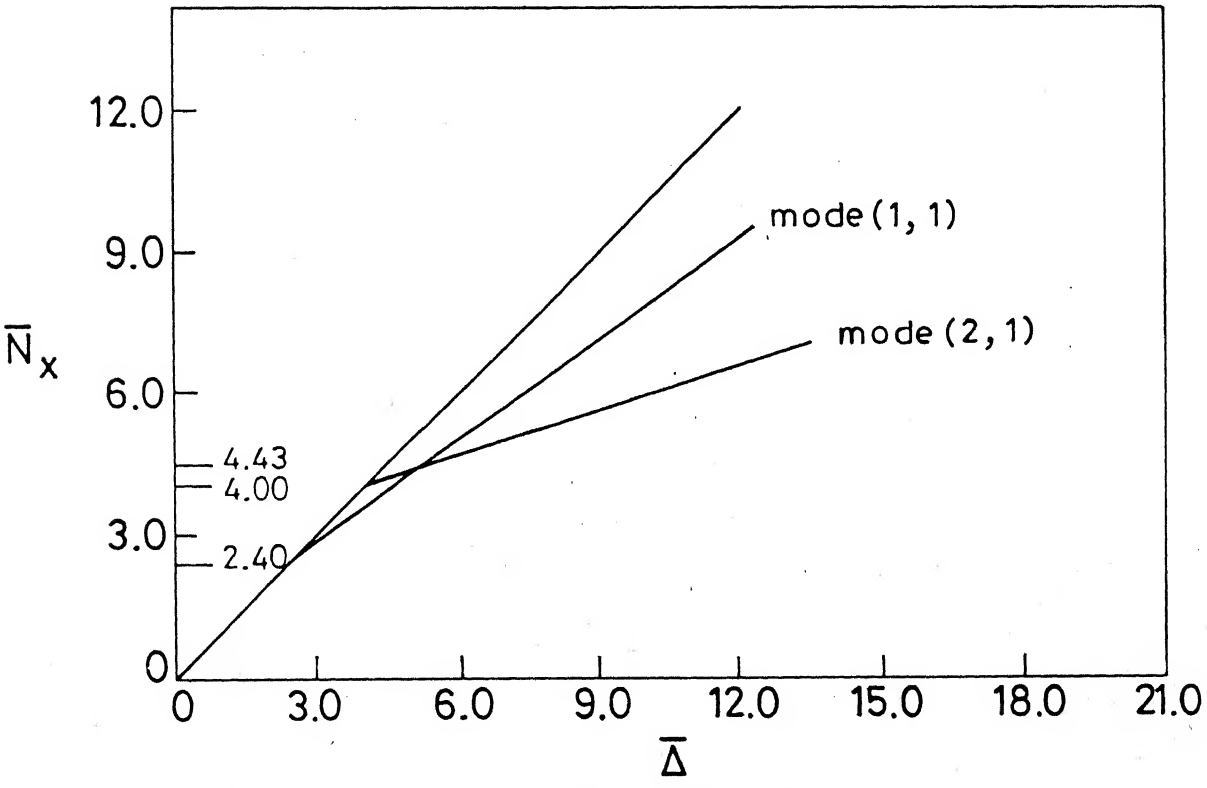

(b) $\lambda = 2.0$, FE condition

Fig. 4.10 Load-shortening curves for boron-epoxy plate.

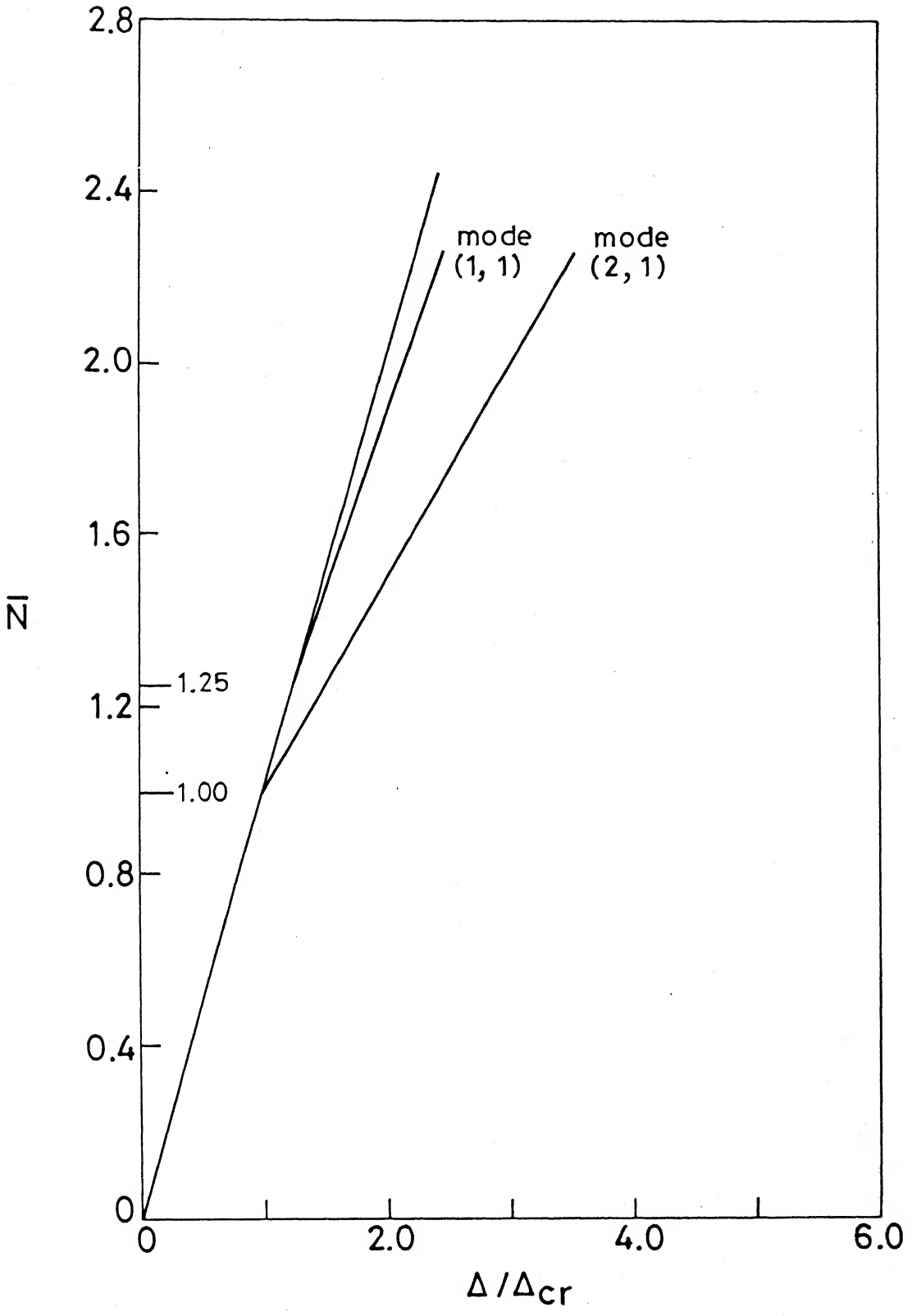

Fig. 4.11 Load-shortening curves for boron-epoxy plate, $\lambda = 3.0$, FE condition.

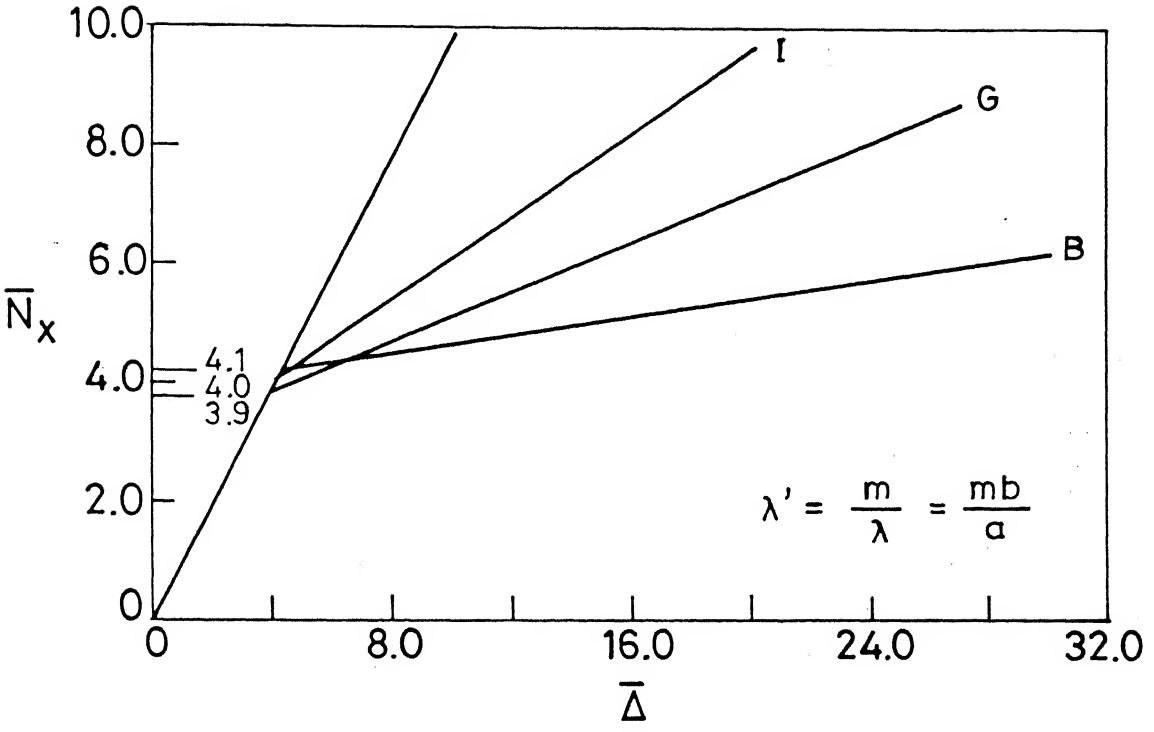

(a) ME condition

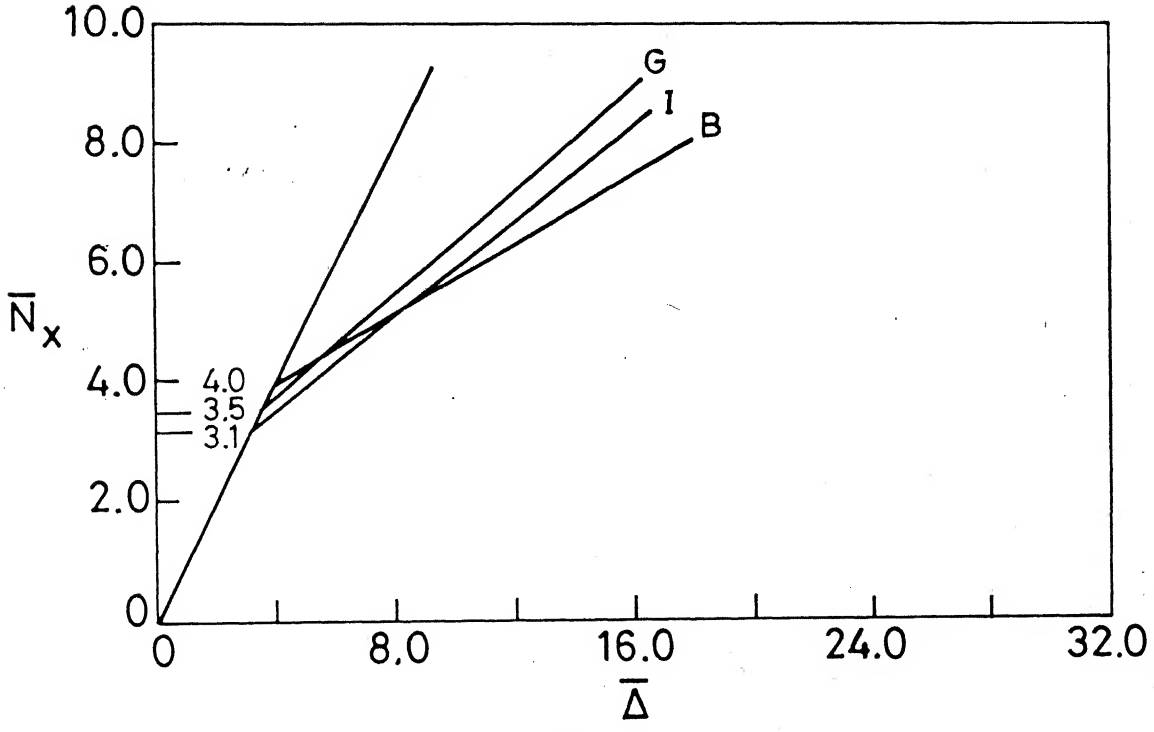

(b) FE condition

Fig. 4.12 Load-shortening curves for plates with $\lambda' = 1.0$.

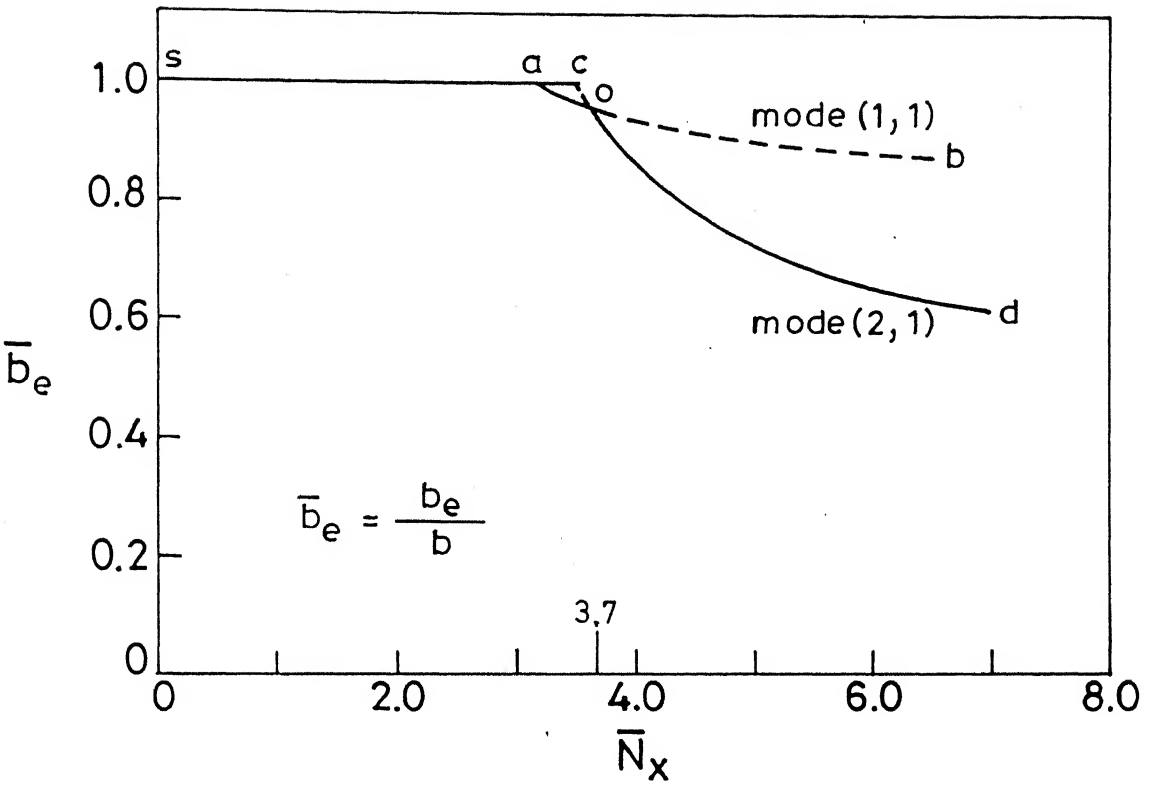

(a) $\lambda = 2.0$, FE condition

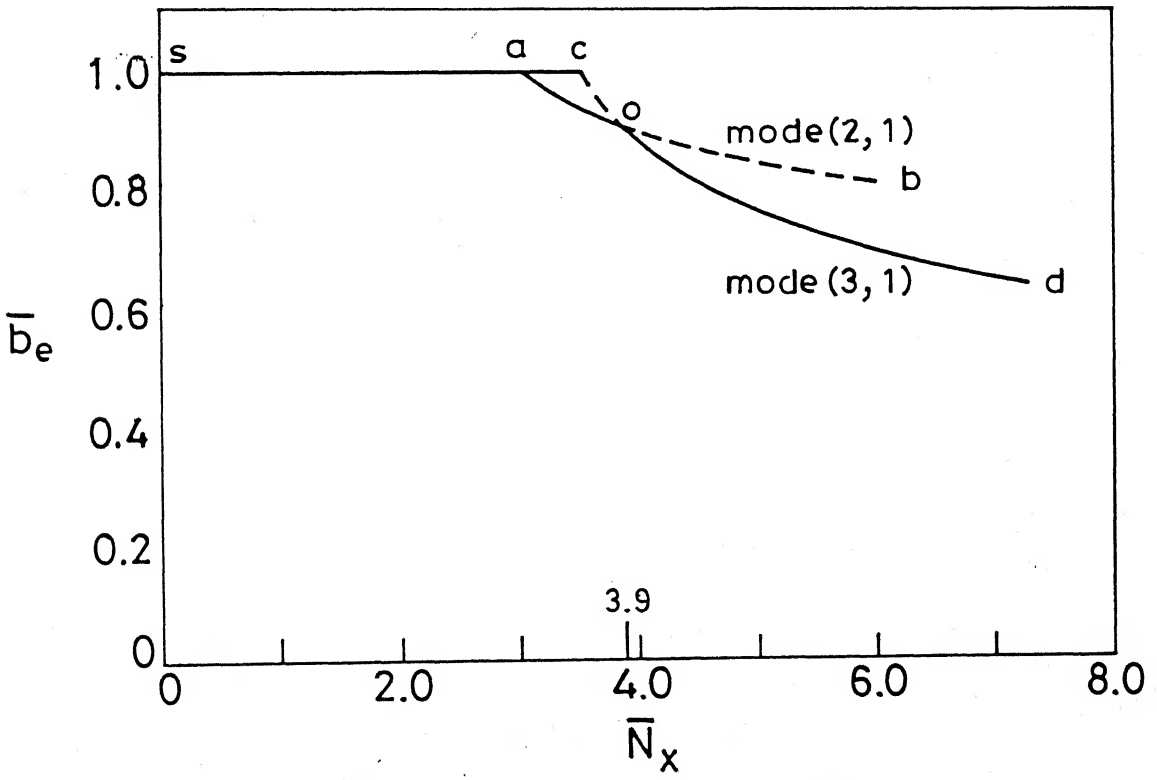

(b) $\lambda = 3.0$, FE condition

Fig. 4.13 Effective with curves for glass-epoxy plates.

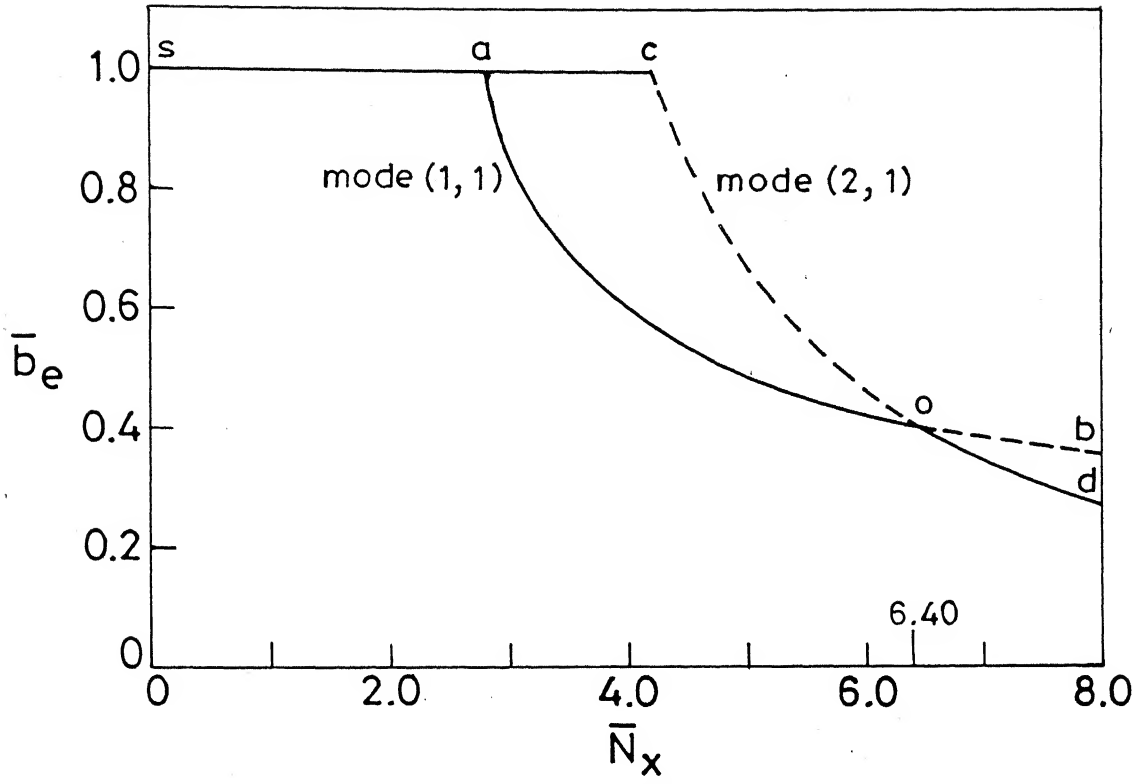

(a) $\lambda = 2.0$, ME condition

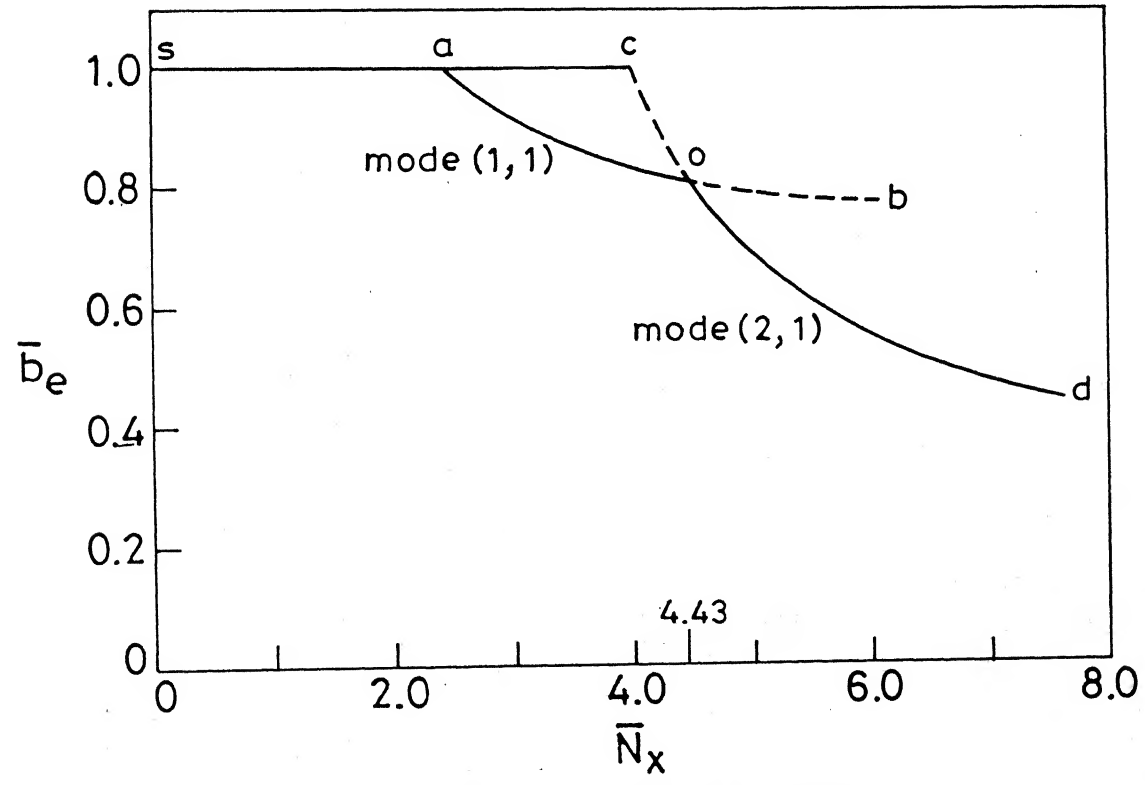

(b) $\lambda = 2.0$, FE condition

Fig. 4.14 Effective width curves for a boron-epoxy plate.

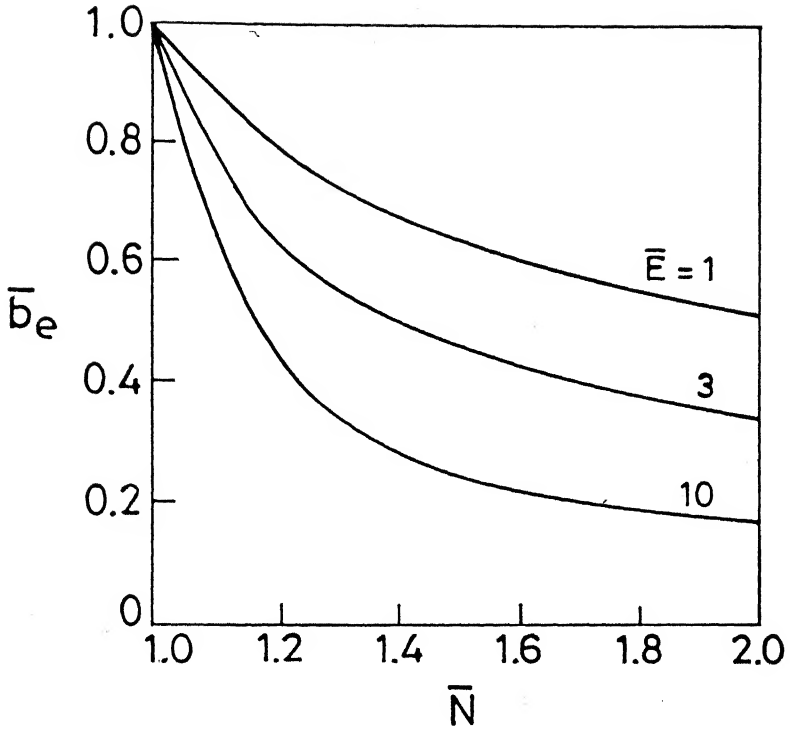

(a) ME condition

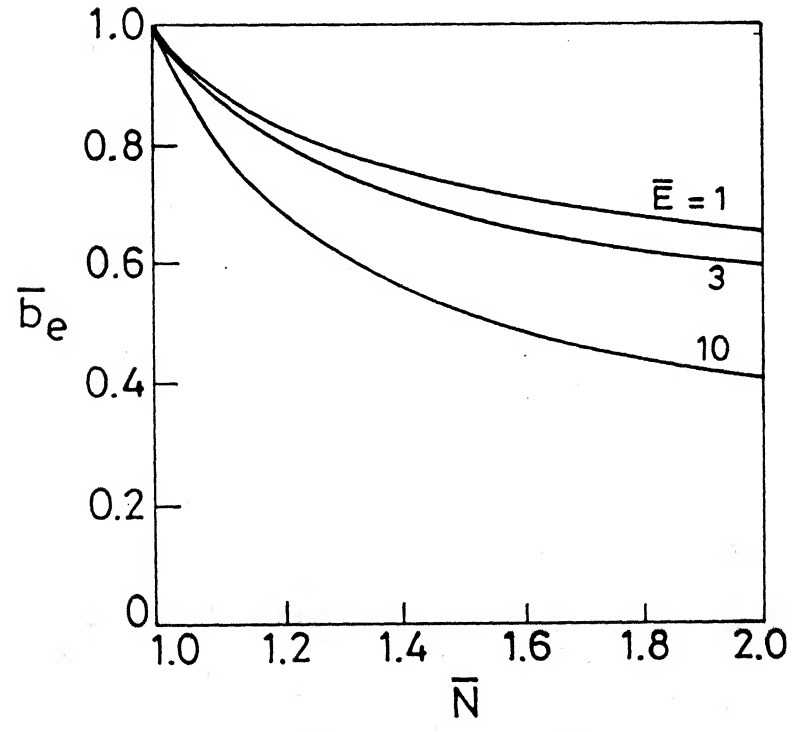

(b) FE condition

Fig. 4.15 Effective width curves for plates with $\lambda' = 1.0$.

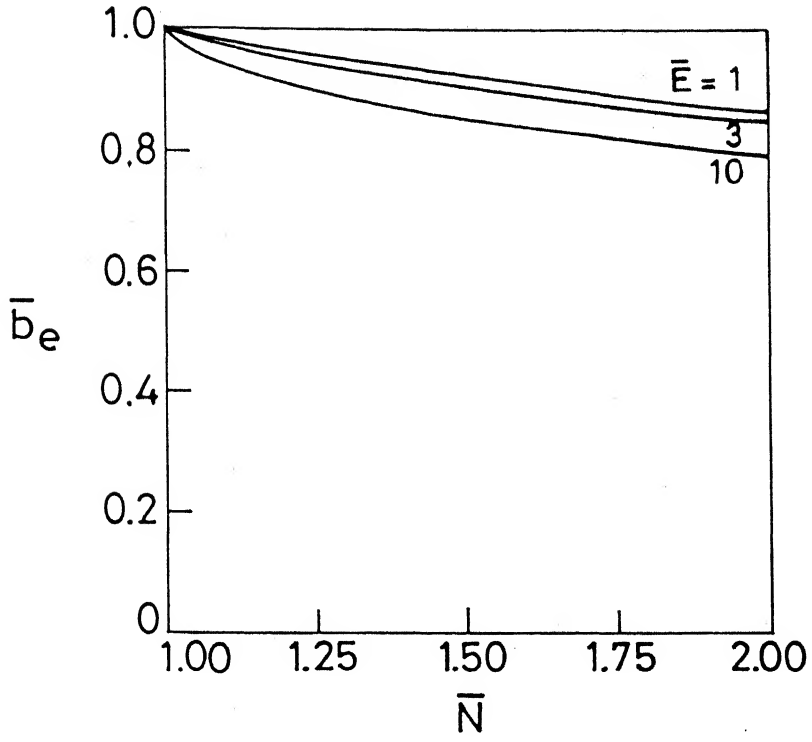

(a) $\lambda' = 0.50$, FE condition

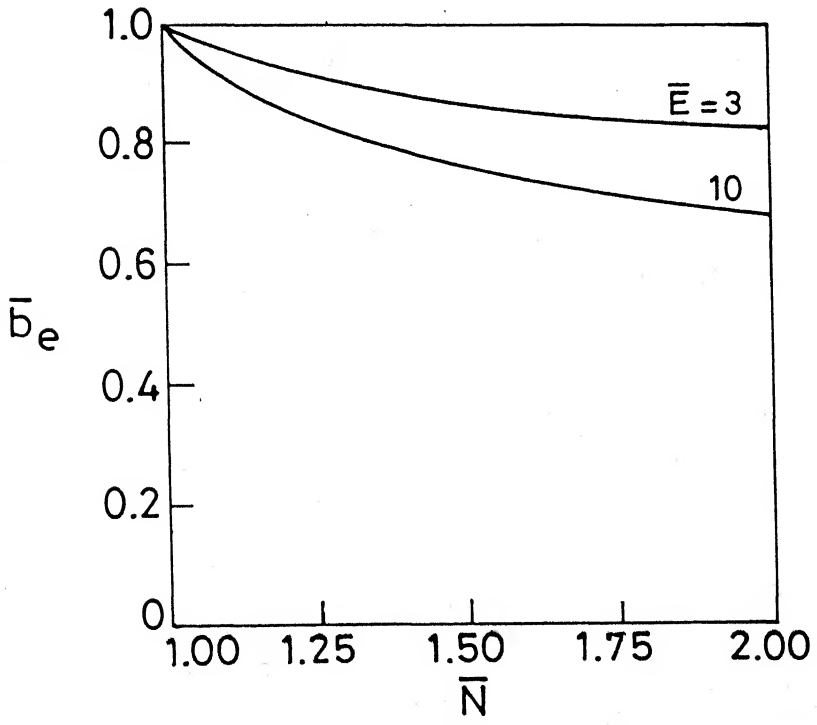

(b) $\lambda' = 0.67$, FE condition

Fig. 4.16 Effective width curves.

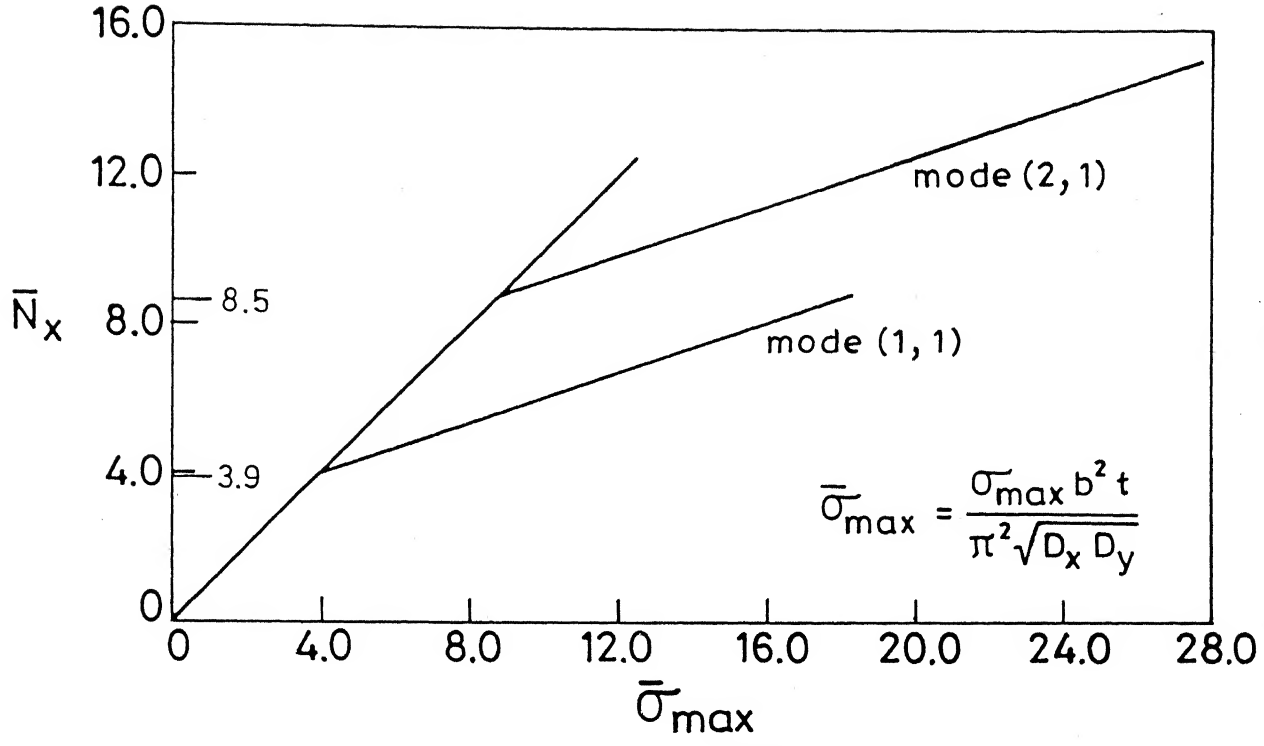

(a) Glass-Epoxy, ME condition

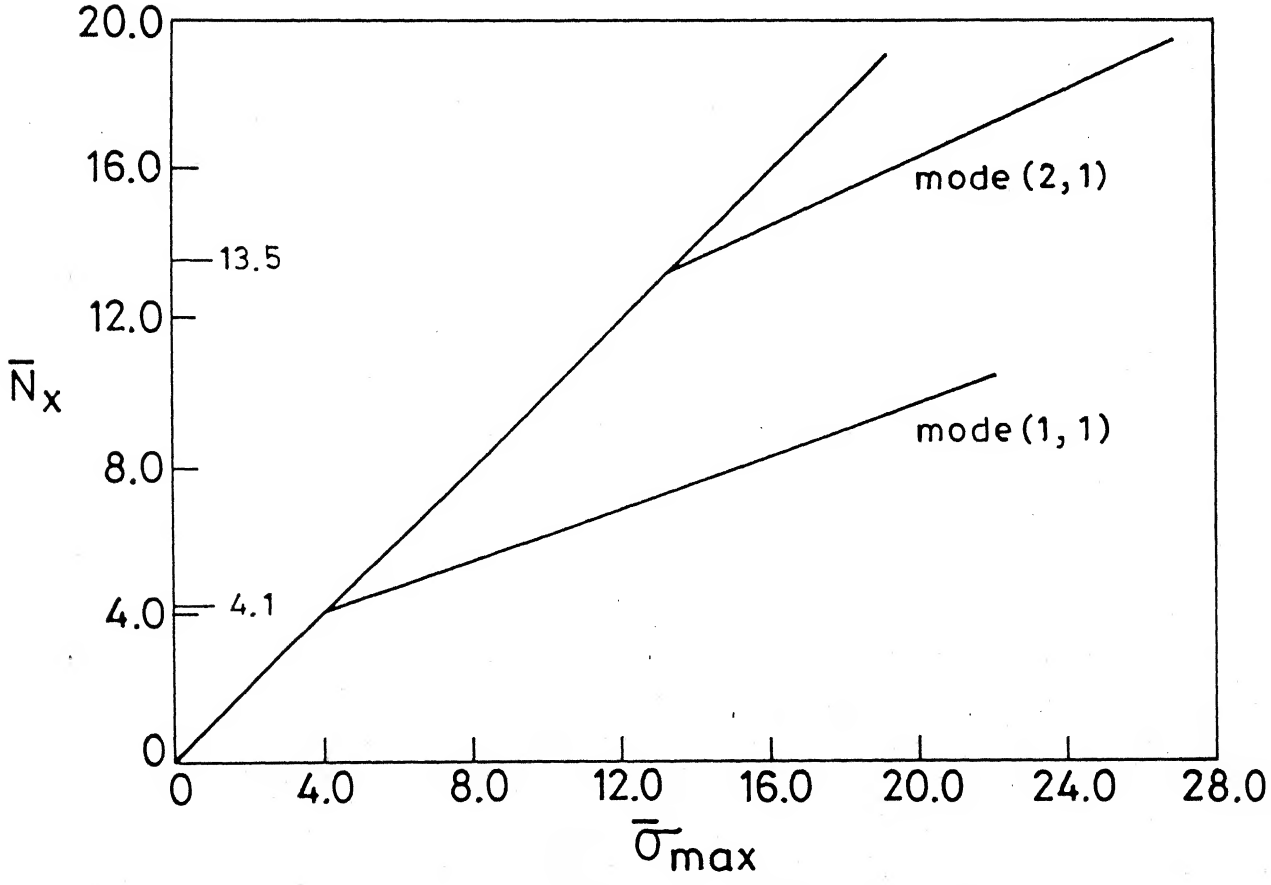

(b) Boron-Epoxy, ME condition

Fig. 4.17 Variation of maximum longitudinal stress with the load for square plates.

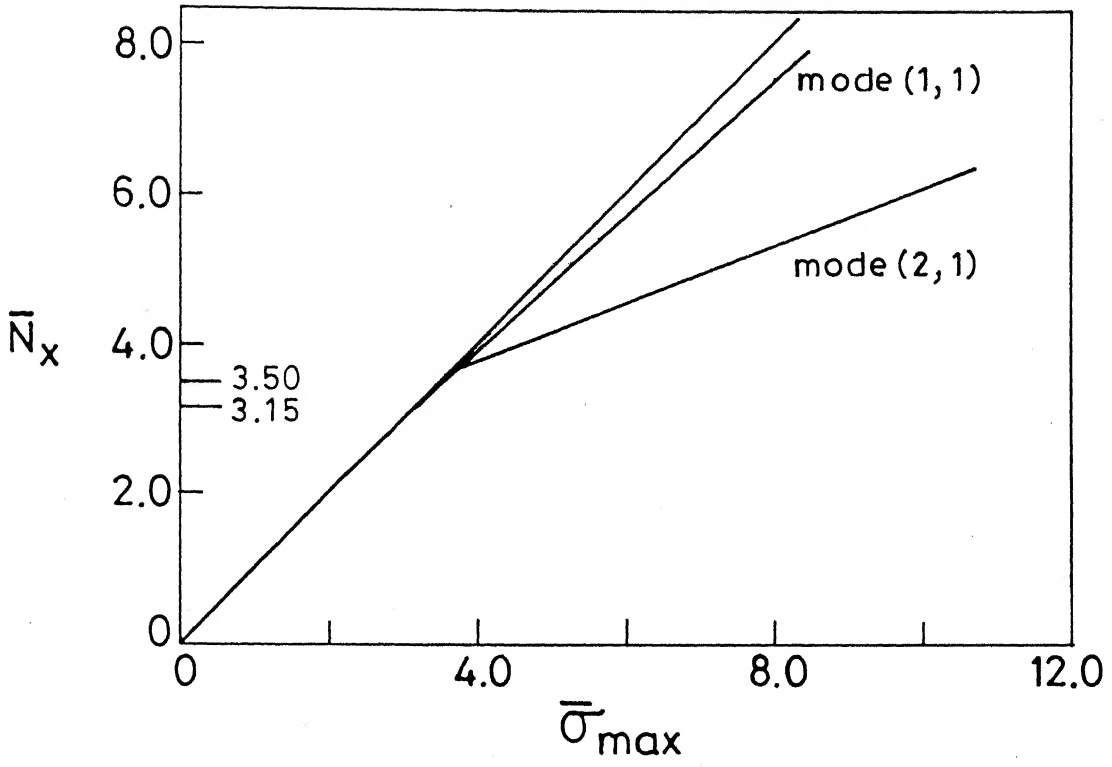

(a) $\lambda = 2.0$, FE condition

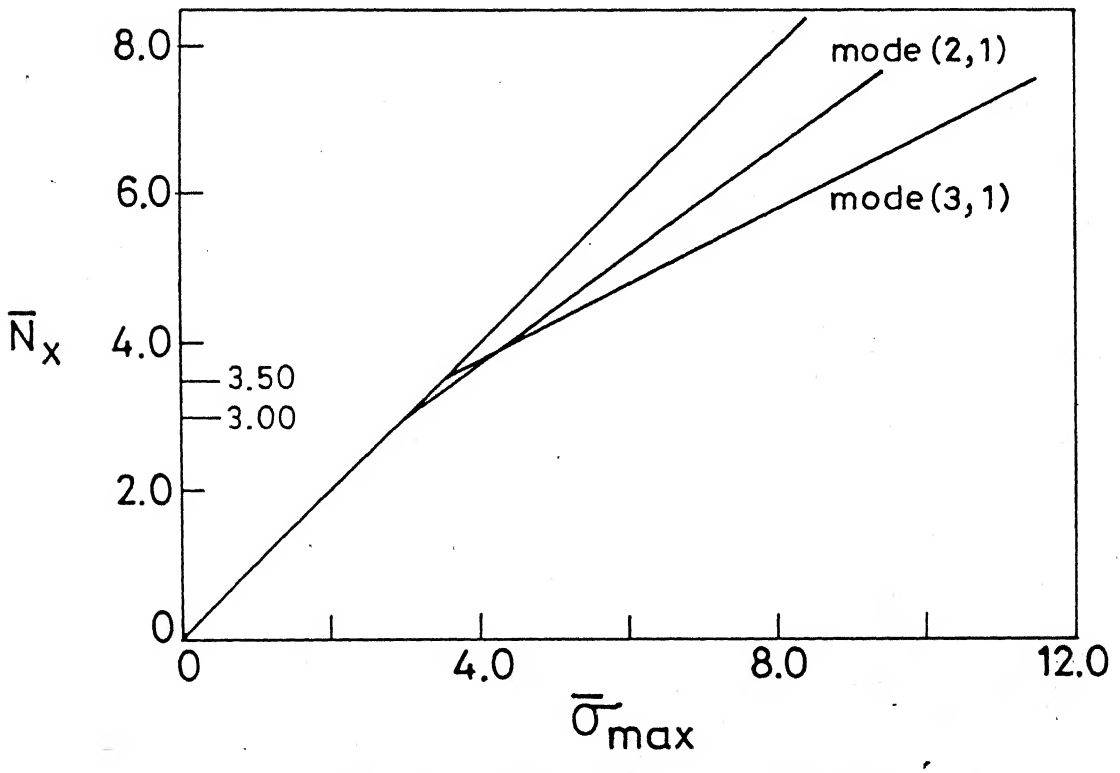

(b) $\lambda = 3.0$, FE condition

Fig. 4.18 Variation of maximum longitudinal stress with the load for glass-epoxy plates.

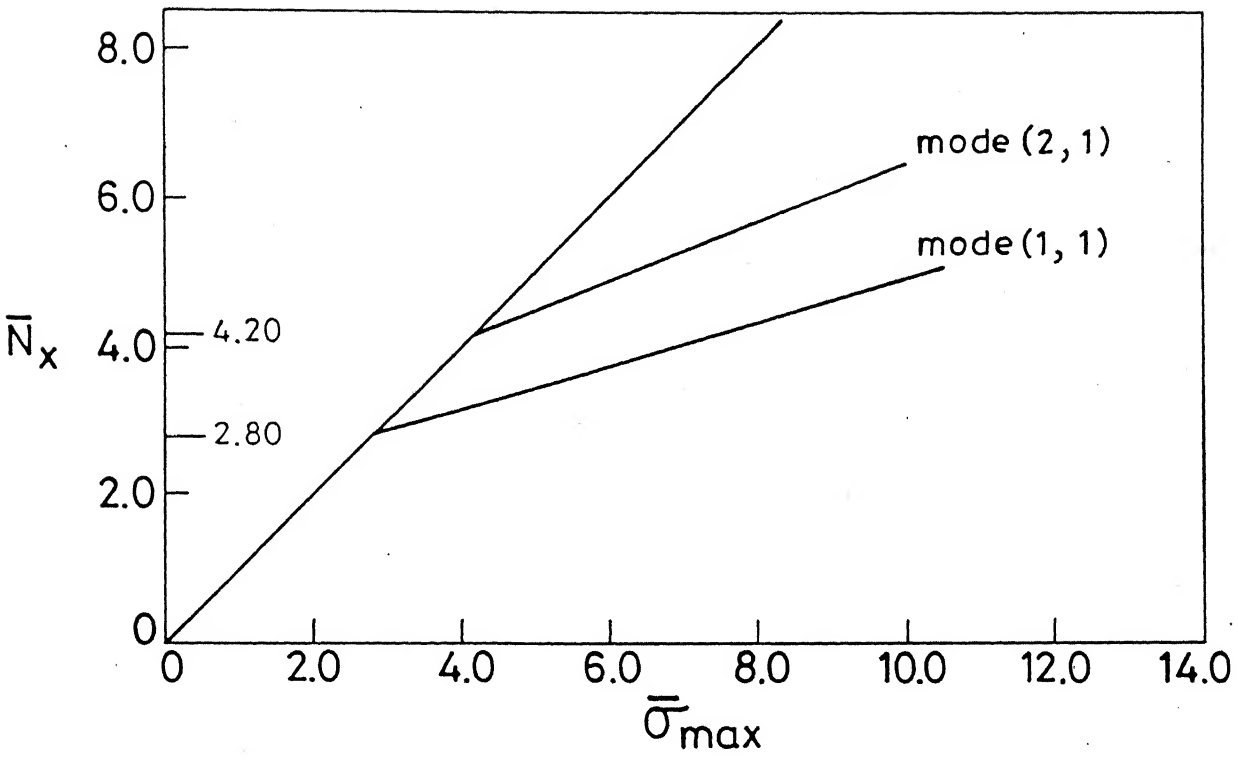

(a) $\lambda = 2.0$, ME condition

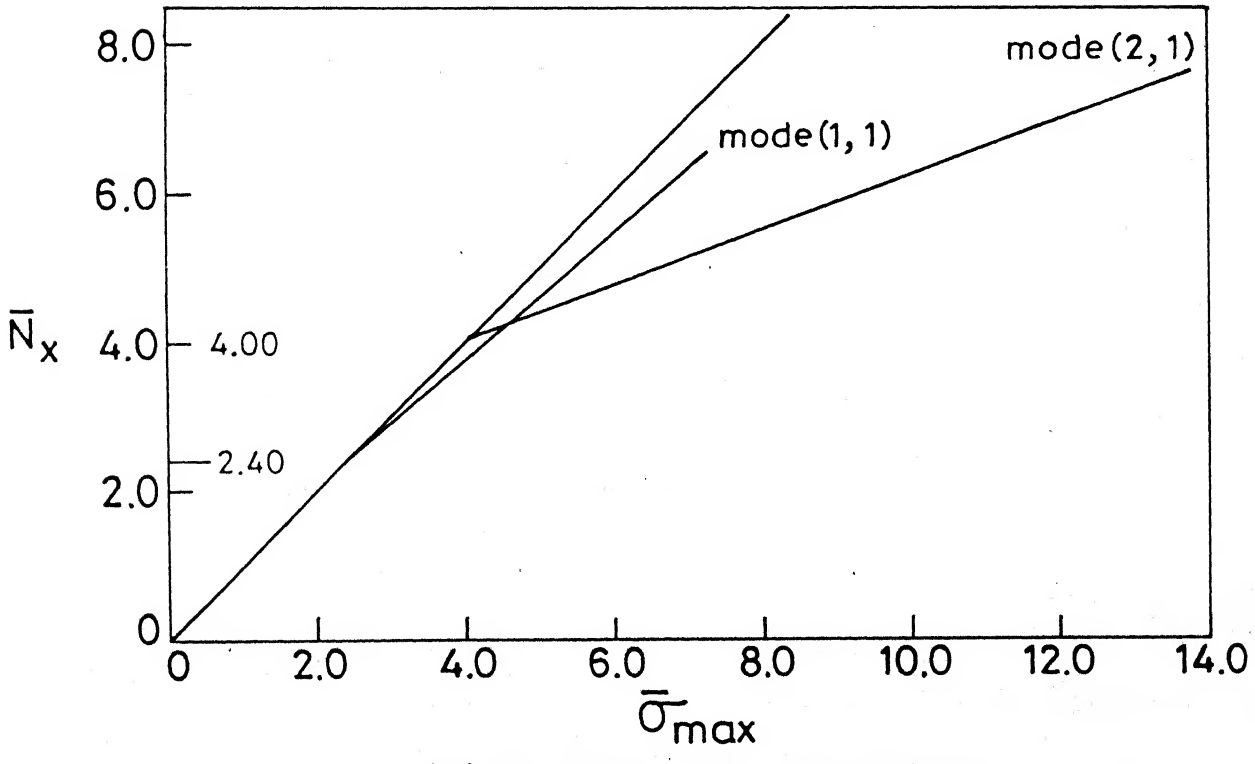

(b) $\lambda = 2.0$, FE condition

Fig. 4.19 Variation of maximum longitudinal stress with the load for boron-epoxy plate.

CHAPTER 5

PLATES SUBJECTED TO SHEAR LOADING

5.1 INTRODUCTION

For buckling to take place, it is not necessary that the plate be loaded in compression only. A system of forces that can cause compressive stresses anywhere in the plate is responsible for its instability. The pure shear, for example, produces compression on planes inclined at 45^{o} and when these forces become increasingly large, buckling takes place. Since the compressive stresses are developed on planes that are inclined, the buckle pattern tends to become skew. In case of long plates, it is reported (Gerard, 1962) that the half wave length equals to 1.25 times the width.

From the review of literature, presented in Chapter 1, it is seen that not much work has been done on the postbuckling analysis of shear loaded plates. Moreover, the Finite Element Method has hardly been attempted. In this chapter, simply supported isotropic and orthotropic rectangular plates, subjected to pure shear load, are analysed with the view to study their postbuckling behavior.

5.2 ANALYSIS DETAILS

In Chapters 3 and 4, only a quadrant of the plate was considered because of the symmetry with respect to loading as well as geometry. In case of a plate subjected to pure shear, symmetry with respect to loading is violated. Hence, the full

plate needs to be analysed, as shown in Figures 5.1. It is discretized in 16 equal 4-noded rectangular finite elements. A uniform load (in x-direction) along the edge y = b (in the form of concentrated loads at the edge nodes) is applied, while the edge y = 0 is restrained to move in its own direction, thus causing a pure shear. The other pair of edges viz. x = 0, a are not allowed to translate in the y-direction. These inplane conditions correspond to the NASTRAN model as reported by Agarwal (1981). The plate is assumed simply supported on all the four edges and hence the appropriate boundary conditions of zero deflection and zero moment, namely the Eq. (1.4) are applied.

Buckling Pattern/Mode

Unlike a longitudinally compressed plate, a plate subjecte to shear loading, does not buckle in a simple (uncoupled or couple mode with n equal to unity. The buckling pattern is actually a mixture of various uncoupled modes with different combination of m and n values. In the case of an isotropic plate, it is well known that the resulting buckled pattern is such that the sum (m+n), for each constituent (uncoupled) mode is either even or odd. When (m+ is even, it requires the slopes to be zero ($\partial w/\partial x = \partial w/\partial y = 0$) at the centre of the plate, while for odd values of (m+n), the condi of zero deflection (w = 0) is needed. The two patterns (modes) may, therefore, be called as symmetric and anti-symmetric, respec ively. Hence, for a plate of given aspect ratio, either of these modes will yield the minimum critical load.

To initiate a symmetric mode, a small lateral load is applied at the centre, 'O' of the plate (Figure 5.1a) and for an anti-symmetric mode, two loads (in opposite directions) at nodes M and N are applied as has been the case with plates under edge compression. But, the condition of zero slope for the symmetric mode and the zero deflection condition for the anti-symmetric mode are imposed only at the centre of the plate O and not on the whole line PR, so that buckling pattern is free to take its own shape.

5.3 CURVES FOR SHEAR BUCKLING COEFFICIENTS

For a simply supported, rectangular, isotropic plate, under the edge shear, the critical load N_{xycr} (per unit length) is given by (Kumar, 1985)

$$N_{xycr} = k_s \frac{\pi^2 D}{b^2} \qquad (5.1)$$

where k_s is the shear buckling coefficient. In terms of critical shear stress τ_{cr} the above formula may be re-written as :

$$\tau_{cr} = k_s \frac{\pi^2 E}{12(1 - \nu)^2} \left(\frac{t}{b}\right)^2 \qquad (5.2)$$

In these equations b is always the shorter dimension of the plate, as all the edges are loaded in shear. Hence, in this case the aspect ratio $\lambda (= a/b) < 1$ does not have any meaning; λ will always be ≥ 1.0. For an orthotropic plate, the corresponding expression for the critical load is

$$N_{xycr} = k_s \frac{\pi^2 \sqrt{D_x D_y}}{b^2} \qquad (5.3)$$

In Eq. (5.1) or (5.3), the expression for k_s is not a simple function of m,n, and λ, unlike the case for plates under edge compression; in fact k_s has to be evaluated numerically for each case.

Based on Eq. (5.1), curves for the shear buckling coefficien k_s, for isotropic plates, are shown in Figure 5.2.

Following important points are worth noting with respect to these curves :

i) Curves start from $\lambda = 1.0$ and the value of k_s is highest at this aspect ratio. The minimum value of k_s is 5.35 for $\lambda \to \infty$ (i.e. a long plate).

ii) Each curve is the combination of curves corresponding to m (= 1,2,3,...) and n (= 1,2,3,...) number of half waves in x- and y-direction, respectively.

iii) The symmetric pattern (of one large buckle) and the anti-symmetric pattern (of two large buckles) intersect at $\lambda = 2.05$ and thus from $\lambda = 1.0$ to 2.05, the symmetric pattern gives the minimum critical load. Similarly, from $\lambda = 2.05$ to 3.50 (where the next two curves of anti-symmetr and symmetric patterns meet), the anti-symmetric pattern governs the buckling, and so on.

The critical load and even the postbuckling path is independent of the direction of the shear (Figures 5.1b,c) for isotropic as well as for specially orthotropic plates. However,

for anisotropic plates (not discussed here) there are two different critical loads and the postbuckling paths for the two alternative directions of the shear (Zhang and Matthews,1984).

5.4 ILLUSTRATIVE EXAMPLES

Following illustrative examples are taken in order to study the postbuckling behaviour of isotropic and orthotropic plates under shear :

I : square plate ($\lambda = 1.0$); 1.0 m x 1.0 m and 10 mm thick, E = 200 GPa , ν = .316, buckling in symmetric and anti-symmetric modes.

II : rectangular plate ($\lambda = 1.5$); 1.5 m x 1.0 m and 10 mm thick, E = 200 GPa , ν = .316 , buckling in symmetric and anti-symmetric modes.

III : rectangular plate ($\lambda = 2.5$); 2.5 m x 1.0 m and 10 mm thick, E = 200 GPa , ν = .316, buckling in symmetric and anti-symmetric modes.

IV : Glass-Epoxy square plates ($\lambda = 1.0$); 1.0 m x 1.0 m and 10 mm thick, E_x = 42 GPa, E_y = 14 GPa, G_{xy} = 7 GPa, ν_x = .25, ν_y = .0833, buckling in symmetric and anti-symmetric modes.

V : Boron-Epoxy, square plate ($\lambda = 1.0$); 1.0 m x 1.0 m and 10 mm thick, E_x = 210 GPa, E_y = 21 GPa, G_{xy} = 7 GPa, ν_x = .30, ν_y = .03, buckling in symmetric and anti-symmetric modes.

5.5 NUMERICAL RESULTS

5.5.1 Critical Loads

As before, the critical loads are obtained from the load-deflection/shear displacement curves (ref. Section 3.4.1), for each example. The values of shear buckling coefficients k_s are tabulated in Table 5.1. These values for an isotropic plate, are compared with those obtained by Stein (1947), both for symmetric as well as for anti-symmetric modes. The agreement, between the two set of values is found to be very good.

Table 5.1 Comparison of shear buckling coefficients k_s

Isotropic plates

λ $(= \frac{a}{b})$	Mode	Value of k_s	
		Exact (Stein,1947)	Present work
1.0	S	9.35	9.43
1.0	A	11.63	11.76
1.5	S	7.07	7.11
1.5	A	7.97	8.04
2.5	S	6.29	6.34
2.5	A	6.06	6.12

S : Symmetric A : Antisymmetric

Orthotropic plates

λ = 1.0, Glass-Epoxy, Symmetric Mode : k_s = 8.65

λ = 1.0, Boron-Epoxy, Symmetric Mode : k_s = 9.05

5.5.2 Load-Deflection/Shear Displacement Curves

The applied shear load N_{xy} along the edges is non-dimensionalized as $\bar{N}_{xy} = N_{xy}\, b^2/\pi^2 D$ for isotropic plates and as $N_{xy}\, b^2/\pi^2 \sqrt{D_x D_y}$ for orthotropic plates. The load is also expressed as the load ratio $\bar{N}$ ($= N_{xy}/N_{xycr} = \bar{N}_{xy}/k_s$), where N_{xycr} is the critical shear load. Load-deflection curves between $\bar{N}$ and $\bar{w}_o$ ($= w_o/t$; w_o being the maximum lateral deflection, as usual) are shown in Figure 5.3, for isotropic plates, having $\lambda = 1.0$, 1.5 and 2.5. Both, symmetric as well as anti-symmetric modes are considered. Figure 5.4(a) shows such curves for glass-epoxy and boron-epoxy square plates. To have an overall picture of the shape of the buckle patterns, the deflection contours are drawn on the plan of the plate, (Figures 5.6 - 5.8).

Corresponding to the term 'shortening' (Δ), in a longitudinally compressed plate, a term 'shear displacement' (Δ_{sh}), has been used in the present case of a shear loaded plate. This may be defined as the relative displacement of the longitudinal edges, parallel to itself, and is normalized as $\bar{\Delta}_{sh}$ ($= \Delta_{sh}\, G\, bt/\pi^2 D$) for an isotropic plate and as $(\Delta_{sh}\, G_{xy}\, b\, t)/(\pi^2 \sqrt{D_x D_y})$ for an orthotropic plate. Plots of load $\bar{N}_{xy}$ versus shear displacement $\bar{\Delta}_{sh}$ are presented in Figure 5.5 for isotropic and in Figure 5.4(c) for orthotropic plates (glass-epoxy and boron-epoxy square plates buckling in symmetric modes). The $\bar{N}_{xy} - \bar{\Delta}_{sh}$ curve for a plate with $\lambda = 2.5$ (Figure 5.5) is close enough to that of Stein (1985), who has analysed a long plate only with edges held straight.

5.5.3 Stresses

For each illustrative example, stresses have also been calculated. The shear stress values have been marked on the edges of the plates in Figures 5.6 - 5.8. Figure 5.9 depicts the variation of maximum shear stress with the load, for plates with $\lambda = 1.0$, 1.5 and 2.5 and buckling in symmetric or anti-symmetric modes. Similar curves for glass-epoxy and boron-epoxy square plates are shown in Figure 5.4(b).

The direct membrane stresses σ_x and σ_y are zero, in a shear loaded plate, until buckling starts. In the postbuckling range, these stresses, which could be tensile or compressive, also get developed. The maximum values of longitudinal tensile stress $\sigma_{x\ max}$ and transverse tensile stress $\sigma_{y\ max}$ are normalized with respect to the critical load N_{xcr} (of uniaxial compression) as $\bar{\sigma}_{x\ max} = \sigma_{x\ max}\ t/N_{xcr}$ and $\bar{\sigma}_{y\ max} = \sigma_{y\ max}\ t/N_{xcr}$, respectively. These are plotted against the load ratio $\bar{N}$ in Figure 5.10, for isotropic, glass-epoxy and boron-epoxy square plates, buckling in symmetric mode. The magnitude of the longitudinal tensile stress σ_x, produced in an isotropic plate with $\lambda = 2.5$, at the load $\bar{N} = 1.5$ is compared with the long plate results of Stein (1985). This value in the present case is $0.39\ N_{xcr}$ while for the long plate it is approximately $0.30\ N_{xcr}$. The difference in the two values is, perhaps, due to the fact that Stein maintained the loaded edges of the long plate to be straight.

5.6 DISCUSSIONS

5.6.1 Deflections

Some conclusions drawn from the various deflection curves, for the shear loaded plates are :

(i) The deflection $\bar{w}_o$ increases with the aspect ratio of the plate for the same load ratio $\bar{N}$ and for the same mode (Figure 5.3).

(ii) For a particular value of $\bar{N}$ the deflection $\bar{w}_o$ is less for a shear loaded plate than for a plate loaded in compression (Figures 5.3a, 4.7a).

(iii) In regions near the corners of the compression diagonal of a buckled plate the lateral deflections are of opposite nature to that of the rest of the plate.

(iv) For the loads considered (upto about twice the critical load value), it is observed that the load-shear displacement lines, for all aspect ratios, are almost parallel (Figure 5.5).

(v) There is only a slight deviation of the postbuckled line from the original (prebuckled) line. This shows that for a shear loaded plate, the reduction in the shear stiffness after buckling is very small (about 11%)

(vi) As the $\bar{N}_{xy} - \bar{\Delta}_{sh}$ lines (for loads upto twice the critical corresponding to the two modes (symmetric and anti-symmetric) do not meet for the plate of any aspect ratio (Figure 5.5); the question of change of wave pattern fr a symmetric to an anti-symmetric mode (or vice versa) d

not arise. Stein (1985) also has stated that the mode at the instant of buckling remains same, in the initial postbuckling regime.

(vii) For orthotropic plates (glass-epoxy and boron-epoxy) the deflections $\bar{w}_o$ are greater than those of an isotropic plate for the same load ratio $\bar{N}$ and the mode; $\bar{w}_o$ increases with degree of orthotropy $\bar{E}$, (Figures 5.3a, 5.4a).

(viii) The reduction in shear stiffness decreases with the increase in value of $\bar{E}$; thus the shear displacement for a boron-epoxy plate is less than that for a glass-epoxy and for an isotropic plate, for the same load $\bar{N}_{xy}$ (Figures 5.4c, 5.5). It may be noted here that just the opposite observation holds for orthotropic plates loaded in compression.

5.6.2 Stresses

Following points are observed from the results on stresses:

(i) The variation in shear stress τ_{xy} is symmetrical with respect to the two diagonals of the plate.

(ii) The maximum value of the shear stress τ_{max} occurs at the two corners (diagonally opposite), for isotropic as well orthotropic plates, buckling in the mode corresponding to the minimum critical shear load, (e.g. for $\lambda = 1.0$, 1.5 in symmetric mode and for $\lambda = 2.5$ in anti-symmetric mode). τ_{xy} is minimum at the other two corners.

(iii) For plates of low aspect ratio (λ = 1.0, 1.5), buckling in an anti-symmetric mode, τ_{max} occurs at some distance (about one quarter) from the above corners (Figures 5.6, 5.7). Thus its position is at nodes 2,6,20 and 24 (Figure 5.1a).

(iv) The magnitude of the maximum longitudinal tensile stress $\sigma_{x\ max}$ and transverse tensile stress $\sigma_{y\ max}$ increases linearly with the load (Figure 5.10). For a particular value of the load ratio $\bar{N}$, $\bar{\sigma}_{x\ max}$ increases and $\bar{\sigma}_{y\ max}$ decreases with the increase in the value of $\bar{E}$ (Figure 5.10a,b).

(v) For the same value of $\bar{N}$, the stresses $\bar{\sigma}_{x\ max}$ and $\bar{\sigma}_{y\ max}$ reduce as the aspect ratio increases.

(vi) For a fixed value of the shear load $\bar{N}_{xy}$, the maximum shear stress $\bar{\tau}_{max}$ is greater in symmetric mode than in anti-symmetric mode, for plates with λ = 1.0, 1.5 and it is greater in anti-symmetric mode than in symmetric mode, for the plate with λ = 2.5 (Figures 5.6 - 5.8). This shows that the magnitude of the absolute maximum shear stress occurs when a plate buckles in its fundamental mode (mode in which the critical load is absolute minimum.

(vii) From Figure 5.8, it can be interpreted that for a given load ratio $\bar{N}$, the magnitude of $\bar{\tau}_{max}$ decreases with the increase in the aspect ratio. For example, the values $\bar{\tau}_{max}$ for λ = 1.0,1.5 and 2.5 are approximately 27.0, 20 and 14.4 respectively.

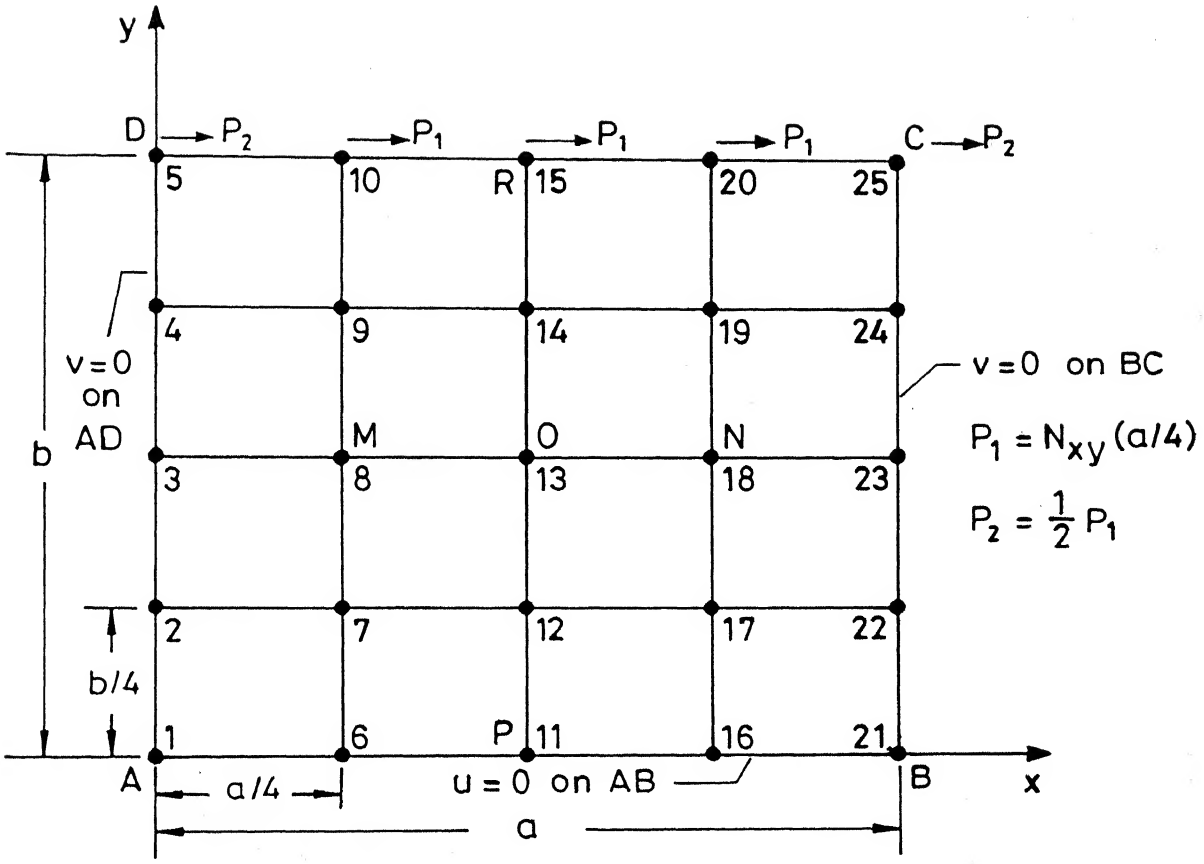

Fig. 5.1(a) Rectangular plate under shear loading.

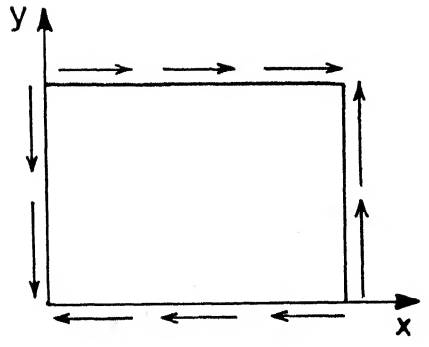

Fig. 5.1(b) Positive shear.

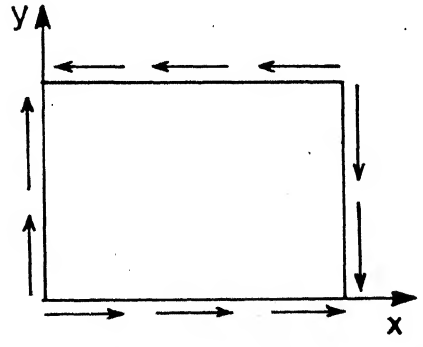

Fig. 5.1(c) Negative shear.

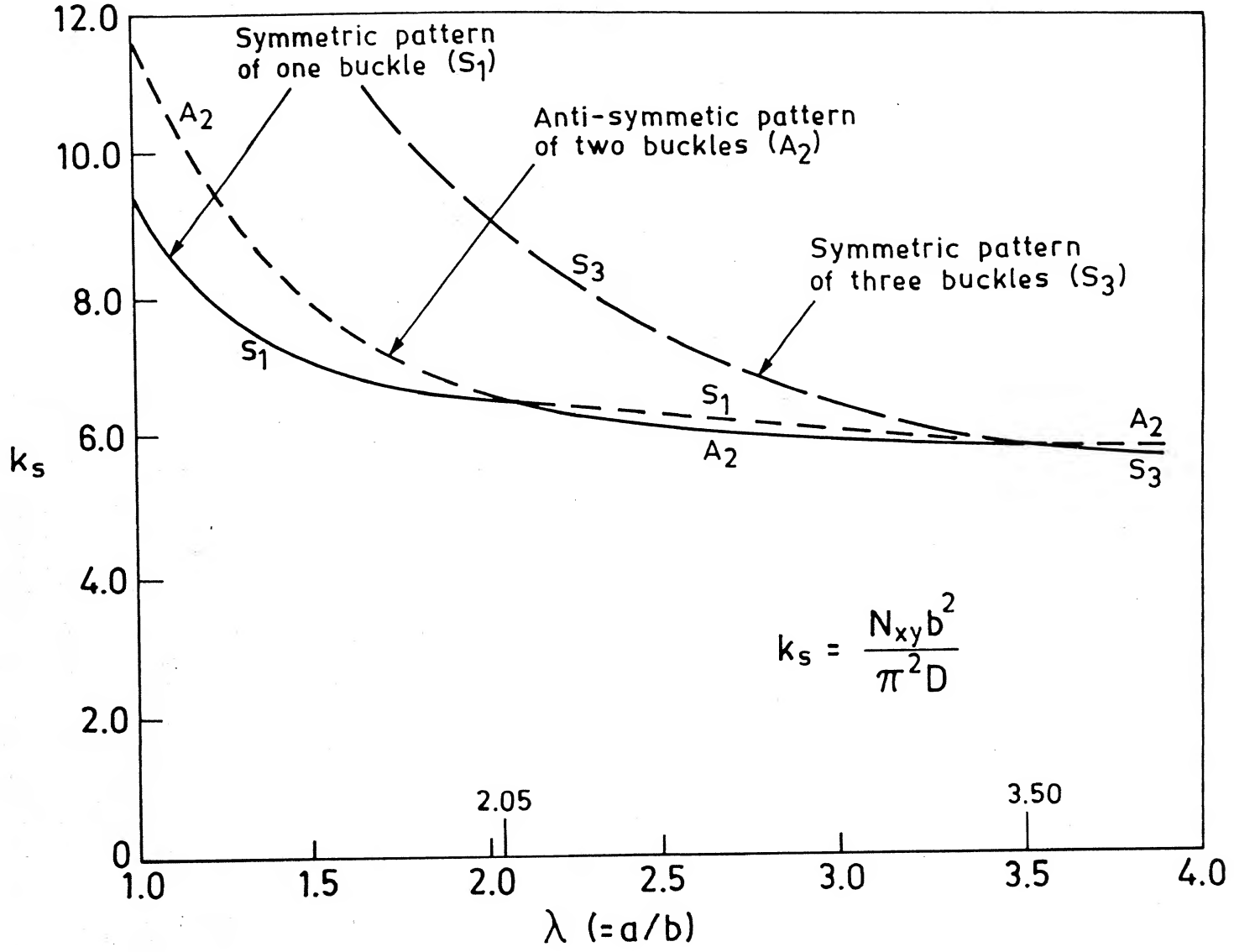

Fig. 5.2 Shear buckling coefficients for simply supported isotropic plates.

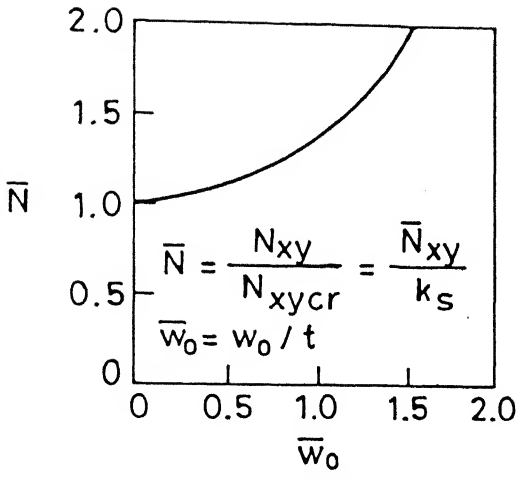

λ = 1.0, (a) Symmetric mode

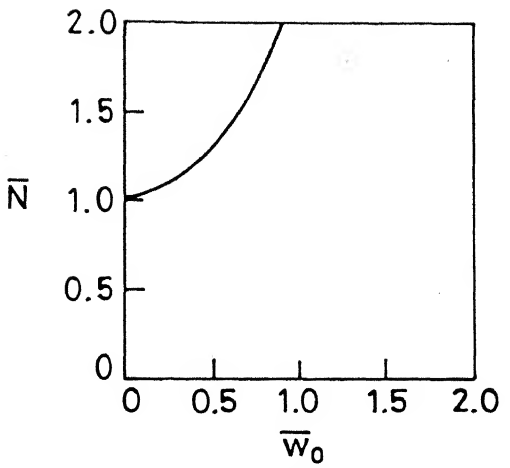

(b) Anti-symmetric mode

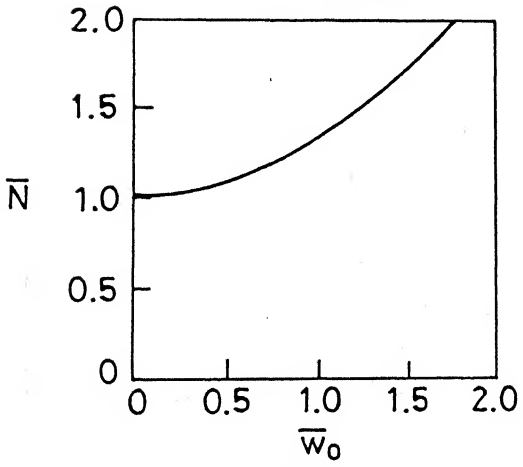

λ = 1.5, (c) Symmetric mode

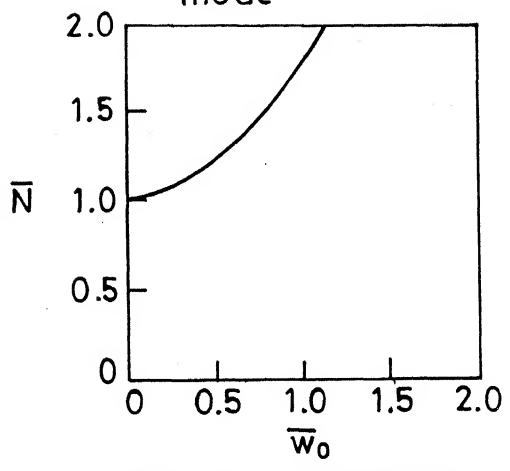

(d) Anti-symmetric mode

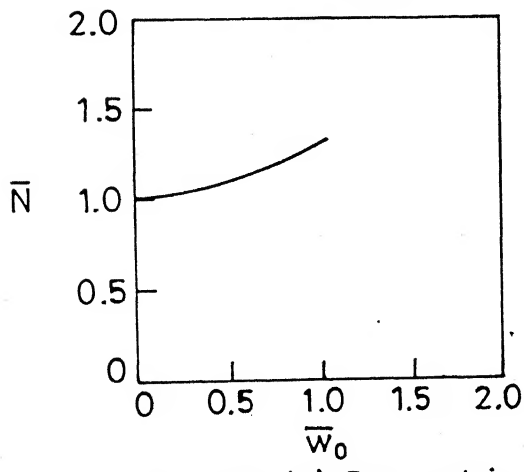

λ = 2.5, (e) Symmetric mode

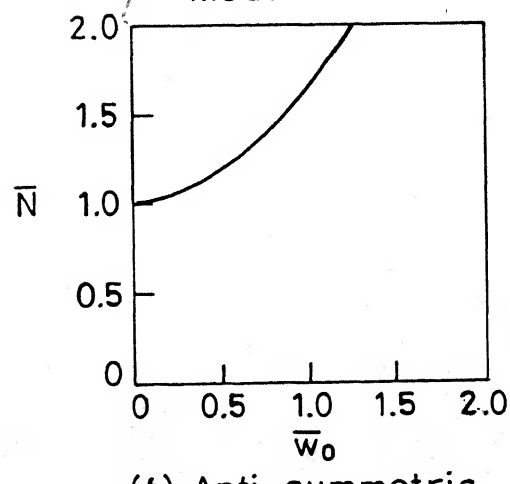

(f) Anti-symmetric mode

Fig. 5.3 Load-deflection curves for isotropic plates loaded in shear.

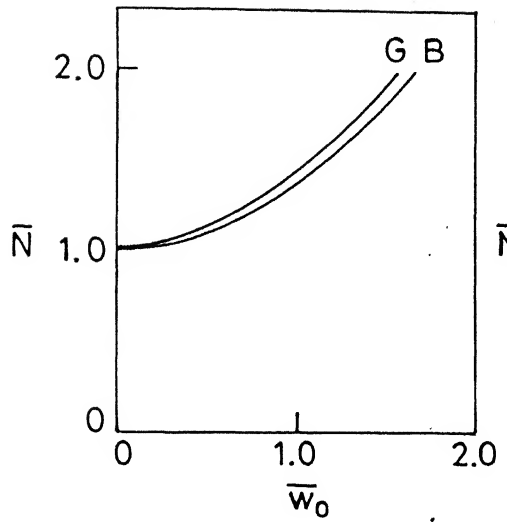

(a) Load-deflection curves

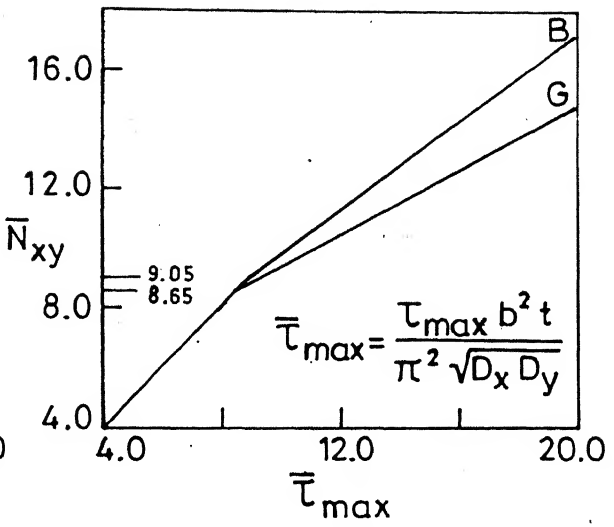

(b) Variation of maximum shear stress with load

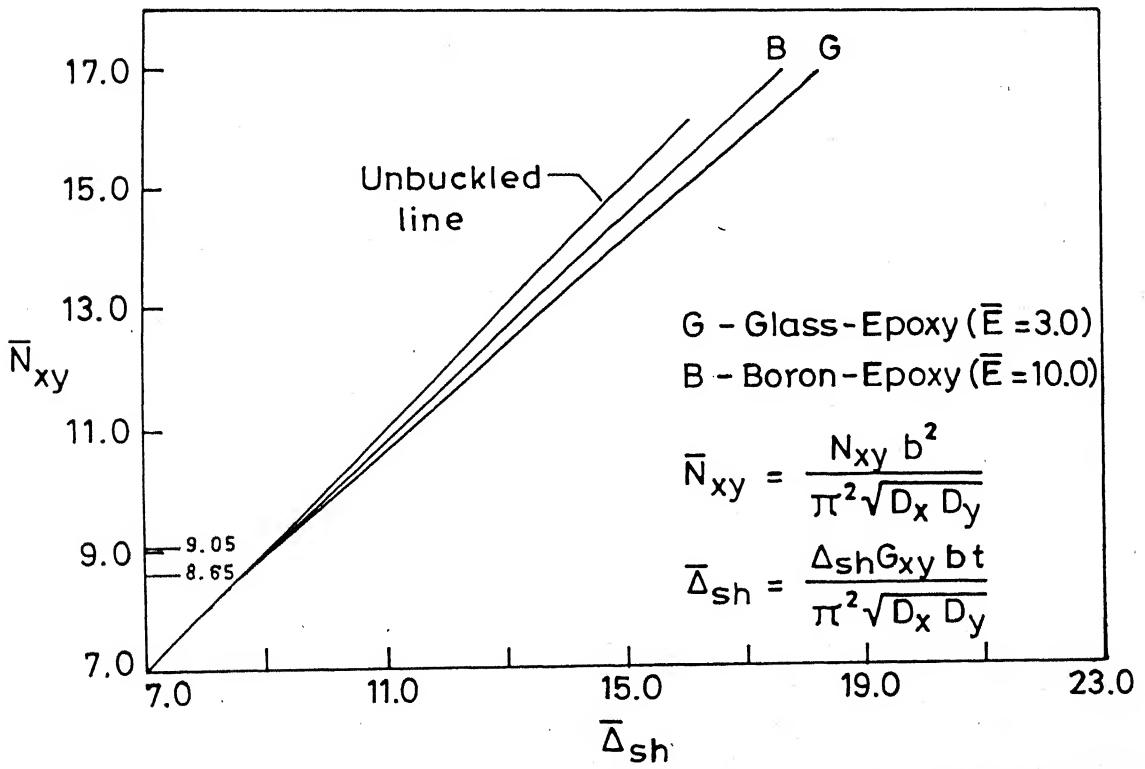

(c) Load-shear displacement curves

Fig. 5.4 Various curves for orthotropic square plates, loaded in shear, buckling in symmetric mode.

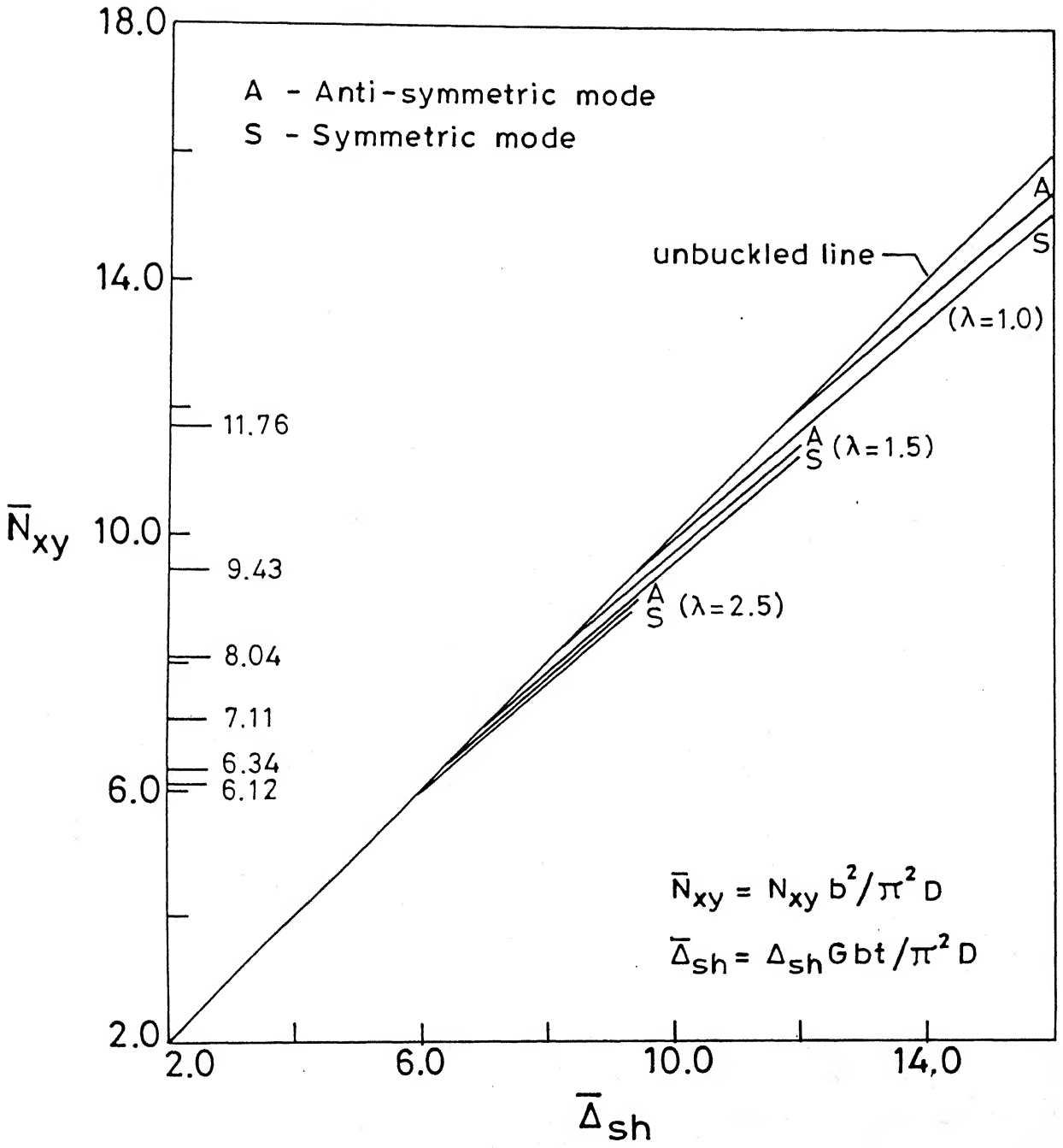

Fig.5.5 Load-shear displacement curves, for isotropic plates, loaded in shear.

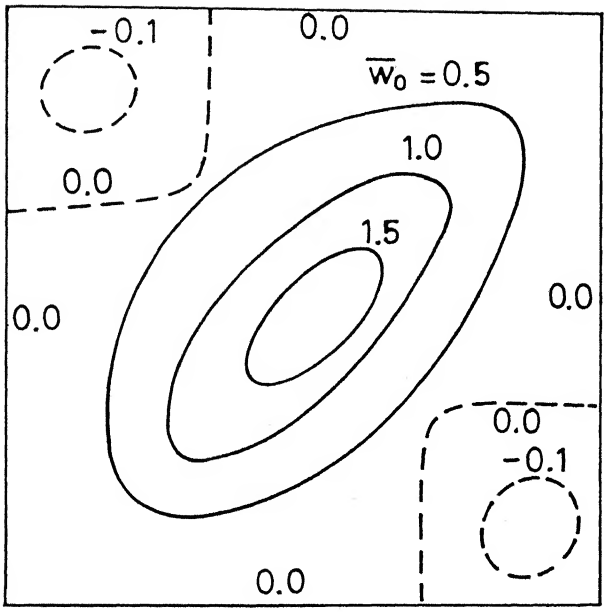

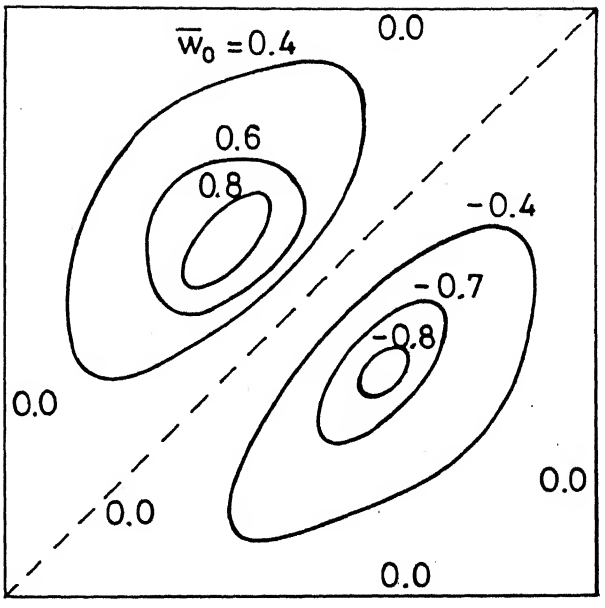

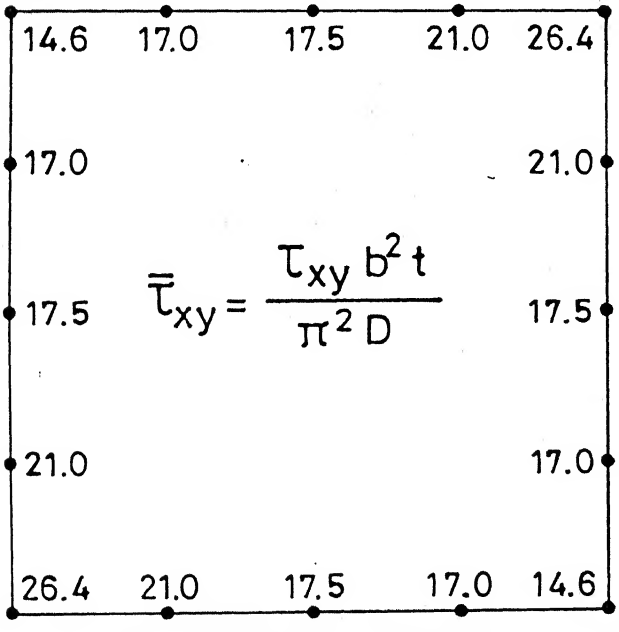

Symmetric mode
($\bar{N} = 2.05$, $\bar{N}_{xy} = 19.2$)

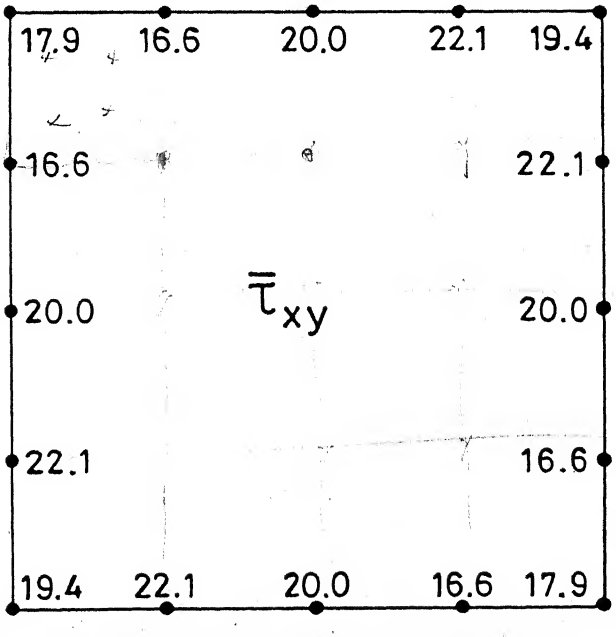

Anti-symmetric mode
($\bar{N} = 1.63$, $\bar{N}_{xy} = 19.2$)

Fig. 5.6 Deflection contours and shear stress distribution for isotropic square plate loaded in shear.

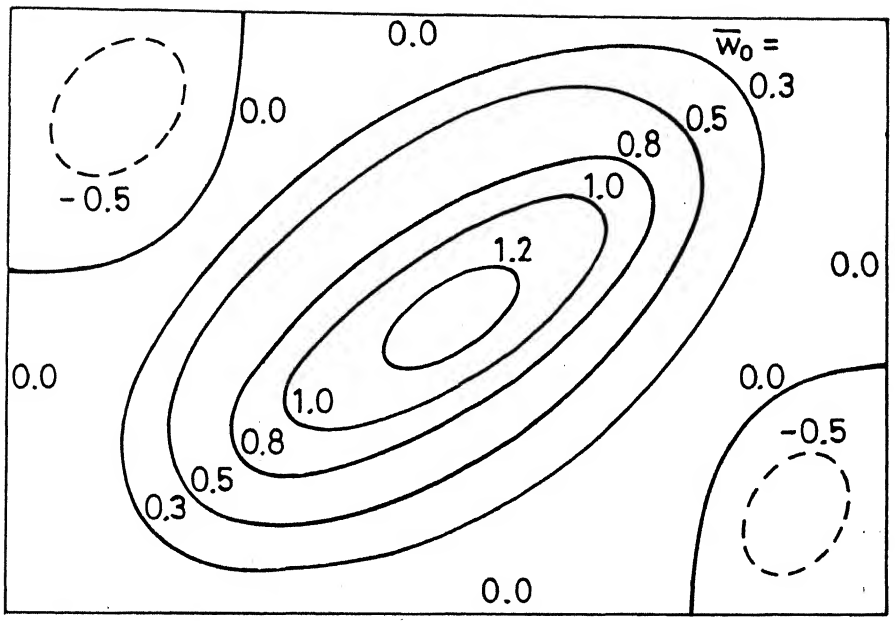

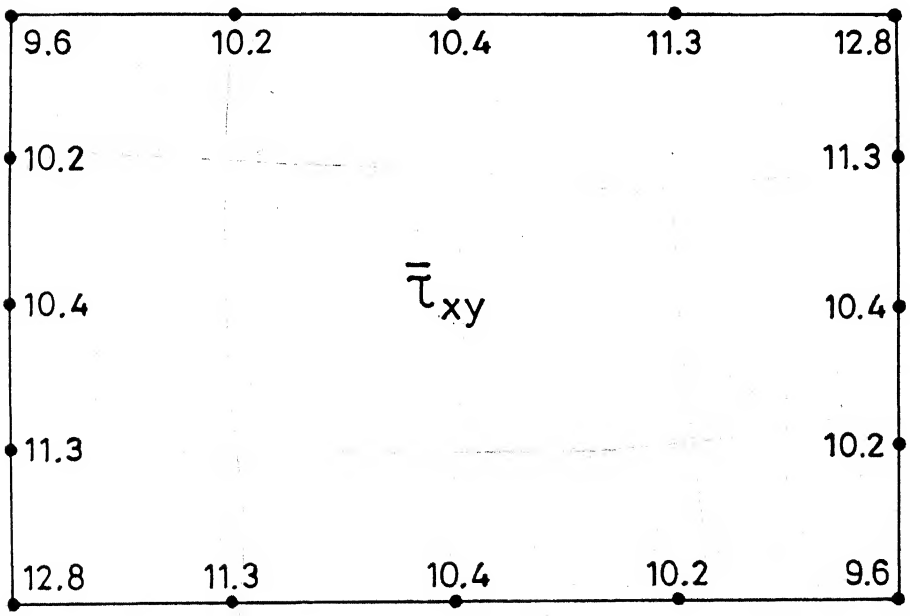

Fig. 5.7 Deflection contours and shear stress distribution for isotropic rectangular plate, $\lambda = 1.5$, symmetric mode, ($\bar{N} = 1.52$, $\bar{N}_{xy} = 10.8$)

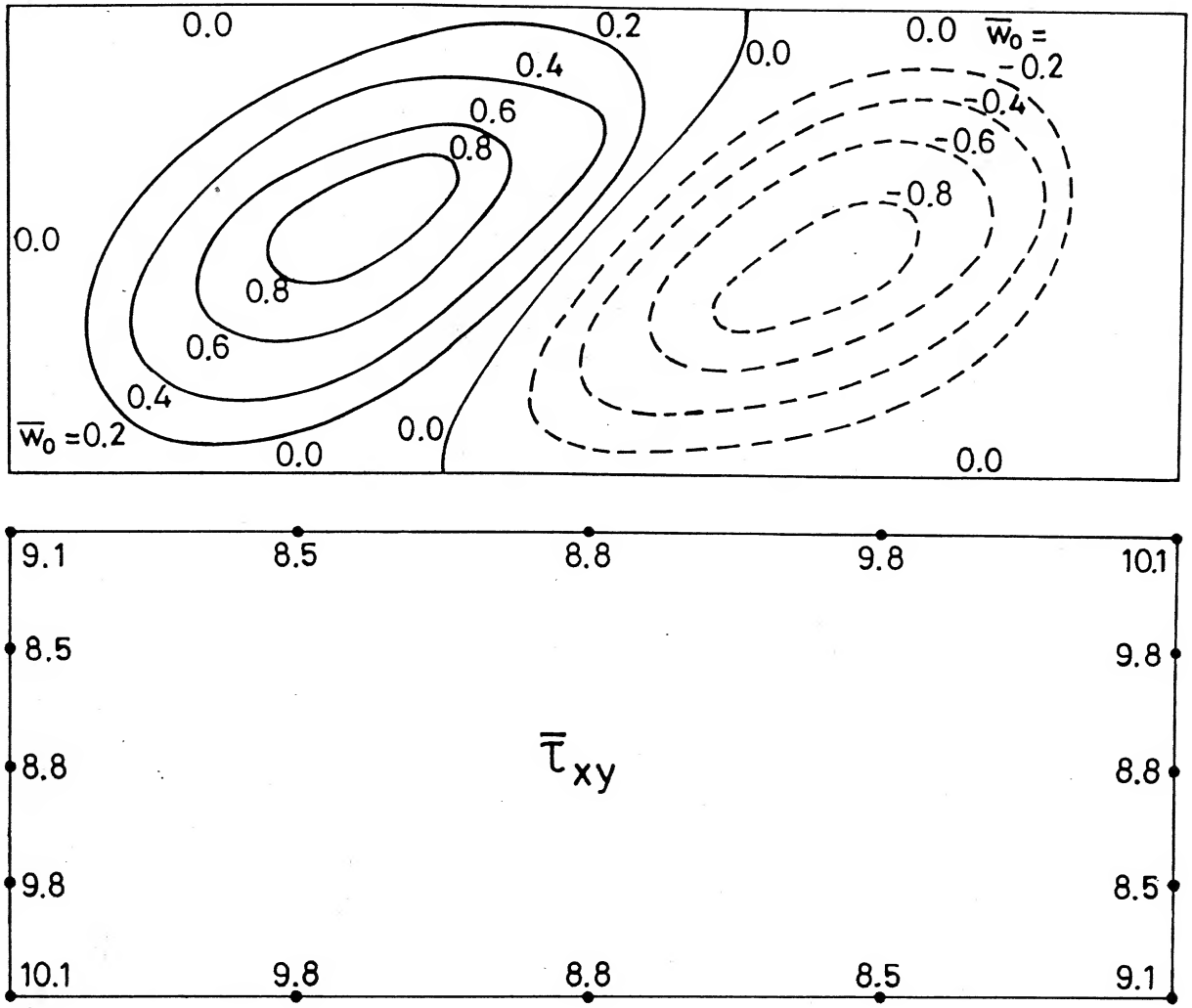

Fig. 5.8 Deflection contours and shear stress distribution for isotropic rectangular plate, $\lambda = 2.5$, anti-symmetric mode, ($\bar{N} = 1.5$, $\bar{N}_{xy} = 9.2$)

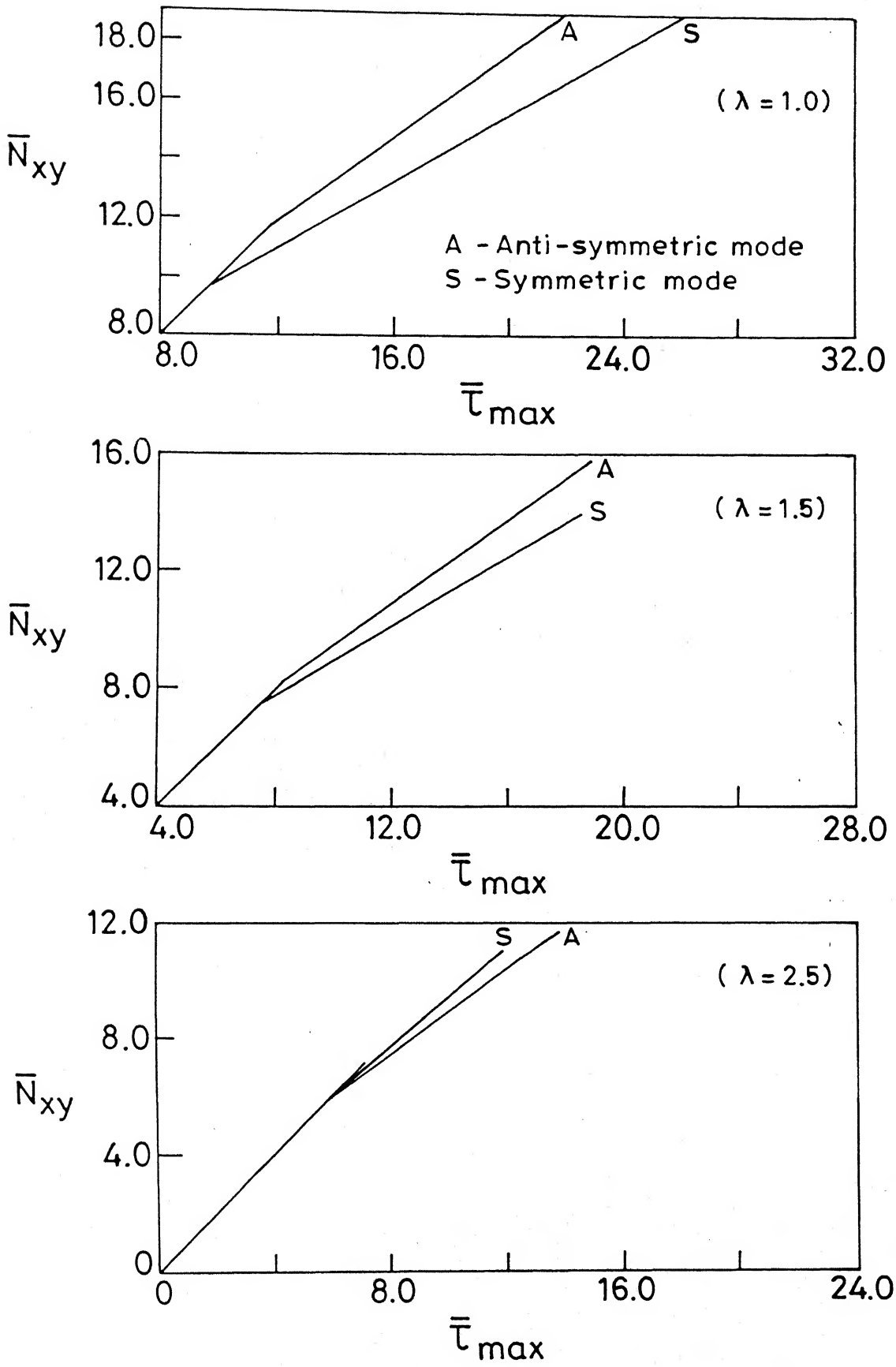

Fig. 5.9 Variation of maximum shear stress with the load.

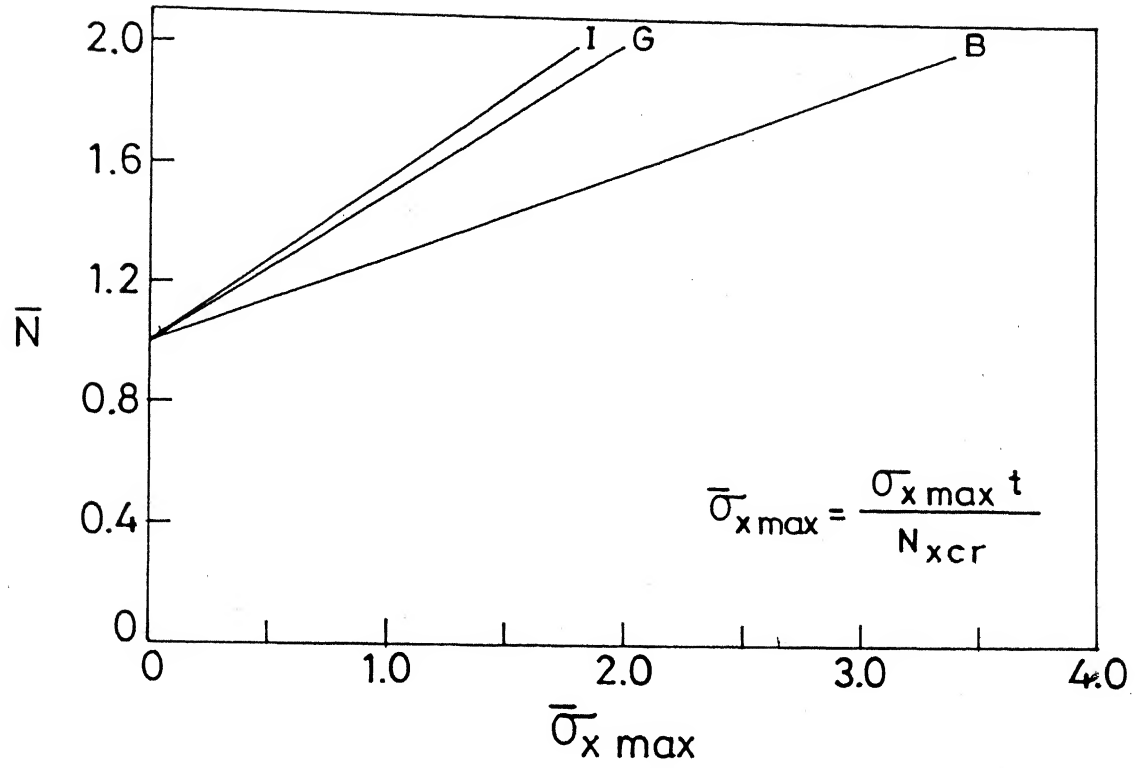

(a) Longitudinal stress

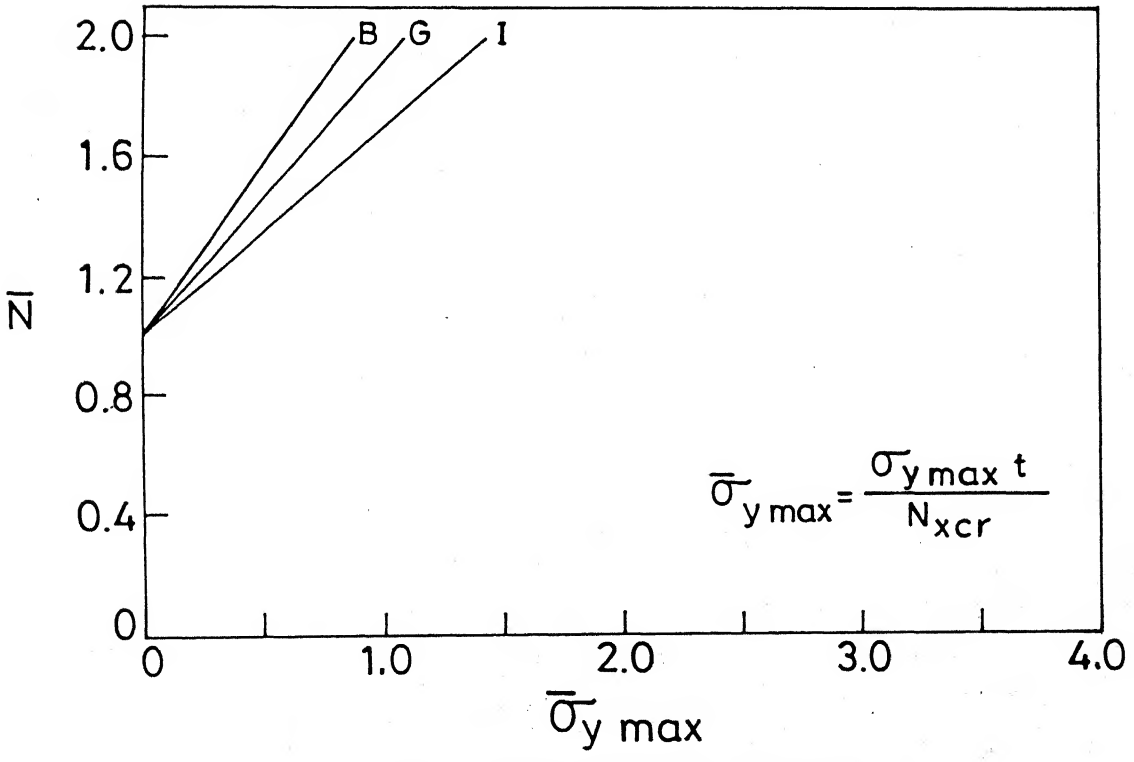

(b) Transverse stress

Fig. 5.10 Variation of maximum tensile stress with the shear load for a square plate buckling in symmetric mode.

CHAPTER 6

SUMMARY AND CONCLUSIONS

6.1 SUMMARY

The main aim of the present work has been to investigate the postbuckling behavior of isotropic and orthotropic thin rectangular plates subjected to either longitudinal compression or edge shear. Plates are assumed to be simply supported on all edges. Two inplane boundary conditions on unloaded edges have been considered : (i) edges free to move (ii) edges fully restrained. Throughout the investigation, the finite element method has been employed; a 16 element mesh is used to discretiz the quadrant of the plate (for compression loading) and the full plate (for shear loading). Each element is a 4-noded rectangle with 6 degrees of freedom at each node. The governing different equations have been derived by minimizing the total potential energy of the element and then assembled to obtain a set of simultaneous nonlinear algebraic equations which have been solve by an incremental-cum-iterative method.

Main contributions of the present study are :

(1) It has been shown that the finite element method is quite versatile in handling complex non-linear problems such as one dealt in this thesis.

(2) A method has been suggested to predict a possible change in the buckling mode for a given size of the plate and for specified boundary conditions.

(3) Empirical formulae have been deviced to predict the magnitude of the load at which a possible changeover in the buckling mode takes place. Equations (3.15) and (4.9) are applicable for longitudinally compressed plates and are valid for isotropic as well as orthotropic plates and for any inplane boundary condition.

(4) A useful set of effective width curves has been presented these curves are valid even after the change in the buckled configuration has taken place.

(5) The FE inplane boundary condition has been explored in detail for the postbuckling analysis; not much work is available in literature for this condition.

(6) By investigating plates of different aspect ratio, under shear loading, it has been shown that the primary mode at the instant of buckling remains unchanged in the postbuckling range. The buckling mode is a coupled one consisting of either symmetric uncoupled modes or anti-symmetric uncoupled modes.

6.2 CONCLUSIONS

Following useful conclusions can be drawn for plates subjected to longitudinal compression :

(i) The values of the critical load obtained using finite element method are very close to the exact ones.

(ii) The postbuckling behavior is greatly influenced by inplane boundary conditions on unloaded edges.

(iii) A plate of given aspect ratio may buckle in different modes under different inplane conditions. For example, an isotropic plate with $\lambda = 2.0$ buckles in (2,1) mode under ME condition but in (1,1) mode under FE condition

(iv) A plate initiated to buckle in a particular symmetric mode, converges, for a given load, to a mode which is a symmetric but not necessarily to the same one. On the other hand, a plate initiated to buckle in a particular anti-symmetric mode would finally converge to the same anti-symmetric mode.

(v) For a plate of given aspect ratio λ and a specified mode (m,n), i.e. for a fixed value of λ' $(= m/\lambda)$, the maximum lateral deflection is greater under ME condition than that under FE condition.

(vi) For the same load ratio, the lateral deflection of an orthotropic plate is greater than that of an isotropic plate and it increases with the value of rigidity ratio $\bar{E}$ of the material.

(vii) The axial stiffness of a plate after buckling reduces to about 50% to 70% of the prebuckled value, the actual value being dependent on plate boundary conditions, plate dimensions and the mode of buckling. A further reduction takes place after the secondary buckling to about 40% to 50% of the original (unbuckled) value. The reduction in stiffness is greater under ME condition than under FE condition.

(viii) The effective width reduces with an increase in the axial load; the reduction is large enough in the beginning but is very small for loads beyond 1.75 P_{cr}.

(ix) The effective width of a plate is greater under FE condition than under ME condition, keeping other factors same.

(x) For a given λ' and for prescribed boundary conditions, the effective width $\bar{b}_e$ decreases with an increase in the degree of orthotropy $\bar{E}$.

(xi) In the postbuckling regime, a plate undergoes differential shortenings causing non-uniform strains and stresses. The longitudinal stress under ME condition is maximum at the crest of the buckle whereas, for FE condition, it is maximum at the corners (junctions of loaded and unloaded edges).

(xii) For the same load ratio, $\bar{\sigma}_{max}$ decreases with the increase in the value of $\bar{E}$. For example, the ratio $\bar{\sigma}_{max}/\bar{\sigma}_{cr}$ for boron-epoxy is lower than that for glass-epoxy.

Additional comments on 'change in buckle pattern' of the plate subjected to longitudinal compression:

Throughout the investigation of longitudinally compressed plates, uncoupled modes only have been examined. Each time the plate was initiated to buckle in a particular uncoupled mode. The change in buckle pattern from lower uncoupled mode (i.e. primary mode) to the higher uncoupled mode (i.e. secondary mode)

was then obtained as point of intersection of the corresponding load-shortening lines. However, Supple (1966) has found that the change in buckle pattern is in the form of a coupled mode and it branches from the secondary mode (i.e. the one with higher critical load). But, for plates under FE condition, Supple (1970) shows that the change from primary to secondary mode does take place.

Since the present work does not examine coupled modes, the author feels that the results of effective width curves of Chapters 3 and 4 (involving change in buckle pattern) are approximate only. The curves however represent the qualitative picture as to how these curves get effected if the change in buckling pattern is to be accounted for.

Following useful conclusions can be drawn for plates subjected to edge shear :

(i) The mode at the instant of buckling is a mixed one consisting of either uncoupled symmetric modes or uncoupled anti-symmetric modes.

(ii) The load-shear displacement lines for a plate of a given λ are parallel; hence a change in buckled pattern is not possible, atleast in the postbuckling range.

investigated ($P \leq 2 P_{cr}$). This has been found true for all the three values of λ considered.

(iii) The reduction in the shear stiffness after primary buckling is rather small.

(iv) As expected, the deflection profiles are skewed making some angle with the edges.

(v) Longitudinal and transverse tensile membrane stresses are produced which tend to stiffen the plate in its postbuckling range.

(vi) Distribution of shear stress is symmetrical with respect to the two diagonals of the plate, with maximum value occuring at the two ends of the elongated (tension) diagonal.

6.3 SUGGESTIONS FOR FUTURE WORK

There is a tremendous scope of further research the subject of postbuckling behavior of plates. Some sug in this regard are :

* The effect of different flexural boundary cond should be studied, both for isotropic and orthotropic pla

* The postbuckling behavior of laminated composi plates should be studied.

* The effect of combined loading should be inves so as to make the problem more realistic.

* The effect of transverse shear in the plate theory can be included to make the large-deflection analysis more rational.

* The experiment work needs to be carried out to support findings of the theoretical investigation such as the present one.

REFERENCES

For explanation of the abbreviations used for journals, see NOTATIONS.

Aalami, B. and Chapman, J.C., 'Large Deflection Behavior of Rectangular Orthotropic Plates under Transverse and In-Plane Loads', PICEL, v. 42, pp. 347-382 (1969).

Agarwal, B.D. and Broutman, L.J., 'Analysis and Performance of Fibre Composites', John Wiley and Sons (1980).

Agarwal, B.L., 'Post-Buckling Behavior of Composite Shear Webs', AIAAJ, v. 19, pp. 933-939, July (1981).

Basu, A.K. and Chapman, J.C., 'Large Deflection Behavior of Transversly Loaded Rectangular Orthotropic Plates', PICEL, v. 39, pp. 79-110, Sept. (1966).

Carnoy, E.G. and Hughes, T.J.R., 'Finite Element Analysis of the Secondary Buckling of a Flat Plate under Uniaxial Compression', IJNLM, v. 18, n. 2, pp. 167-175 (1983).

Chajes, A., 'Principles of Structural Stability Theory', Prentice-Hall Int. (1974).

Chandra, R. and Raju, B.B., 'Post-Buckling Analysis of Rectangular Orthotropic Plates', IJMS, v. 15, pp. 81-97 (1973).

Chang, Y.W. and Masur, E.F., 'Vibrations and Stability of Buckled Panels', JEMD, EM5, pp. 1-26 (1965).

Cheung, Y.K. and Yeo, M.F., 'A Practical Introduction to Finite Element Analysis', Pitman Publishing Limited, London (1979).

Chia, C.Y., 'Large Deflection of Rectangular Orthotropic Plates', JEMD, EM5, pp. 1285-1298 (1972).

Chia, C.Y., 'Non-Linear Analysis of Plates', McGraw Hill Int., New York,

Chia, C.Y. and Prabhakara, M.K., 'Non-linear Analysis of Orthotropic Plates', JMES, v. 17, n. 3, pp. 133-138 (1975).

Coan, J.M., 'Large Deflection Theory of Plates with Small Initial Curvature Loaded in Edge Compression', JAM, pp. 407-414 (1951).

Colville, J., Becker, E.B., and Furlong, R.W., 'Large Displacement Analysis of Thin Plates', JSD, ST3, pp. 349-364 (1973).

Cook, R.D., 'Concepts and Applications of Finite Element Analysis', John Wiley and Sons (1981).

Crisfield, M.A., 'A Faster Modified Newton-Raphson Iteration', CMAME, v. 20, pp. 267-278 (1979).

Cui, E.J. and Dowell, E.H., 'Post-Buckling Behavior of Rectangular Orthotropic Plates with Two Free Side Edges', IJMS, v. 25, n. 6, pp. 429-446 (1983).

Desai, C.S. and Abel, J.F., 'Introduction to the Finite Element Method', Affiliated East-West Press Pvt. Ltd., New Delhi (1972).

Dombourian, E.M., Smith, C.V., and Carlson, R.L., 'A Perturbation Solution to a Plate Post-Buckling Problem', IJNLM, v. 11, pp. 49-58 (1976).

Gerard, G., 'Introduction to Structural Stability Theory', McGraw-Hill Book Co. (1962).

Harris, G.Z., 'The Buckling of Orthotropic Rectangular Plates Including the Effect of Lateral Edge Restraint', IJSS, v. 11, pp. 877-885 (1975).

Harris, G.Z., 'The Buckling and Post-Buckling Behavior of Composite Plates under Bi-axial Loading', IJMS, v. 17, pp. 187-202, March (1975).

Johns, D.J., 'Shear Buckling of Isotropic and Orthotropic Plates - A Review', British Aeronautical Research Council, R. and M., 3677 (1970).

Kaminski, B.E. and Ashton, J.E., 'Diagonal Tension Behavior of Boron-Epoxy Shear Panels', JCM, v. 5, pp. 553-558 (1971).

Kawai, T. and Yoshimura, N., 'Analysis of Large Deflection of Plates by the Finite Element Method', IJNME, v. 1, pp. 123-133 (1969).

Kobayashi, S., Sumihara, K., and Koyama, K., 'Shear Buckling Strength of Graphite-Epoxy Laminated Panels', Composite Materials, Proceedings of Japan-U.S. Conference, Tokyo (1981).

Kumar, A., 'Stability Theory of Structures', Tata McGraw-Hill Publishing Co. Ltd., New Delhi (1985).

Levy, S., 'Bending of Rectangular Plates with Large Deflections', NACA, TR 737 (1942).

Lind, N.C., Ravindra, M.K., and Schron, G., 'Empirical Effective Width Formula', JSD, ST9, pp. 1741-1757 (1976).

Murray, D.W. and Wilson, E.L., 'Finite Element Post-Buckling Analysis of Thin Elastic Plates', AIAAJ, pp. 1915-1920, Oct. (1969).

Nakamura, T. and Uetani, K., 'The Secondary Buckling and Post-Secondary Buckling Behaviors of Rectangular Plates', IJMS, v. 21, pp. 265-286 (1979).

Narayanan, R. and Chow, F.Y., 'Effect of Support Conditions on Plate Strengths', JSD, v. 111, n. 1, pp. 175-189 (1985).

Niyogi, A.K., 'Non-Linear Bending of Rectangular Orthotropic Plates', IJSS, v. 9, pp. 1133-1139 (1973).

Prabhakara, M.K. and Chia, C.Y., 'Post-Buckling Behavior of Rectangular Orthotropic Plates', JMES, v. 15, n. 1, pp. 25-33 (1973).

Rhodes, J. and Harvey, J.M., 'Plates in Uniaxial Compression with Various Support Conditions at the Unloaded Boundaries', IJMS, v. 13, pp. 787-802 (1971).

Rhodes, J. and Harvey, J.M., 'Examination of Plate Post-Buckling Behavior', JEMD, EM3, pp. 461-478 (1977).

Roberts, T.M. and Ashwell, D.G., 'The Use of Finite Element Mid-Increment Stiffness Matrices in the Post-Buckling Analysis of Imperfect Structures', IJSS, v. 7, pp. 805-823 (1971).

Rushton, K.R., 'Post-Buckling of Rectangular Plates with Various Boundary Conditions', AQ, pp. 163-181, May (1970).

Rushton, K.R., 'Post-Buckling of Tapered Plates', IJMS, v. 11, pp. 461-480 (1969).

Shye, K.Y. and Colville, J., 'Post-Buckling Finite Element Analysis of Flat Plates', JSD, ST2, pp. 297-311 (1979).

Stein, M., 'Buckling Stresses of Simply Supported Rectangular Flat Plates in Shear', NACA TN 1222 (1947).

Stein, M., 'Behavior of Buckled Rectangular Plates', JEMD, EM2, pp. 59-76 (1960).

Stein, M., 'Post-Buckling of Orthotropic Composite Plates Loaded in Compression', AIAAJ, v. 21, n. 12, pp. 1729-1735 (1983).

Stein, M., 'Post-Buckling of Long Orthotropic Plates in Combined Shear and Compression', AIAAJ, v. 23, n. 5, pp. 788-794 (1985).

Stricklin, J., Haisler, W.E., and Von-Riesemann, W., 'Geometrically Non-Linear Structural Analysis by Direct Stiffness Method', JSD, ST9, pp. 2299-2314 (1971).

Supple, W.J., 'Coupled Buckling Modes of Structures', Ph.D. thesis, University of London (1966).

Supple, W.J., 'Coupled Branching Configurations in the Elastic Buckling of Symmetric Structural Systems', IJMS, v. 9, pp. 97-112 (1967).

Supple. W.J., 'On the Change in Buckle Pattern in Elastic Structures', IJMS, v. 10, pp. 737-745 (1968).

Supple, W.J., 'Changes of Wave Form of Plates in the Post-Buckling Range', IJSS, v. 6, pp. 1243-1258 (1970).

Szilard, R., 'Theory and Analysis of Plates', Prentice-Hall Inc. (1974).

Szilard, R., 'Critical Load and Post-Buckling Analysis by FEM Using Energy Balancing Techniques', CS, v. 20, n. 1-3, pp. 277-286 (1985).

Timoshenko, S.P. and Gere, J.M., 'Theory of Elastic Stability' McGraw-Hill Book Co. (1961).

Uemura, M. and Byon, O-IL., 'Secondary Buckling of a Flat Plate under Uni-axial Compression, Part I: Theoretical Analysis of Simply Supported Flat Plate', IJNLM, v. 12, pp. 355-370 (1977).

Walker, A.C., 'Post-Buckling Behavior of Simply Supported Square Plates', AQ, v. 20, pp. 203-222 (1969).

Wittrick, W.H., 'Correlation Between Some Stability Problems for Orthotropic and Isotropic Plates under Biaxial and Uniaxial Direct Stress', AQ, v. 4, pp. 83-92 (1952).

Yamaki, N., 'Post-Buckling Behavior of Rectangular Plates with small Initial Curvature Loaded in Edge Compression', JAM, Trans. ASME, pp. 407-414 (1959) and pp. 335-342 (1960).

Yang, T.Y., 'Flexible Plate Finite Element on Elastic Foundation', JSD, ST10, pp. 2083-2101 (1970).

Yang, T.Y., 'Elastic Post-Buckling Predictions of Plates using Discrete Elements', AIAAJ, v. 9, n. 9 (1971).

Yang, T.Y. and Han, A.D., 'Buckled Plate Vibrations and Large Amplitude Vibrations using High Order Triangular Elements', AIAAJ, v. 21, n. 5, pp. 758-766 (1983).

Zhang, Y. and Matthews, F.L., 'Post-Buckling Behavior of Anisotropic Laminated Plates under Pure Shear and Shear Combined with Compressive Loading', AIAAJ, v. 22, n. 2, pp. 281-286 (1984).

Zienkiewicz, O.C., 'The Finite Element Method', Tata McGraw-Hill Publ. Co. Ltd., New Delhi (1977).